Late-Time Acceleration:

Interacting Dark Energy and Modified Gravity

by

Timothy Clemson

This thesis is submitted in partial fulfilment of
the requirements for the award of the degree of
Doctor of Philosophy of the University of Portsmouth.

September 23, 2013

Abstract

In 1998 astronomical observations of distant stars exploding at the ends of their lives led to the discovery that the expansion of the Universe is accelerating. This is likely to be caused by an intrinsic part of Einstein's General Theory of Relativity known as the cosmological constant, but naturalness issues and the need to improve observational tests have motivated the study of alternative models of the Universe. The research in this thesis is part of ongoing efforts to pin down the cause of late-time acceleration by better understanding these alternatives and their signatures in cosmological observations.

One such alternative is known as interacting dark energy and would be caused by additional matter in the Universe, as yet unknown to particle physics. This would interact with another unknown particle called dark matter that has been part of the standard model of cosmology since the 1970's. The first part of this thesis contains a review of works on interacting dark energy and investigates a particular version of the model which had not been studied in detail before, placing recent observational constraints on its parameters.

Another alternative to the cosmological constant is known as modified gravity, where General Relativity is extended by the addition of new degrees of freedom. Theories of modified gravity are mathematically related to some models of interacting dark energy and can appear very similar in cosmological observations. The second part of this thesis investigates the extent to which the two can be distinguished using current observational data.

Table of Contents

List of Tables

List of Figures

Declaration

Whilst registered as a candidate for the above degree, I have not been registered for any other research award. The results and conclusions embodied in this thesis are the work of the named candidate and have not been submitted for any other academic award.

Word count: Approximately 32,000 words.

Acknowledgements

My thanks go to Kazuya and Gong-Bo for giving their time during my PhD, Roy for his insight into the model and to Rachael and my parents for supporting me during my write-up.

Dissemination

Interacting Dark Energy – constraints and degeneracies

Timothy Clemson, Kazuya Koyama, Gong-Bo Zhao,
Roy Maartens and Jussi Valiviita.
Physical Review D, volume 85, (2012), 043007.
arXiv:1109.6234 [astro-ph.CO]

The Distinguishability of
Interacting Dark Energy from Modified Gravity

Timothy Clemson and Kazuya Koyama.
Journal of Cosmology and Astroparticle Physics,
volume 1301, (2013), 010.
arXiv:1209.2618 [astro-ph.CO]

Presentations

September 2011
Interacting Dark Energy,
UKCosmo, ICG.

July 2012
Interacting Dark Energy and Modified Gravity,
Thirteenth Marcel Grossmann Meeting, Stockholm.

Abbreviations

General Relativity	GR
Dark Energy	DE
Interacting Dark Energy	IDE
Dark Matter	DM
Cold Dark Matter	CDM
Modified Gravity	MG
Scalar-Tensor Theory	STT
Dvali-Gabadadze-Porrati	DGP
Quantum Mechanics	QM
Friedmann-Lemaitre-Robertson-Walker	FLRW
Cosmic Microwave Background	CMB
Baryon Acoustic Oscillations	BAO
Supernovae	SNe
Type Ia Supernovae	SNIa
Integrated Sachs-Wolfe	ISW
Big-Bang Nucleosynthesis	BBN
Gamma-Ray Burst	GRB
Wilkinson Microwave Anisotropy Probe	WMAP
Code for Anisotropies in the Microwave Background	CAMB
Chevallier-Polarski-Linder	CPL
European Photon Imaging Camera	EPIC
Dark Universe Explorer	DUNE
Markhov-Chain Monte-Carlo	MCMC
Hubble Space Telescope	HST

Definitions and Notation

Metric tensor	$g_{\mu\nu}$
Perturbation metric tensor	$\delta g_{\mu\nu}$
Partial derivative	$A_{,i} \equiv \partial_i A$
Christoffel symbol	$\Gamma^{\alpha}_{\mu\nu} \equiv \frac{1}{2} g^{\beta\alpha}(g_{\beta\mu,\nu} + g_{\beta\nu,\mu} - g_{\mu\nu,\beta})$
Covariant derivative	$V_{\nu\|\mu} \equiv \nabla_\mu V_\nu \equiv \partial_\mu V_\nu - \Gamma^{\sigma}_{\mu\nu} V_\sigma$
Covariant derivative 'squared'	$(\nabla\phi)^2 \equiv g^{\mu\nu}(\nabla_\mu\phi)(\nabla_\nu\phi)$
D'Alembertian	$\Box \equiv \nabla^\mu\nabla_\mu = g^{\mu\nu}\nabla_\mu\nabla_\nu$
Riemann tensor	$R^{\alpha}_{\ \mu\beta\nu} \equiv \Gamma^{\alpha}_{\mu\nu,\beta} - \Gamma^{\alpha}_{\mu\beta,\nu} + \Gamma^{\alpha}_{\lambda\beta}\Gamma^{\lambda}_{\mu\nu} - \Gamma^{\alpha}_{\lambda\nu}\Gamma^{\lambda}_{\mu\beta}$
Ricci tensor	$R_{\mu\nu} \equiv R^{\alpha}_{\ \mu\alpha\nu}$
Ricci scalar	$R \equiv g^{\mu\nu} R_{\mu\nu}$
Energy-momentum tensor	$T_{\mu\nu}$
Scale factor	a
Redshift	$z = \frac{1}{a} - 1$
Cosmic time	t
Conformal time	τ
$\ln a$	N
$\frac{\mathrm{d}\alpha}{\mathrm{d}\tau}$	$\dot{\alpha}$
$\frac{\mathrm{d}\alpha}{\mathrm{d}N}$	α'

$\frac{1}{a}\frac{\mathrm{d}a}{\mathrm{d}t}$	H
$\frac{1}{a}\frac{\mathrm{d}a}{\mathrm{d}\tau}$	$\mathcal{H}$
Newton's constant	$G \equiv 6.67 * 10^{-11}$
Einstein-Hilbert action	S_{EH}
Interacting dark energy action	S_{IDE}
Scalar-Tensor theory action	S_{STT}
Interacting dark energy quantities	α_x
Cold dark matter quantities	α_c
Baryon quantities	α_b
Modified gravity and transformed quantities	$\tilde{\alpha}$
Fourier mode wavenumber	$k^2 = -\partial_i \partial^i$
Scalar metric perturbations	Ψ, Φ, B, E
Vector metric perturbations	J_{i}, F_{i}
Tensor metric perturbation	h_{ij}
Synchronous gauge metric perturbation	$h = -2\left(3\dot{\Phi} + k^2\dot{E}\right)$
Small changes of coordinates	$\xi, \xi^0, \hat{\xi}$
Projection tensor	$s_{\mu\nu}$
Expansion scalar	Θ
Rotation tensor	$r_{\mu\nu}$
Shear tensor	$\sigma_{\mu\nu}$
Expansion scalar	a_μ
Interacting dark energy field perturbation	φ
Total interacting dark energy field	$\bar{\psi} \equiv \psi + \varphi$
Interacting dark energy potential	$V(\psi)$
Interacting dark energy coupling	$C(\psi)$

Modified gravity field perturbation	χ
Total modified gravity field	$\bar{\phi} \equiv \phi + \chi$
Scalar-Tensor theory function	$\omega(\phi)$
Scalar-Tensor theory potential	$U(\phi)$
Cold dark matter field	ζ
Matter field	η
Baryon field	ς
Energy density perturbation	$\delta \equiv \delta\rho/\rho$
Total energy density	$\bar{\rho} \equiv \rho + \delta\rho = \rho(1+\delta)$
Four-velocity	u^μ
Velocity potential	v_A
Velocity divergence	$\theta_A \equiv -k^2(v_A + B)$
Pressure perturbation	δp
Total pressure	$\bar{p} \equiv p + \delta p$
Dark energy equation of state parameter	$w \equiv p_x/\rho_x$
Density parameter	$\Omega \equiv \frac{8\pi G\rho}{3H^2}$
Anisotropic stress	π^i_j
Physical soundspeed	$c^2_{s,A} \equiv (\delta p_A/\delta\rho_A)_{\text{restframe}}$
Adiabatic soundspeed	$c^2_{a,A} \equiv \dot{p}_A/\dot{\rho}_A$
Interaction rate	Γ
Energy-momentum transfer four-vector	$\bar{Q}^\mu_A$
Energy density transfer perturbation	δQ_A
Energy density transfer rate	$\bar{Q}_A \equiv Q_A + \delta Q_A$
Momentum transfer potential	f_A
Momentum density transfer rate	$F^\mu_A \equiv a^{-1}(0, \partial^i f_A)$
E_G ΛCDM+GR test parameter	E_G
$\mu - \Sigma$ modified gravity parameterisation	μ, Σ

Chapter 1

Perspectives on ΛCDM

At present the standard cosmological model seems to be resilient to observational tests. It was 80 years before the effect of Einstein's Λ was detected in 1998 [1, 2], but the conclusion that the expansion of the Universe is accelerating is now very robust [3]. The Dark Energy Task Force Report [4] laid out a roadmap to understanding the nature of dark energy, (DE), through observations. They categorised these efforts into four stages of increasing sophistication and Stage 3 DE missions such as the Baryon Oscillation Spectroscopic Survey and the Dark Energy Survey are now beginning. Eventually, after two decades of both observational and theoretical efforts, Stage 4 missions such as the Square Kilometre Array, the Large Synoptic Survey Telescope and the Euclid satellite should provide definitive results on whether or not the cosmological constant is sufficient to describe the apparent late-time acceleration of the Universe.

The picture for cold dark matter, (CDM), is less clear however. It is believed to make up more than five times as much of the Universe as matter described by the standard model of particle physics, but 80 years after it was first proposed [5] it is still just inferred through its gravitational effects. The evidence for dark matter, (DM), is compelling, with astronomical observations on a range of scales in support of each other, but laboratory experiments around the world have as yet failed to provide proof of its exis-

tence. Strictly speaking therefore, the age old question perennially faced by astronomers of 'more matter or more gravity' still remains to be answered for this phenomenon, although the consensus amongst the cosmological community has indeed been for many years that DM must be particulate in nature. It may be of course that with the recent discovery of the Higgs boson the standard model of particle physics is complete, but there are finetuning issues within it which make a strong case for the naturalness of extensions such as supersymmetry or axions.

The same can also be said about the cause of the late-time acceleration. It could well be either gravitational or material in nature. Indeed the theorised accelerated expansion of the very early Universe known as inflation is thought to be driven by particle fields. The cosmological constant however sits comfortably within an accepted theory as a natural part of the framework of General Relativity, (GR). In this introductory chapter we discuss the issues that surround Λ, the observations that are used to test it and the possible alternatives that exist.

Chapter 2 presents the basics of perturbation theory as a foundation for later chapters and Chapter 3 reviews works on a particular alternative to the cosmological constant called interacting dark energy, (IDE). The study of IDE forms the basis of this thesis and Chapter 4 is a perturbation analysis of a particular IDE model. The second part of the thesis then considers the relationship of IDE to modified gravity theories, (MG). Chapter 5 develops a dual description of two equivalent models and Chapter 6 investigates the possibility of distinguishing between them using current observations. Conclusions are then drawn in Chapter 7.

1.1 The Cosmological Constant

The simplest explanation for the observed late-time acceleration is the inclusion in GR of the cosmological constant. A number of works have been unable to detect any significant deviation from a pure cosmological constant [6, 7, 8],

but it may yet be possible to observe such a break from ΛCDM as purpose-built missions come online and cosmological measurements become even more precise [9, 10]. For reviews of the subject see [11, 12, 13, 14].

1.1.1 History

The cosmological constant was first mentioned in a footnote in Einstein's 1916 paper on GR [15]. Under the action of gravity, the Universe would be expected to collapse, so he later included it in an attempt to describe a static universe [16], which was in fact still the accepted wisdom until 1929. It may be this that he called his biggest blunder, because he missed the obvious instability of a static universe to small variations in density, as shown by Eddington in 1930 [17].

Although Λ was included in early cosmological models it slipped out of common use, doubtless due to the lack of observational evidence, and even Einstein later asserted in an appendix added to the 1945 version of his popular book on relativity that Λ should be rejected on the grounds of logical economy [18]. In particular there was no need for its inclusion after the development of the Friedmann-Lemaître-Robertson-Walker, (FLRW), model [19], which was perfectly capable of describing the observed expansion of the Universe [20, 21].

Thus Λ was mostly consigned to the textbooks until the cosmological community was caught somewhat by surprise by the observation of late-time acceleration in 1998 [1, 2]. This neatly provided for a flat Universe, ($\Omega_{\text{total}} = 1$), winning a Nobel Prize for the teams involved. Cosmic microwave background, (CMB), data had in fact already shown that the geometry of the Universe was close to flat and by combining it with large-scale structure data it could be shown that $\Omega_{\text{m}} \approx 0.3$, (where m stands for matter), suggesting that Λ might be required to make up the difference [13], but as with DM only conclusive observations solidified the consensus.

1.1.2 The place of Λ in GR

The most general second order action for the metric that there is can be written as,

$$S = \frac{1}{16\pi G}\int \sqrt{-g}(R - 2\Lambda)\mathrm{d}^4x, \tag{1.1}$$

where G is Newton's constant, $g \equiv \det(g_{\mu\nu})$ is the determinant of the space-time metric $g_{\mu\nu}$, $R \equiv R^{\mu}_{\ \mu}$ is the Ricci scalar with $R_{\mu\nu}$ being the Ricci tensor and Λ is the cosmological constant. There is no physical reason why Λ should be removed, so we are led by the variational principle to Einstein's field equations,

$$R_{\mu\nu} - \frac{1}{2}Rg_{\mu\nu} + \Lambda g_{\mu\nu} = 8\pi G T_{\mu\nu}, \tag{1.2}$$

where $T_{\mu\nu}$ is the stress-energy tensor. This is the most general form for the equations to take and Λ has entered them in a perfectly natural way. The actual value of Λ could be seen as arbitrary, but there are plenty of constants throughout physics whose values are set only empirically [22]. A big bang universe without Λ can recollapse, while a large enough Λ prohibits structure formation altogether. In this way a small Λ allows matter to have a greater effect on spacetime than a large Λ would so it can be seen as the inherent elasticity of spacetime [23]. It has been described as the only universal length scale in nature [24] and as a functional part of the apparatus of GR the observational evidence of its existence can even be seen as support for the theory relative to Newtonian gravity.

1.1.3 Problems

After the observational confirmation of late-time acceleration, focus turned to the problems associated with Λ. It should be stressed however that there are no practical issues surrounding its gravitational effects or the cosmology it produces. There are instead two problems often cited with Λ, one somewhat philosophical in nature and one associated with Quantum Mechanics, (QM), which are discussed below.

Coincidence

One issue with considering Λ to be responsible for the late-time acceleration is that its energy density has only become comparable to that of matter very recently in the history of the Universe. The energy density of matter scales as a^{-3} with the expansion of the Universe, where a is the scale factor of the Universe, while the effective energy density of a cosmological constant is unchanged by the expansion. Λ could in theory have any value at all, so it can be seen as something of a coincidence that the value it does have leads to acceleration only now, (and likewise parity between $\Omega_{\rm m}$ and Ω_Λ), when we as observers are here to witness it. Indeed the Universe has undergone a large number of e-folds, (expansion by factors of $N = \ln(a)$), even since the end of inflation whereas the Universe has only begun accelerating in the last couple of e-folds [25].

This is known as the coincidence problem and is one of the major motivations for considering alternatives to a simple cosmological constant, with many models being developed to provide alternative explanations as to why the acceleration should only begin at late times. Such coincidences do appear in nature of course, for example the moon is almost exactly the same size in the sky as the sun. It may even be that given the amount of time needed for planets to form and for life to appear on them that it's actually more likely than not that we should observe similar Ω_Λ and $\Omega_{\rm m}$ today [26]. The coincidence is anyway an artefact of the choice of a logarithmic coordinate. When considered in terms of time, (perhaps a more natural way to consider coincidence), or the scale factor itself, the coincidence disappears because the ratio of Ω_Λ to $\Omega_{\rm m}$ has been greater than one third for about half the age of the Universe [22, 26], (or since it was roughly half its current size).

Vacuum Energy

Another issue with admitting Λ into GR is that the existence of a driving force behind the accelerated expansion rate of the Universe has already been predicted by QM. It could potentially be caused by the vacuum energy den-

sity of space, but its approximate value expected from quantum mechanics is 120 orders of magnitude larger than that observed for Λ. This is known simply as the cosmological constant problem and can be made more or less severe depending on where the cut-off of Quantum Field Theory is chosen to be [22]. Given that GR has yet to be reconciled with QM it may be a mistake to identify vacuum energy with Λ anyway. Quantum Field Theory applies only to flat, (Minkowski), spacetimes [22], but GR describes nothing more than the curvature of spacetime. So whilst the effects of Λ and vacuum energy are superficially similar, there is simply no way to relate their causes to one another through a common framework, at least until a method of quantising spacetime is developed.

In truth, what problem there is has always existed in Quantum Field Theory. The Universe is clearly not tearing itself apart due to vacuum energy, but there was no particularly great debate about the issue before 1998 [27], (although see [28]). The Casimir effect is often cited as proof that that vacuum energy exists, but this has been criticised, (e.g. by [29]), as it only demonstrates a change in vacuum energy and says nothing about where the zero point is. Yet another possibility is that the value of Λ is such that it, (nearly), cancels the effect of the vacuum energy in the Universe [30], leading to an effective Λ of the value observed, although this of course suffers from a fine-tuning problem.

1.2 Observations

This section gives a brief overview of the observational probes which are used to constrain cosmological parameters and focuses on those important to DE studies. In particular the disparity between purely geometrical measures and those which involve an understanding of complex astrophysical processes highlighted by recent results from the Planck satellite is discussed, whilst other probes mentioned in later chapters are also introduced.

1.2.1 CMB and BAO

Observations of the CMB offer a unique view of the early Universe. Space-based missions such as the Wilkinson Microwave Anisotropy Probe, (WMAP), [31] and Planck [32] are complemented by ground based observations such as the South Pole Telescope [33] and the Atacama Cosmology Telescope [34]. This has meant that the angular power spectrum of CMB temperature anisotropies is well measured from the largest scales to deep within the damping tail. On their own CMB measurements can provide tight constraints on some cosmological parameters, such as the effective density parameter of curvature $\Omega_{\rm K}$, but they are less well suited to measurements of DE and in the background constraints come only from the shift parameter, which relates Ω_m and $H(z)$.

The fluctuations in the coupled photon-baryon fluid in the early Universe which can be seen in the CMB temperature anisotropies also leave an imprint in the baryon density field after decoupling, (although this becomes washed out somewhat with time due to the underlying smooth DM distribution). The distance that sound waves could have travelled before recombination creates a characteristic excess of power at particular separations in the large scale distribution of galaxies which can be calibrated against the CMB to provide a standard ruler with which to probe the expansion history.

The combination of these baryon acoustic oscillation, (BAO), measurements with CMB data can break the $\Omega_{\rm m}-\Omega_\Lambda$ degeneracy suffered by the CMB and partially break the $\Omega_{\rm m}-w$ degeneracy, (where w is the DE equation of state parameter). This allows useful findings to be gleaned from geometrical measurements alone, the causes of which are better understood theoretically and which have fewer problems with systematic errors than those made from observations of more complex astrophysical processes. Interestingly BAO measurements are now also being made using quasar absorption lines out to redshifts around 2.3, well into the matter dominated era [35].

The recent Planck data [32], when combined with BAO datasets [36, 37, 38], (and WMAP polarization data), have produced some interesting results. $\Omega_{\rm c}$, (where c stands for CDM), is slightly higher than expected, while Ω_Λ and

H_0 are slightly lower, but both data sets are in excellent agreement about the base parameters of ΛCDM. They are also consistent with Λ when allowing for either a constant or time-varying $w \neq -1$, with the conclusion being drawn that "there is no strong evidence that DE is anything other than a cosmological constant" [32].

1.2.2 SNIa and H_0

The original discovery of late-time acceleration came about because of the realisation that Type-Ia supernovae, (SNIa), could be used as normalisable standard candles because they all explode at the same mass limit [39]. This was then made possible by the development of telescope mounted banks of CCD cameras which could be used to quickly and efficiently identify large numbers of supernovae, (SNe). SNIa are excellent at constraining models of DE and are complimentary to both CMB and BAO measurements, but issues about the use of their data remain, such as the existence of 'prompt' and 'late' populations, the nature of the progenitors from which they come and the presence of high luminosity outliers.

Recently a great deal of work has also gone into the determination of H_0. This is especially important for DE studies because the distance measurements made are the first steps on the cosmic distance ladder and also used to calibrate SNIa magnitude-redshift relations. In particular two recent measurements have found $H_0 \approx 74 \mathrm{kms}^{-1}\mathrm{Mpc}^{-1}$ [40, 41], but these are in tension with the lower Planck result of 67.3 at 2.5σ and this tension can not be easily resolved by varying the parameters of ΛCDM [32]. Future improvements in the determination of H_0 hold great promise, with the possibility of detecting exotic physics if measurements can be made with a 1% accuracy [42], but until the error bars on these key measurements can be brought down substantially from today's levels, their predictions seem likely to carry less weight than CMB and BAO data.

Recent SNIa measurements also seem to be at odds with Planck results to some extent. SNe constraints are also geometrical measurements but may

be clouded by the need to understand complex physical systems better than we currently do. It has been suggested that some systematic errors remain unaccounted for in the analysis of their data, so hints of new physics found by combining CMB and SNIa data should be treated with caution [32]. Indeed the combination of one recent SNIa dataset with Planck data, (or equally the H_0 measurements mentioned above), leads to a cosmological constant being disfavoured at 2σ for both constant and variable w models.

1.2.3 Other probes

The number density of cluster-sized DM haloes as a function of halo mass and redshift can be predicted from N-body simulations. The total masses of clusters can be found using x-ray spectroscopy, velocity dispersion and their weak lensing signal, (see below), while their baryon content can be ascertained using x-ray gas emissions, or Sunyaev-Zel'dovich distortions to the CMB's blackbody spectrum. As larger cluster catalogues have become available, N-body predictions have been able to more accurately constrain the Universe's expansion history, (e.g. [43]). The local cluster abundance constrains the amplitude of the matter power spectrum σ_8 and the changes in abundance with redshift constrain $\Omega_{\rm m}$ [44]. The changes in number density are caused by both geometry and structure growth and constraints from cluster counts are complimentary to the probes discussed above. X-ray measurements of the baryonic mass within clusters can also be compared to $\Omega_{\rm m}$ in order to estimate the gas mass fraction in clusters and probe the acceleration of the Universe [45].

Another cosmological probe of increasing relevance is weak lensing, (see e.g. [46, 47]). This quantifies cosmic shear, the gravitational distortion of light from distant galaxies and can be studied tomographically to chart the evolution of DM over time. Like cluster counts it is sensitive to both geometry and structure growth and can be used to constrain σ_8 and $\Omega_{\rm m}$. Techniques are becoming increasingly sophisticated, [48], but cosmic shear measurements are extremely hard to make due to image processing issues and systematic

effects such as galaxy alignment with other galaxies or large scale structures and a great deal of work needs to be done before the technique is implemented in future Stage 4 DE missions.

In a similar way to clusters, galaxies can be used to determine the DM power spectrum. There are more issues with using galaxies however, such as the need to use a homogeneous sample and the effects of DM-baryon bias, non-linear evolution and redshift-space distortions, (deviations from the bulk flow of the Universe due to overdensities). The first of these can be dealt with by using a particular class of galaxies, such as the luminous red galaxies used in [49], whilst the final two can be corrected for either analytically or through numerical modelling. The precise nature of DM-baryon bias is not well understood however and is simply approximated as being scale independent and linear on sufficiently large scales, (where it is nonetheless expected to be a good approximation). The amplitude of anisotropies in the galaxy power spectrum due to redshift-space distortions can also be used to learn about the growth rate of structures [50]

The integrated Sachs-Wolfe, (ISW), effect determines the shape of the large-scale fluctuations in the CMB. It is caused by changes in gravitational potentials as the photons pass through them and so is sensitive to the effects of DE. Ultimately this is of relatively limited use because measurements of the ISW plateau are hugely affected by cosmic variance, although the effect can also be measured as a correlation between CMB anisotropies and the local matter density [51]. Alcock-Paczynski [52] tests use the way the angular size of objects on the sky varies with redshift to learn about cosmology and can be applied to e.g. galaxies or quasar pairs. Other observational constraints come for example from globular cluster limits on the age of the Universe, big-bang nucleosynthesis, (BBN), for which the DE density must be sufficiently small at early times so as not to affect nucleosynthesis and gamma-ray bursts, (GRB's), which may also be standardisable candles like SNIa [53].

$H(z)$ data has been found using stellar population models to determine

the oldest stars in passively evolving galaxies, (those without star formation), which have good spectroscopic redshifts. The difference in ages between galaxies then approximates dz/dt, from which $H(z)$ can be calculated [54]. In a similar way age estimates of passively evolving galaxies or clusters can also be used along with an estimate for the age of the Universe and assumptions about their birth and star formation history to derive their lookback times, (time of observation before the present), which can then be compared to their redshifts to learn about the expansion history [55].

1.3 Alternatives to ΛCDM

The end of the twentieth century saw enormous leaps forward in our ability to observe the Universe, but the success of ΛCDM could very well still be due to the limitations of cosmological observations. For this reason alone it is worth studying alternatives to the standard cosmological model, so that they and their differences from ΛCDM can be better tested for. The two main alternatives at the present time are dark energy, (DE), and MG. Either of these could potentially take the place of Λ as the cause of late-time acceleration. Other possible cause of acceleration also described below seem unlikely to be the whole story.

1.3.1 Dark energy

One possibility for going beyond Λ is to consider the late-time acceleration as being due to some unknown substance in the Universe which is then generally classified under the broad heading of DE. There is now a vast literature on the subject, most of which is summarised in recent reviews [56, 57, 58, 59, 60, 61], while courses are also now being taught in cosmology summer schools [62, 63] and textbooks have even begun to appear which are dedicated to the topic [64, 65].

DE models have predominantly been studied because they are free to admit some form of evolution and so do not necessarily suffer from the smallness

and coincidence problems of the cosmological constant. There are a great variety of possibilities for the precise form that DE may take and so many works have focused on simply trying to get a handle on its nature by studying purely phenomenological models and just parameterising its evolution in some way, (see e.g. [66, 67, 68]). Different techniques such as principle component analysis have been employed to look for the signatures of DE models in observational data [69, 70] and some have found hints of dynamics at low redshifts [8, 71, 72] which forthcoming data will be able to give a more definitive answer on.

DE moves the cause of late-time acceleration to the mass-energy side of Einstein's field equations. Models range from simple decaying cosmological 'constants' to inhomogeneous tachyonic interacting holographic DE, (although not much work has been done on the latter). One model which became popular soon after 1998 is quintessence. This models DE as a scalar field and can lead to scaling solutions for simple scalar field potentials, but it was found that the DE would necessarily have had too much of an influence at early times leading to a potential conflict with BBN bounds [73]. Scaling solutions are still possible with quintessence, but require complex potentials without motivation from particle physics.

A drawback of DE models is that their energy density today is small compared to what would be expected from an equipartition of energy in the early Universe. The cosmological constant does not suffer this precise issue because we only assign an effective Ω_Λ to it, when really it lives on the curvature side of Einstein's field equations rather than the mass/energy side. This gives DE models a finetuning problem to solve, again requiring tailored dynamics, although for sufficiently steep potentials this may be significantly relieved by quantum effects during inflation [74].

At least with the confirmation of the recent Higgs boson discovery, a fundamental scalar particle has now been observed in nature for the first time. Whether it is the only one which exists, at low energies anyway, remains to be seen. As previously noted, DE models can be modified in many unusual

ways, but one natural extension of DE is to allow it to couple to DM non-gravitationally. Models such as these are known as IDE models and the study of particular forms and applications of IDE shall form the majority of this thesis.

1.3.2 Modified gravity

MG theories are extensions or departures from GR, (see [75, 76, 77] for reviews). Historically, they have been studied since GR's inception, motivated by ideas such as the possibility of time-varying constants, theories of extra dimensions from fundamental particle physics and the possibility that GR is an approximation to an even more general theory as it was itself to Newtonian gravity. They include theories with extra scalar, vector or tensor fields in the gravitational sector such as Scalar-Tensor theory, (STT), Einstein-Aether, Tensor-Vector-Scalar, and Bimetric theories. Another modification of gravity is to go beyond second order derivatives of the metric in the field equations or allow more complex derivative terms such as one finds in $f(R)$, Horava-Lifschitz gravity, Galileons and Ghost Condensates. Alternatively the motivation to modify gravity can come from the existence of higher dimensions in a theory such as Kaluza-Klein, Randall-Sundrum, Dvali-Gabadadze-Porrati, (DGP), or higher co-dimension braneworlds [77].

The primary application of MG in modern cosmology is as an explanation for late-time acceleration and STT shall be the subject of study in Chapters 5 and 6. The gravitational alternative to particulate DM is known as Modified Newtonian Dynamics. It was originally very successful and can neatly replicate the rotation curves of galaxies but the theory was unsuited to its relativistic description as Tensor-Vector-Scalar theory and became inconsistent with observations, especially the CMB power spectrum [77].

1.3.3 Other possibilities

Late-time acceleration might also arise from effects due to structure in the Universe, (see [78] for a review). These do not appear to be able to explain all of the acceleration observed but their study is none the less hugely important as observations become increasingly accurate. There are two types of effect which are studied and they both involve dropping our basic assumptions about cosmology to some extent. Dropping the Copernican principle that we do not live in a special place in the Universe allows for us to be located at the centre of a large underdensity which could cause an apparent global acceleration from a relatively local effect, (see e.g. [79]). Also, on scales larger than around 200 Mpc the Universe appears to be homogeneous, but dropping the assumption that such inhomogeneities as there are have no effect might lead to an actual global acceleration caused by a backreaction from structure, (see e.g. [80]).

Chapter 2

Cosmological Perturbations

This chapter provides a brief introduction to the formalisms and conventions underlying cosmological perturbation theory for structure formation at linear order. It also outlines the procedures used to derive evolution equations from the GR+ΛCDM action and underpins the analyses in later chapters. Sections involving metric perturbations are primarily based on [81], whilst the derivation of the evolution equations draws heavily on [82] and [83].

2.1 Perturbing the Metric

The high degree of non-linearity inherent in GR makes the full theory difficult to use in anything other than very simplified situations [84]. Consequently the evolution of density fluctuations is studied using perturbation methods, i.e. identifying a homogeneous isotropic background and studying small perturbations about that background. GR can then be studied at linear order in the perturbations, making the system amenable to analysis and the study of linear perturbations in cosmology is now well developed, see e.g. [85, 86, 87, 88, 89, 90].

The Copernican principle asserts the homogeneity and isotropy of the Universe. Assuming that both of these two conditions hold requires that the geometry of space must have constant curvature [83], (we shall assume a flat

geometry throughout this thesis). The resulting FLRW metric depends only on time and may be written as,

$$g_{\mu\nu}^{\mathrm{FLRW}} = a^2(\tau) \begin{pmatrix} -1 & 0 \\ 0 & \delta_{ij} \end{pmatrix}, \tag{2.1}$$

where the scale factor of the universe $a(\tau)$ is a function of the conformal time defined by $\mathrm{d}t = a(\tau)\mathrm{d}\tau$ and δ_{ij} is the flat spatial 3-metric. In the application of linear perturbation theory to GR, the metric tensor $g_{\mu\nu}$ is split into the FLRW metric $g_{\mu\nu}^{\mathrm{FLRW}}$ and a perturbation metric $\delta g_{\mu\nu}$ which represents small deviations around the FLRW background and as such depends on both space and time,

$$g_{\mu\nu} = g_{\mu\nu}^{\mathrm{FLRW}} + \delta g_{\mu\nu}. \tag{2.2}$$

This allows for a systematic mathematical decomposition of the perturbations into scalar, vector and tensor parts and small variations in the density of matter and energy in the Universe can be related to the small perturbations in the geometry of spacetime that they cause. Importantly, the different modes, (i.e. scalar vector and tensor parts), are decoupled at first order, allowing their evolutions to be studied separately in linear theory [85]. This is especially useful for the study of structure formation, because although all three modes have effects on the CMB only the scalar mode produces density perturbations, which are ultimately what lead to the galaxies and clusters etc. that we observe today [91].

Perhaps the most elementary approach to describing the different perturbation modes is to build the perturbation metric from the ground up, beginning with its simplest components first. The 'scalar' mode can in general be fully described using four scalars, (which we shall denote Ψ, B, Φ and E), along with their derivatives. The one dimensional temporal component of the metric simply requires the addition of a single scalar,

$$\delta g_{00} = -a^2 2\Psi, \tag{2.3}$$

where the sign and factor of 2 is a convention chosen to simplify later expressions, e.g. the GR 'Poisson' equation, (see Section 2.7). The other zero

index components can be represented by a vector obtained from taking the gradient of a scalar, denoted here as B, (if the geometry were not flat it would be necessary to take the covariant derivative in order that the vector transformed correctly), so for the scalar mode we have,

$$\delta g_{0i} = \delta g_{i0} = a^2 \partial_i B, \tag{2.4}$$

The 3-vector $\partial_i B$ is necessarily curl-free by virtue of having been obtained from a scalar, i.e.,

$$\partial_{[ij]} B = \frac{1}{2!}(\partial_i \partial_j B - \partial_j \partial_i B) = 0. \tag{2.5}$$

Furthermore, by Helmholtz's theorem it forms the longitudinal part of some more general vector, along with a transverse, i.e. divergence-free part, (the terms longitudinal and transverse come from the two parts being parallel or perpendicular to the wavevector in Fourier space). Thus a general vector has effectively been decomposed into these two parts and only that which is obtainable from a scalar, (the longitudinal part), contributes to the scalar mode.

Similarly, a tensor can be split into three parts with either two longitudinal indices, two transverse indices or one of each. Thus the remaining spatial components of the scalar mode are described by the doubly longitudinal part of a general 3-tensor, it being that which is obtainable from scalars,

$$\delta g_{ij} = -2a^2(\Phi \delta_{ij} - \partial_i \partial_j E). \tag{2.6}$$

The vector mode is described here using the vectors J_i and F_i. In order that it remains decoupled from the scalar mode it is necessarily traceless, (i.e. divergence free), meaning that it is absent from the purely temporal component of the perturbation metric in linear theory. It appears in the other 0-index components as the remaining part of the general 3-vector which can not be obtained from a scalar, i.e. the transverse counterpart of the longitudinal 3-vector found in the scalar mode. Including the vector part then we now have,

$$\delta g_{0i} = \delta g_{i0} = a^2(\partial_i B - J_i), \tag{2.7}$$

where $\partial_j J_i \delta^{ij} = 0$. The vector mode also contributes to the spatial 3-metric as that part of a general 3-tensor which can be obtained from the derivatives of a transverse vector and corresponds to the singly longitudinal/transverse part of the tensor, such that we now have,

$$\delta g_{ij} = a^2(-2\Phi\delta_{ij} + 2\partial_i\partial_j E + \partial_j F_i + \partial_i F_j). \tag{2.8}$$

Finally, the tensor mode h_{ij} appears only in the spatial 3-metric and is the remaining part of the general 3-tensor which can not be obtained from either a scalar or a vector. As such it is the doubly transverse part and is again necessarily traceless, giving,

$$\delta g_{ij} = a^2(-2\Phi\delta_{ij} + 2\partial_i\partial_j E + \partial_j F_i + \partial_i F_j + h_{ij}). \tag{2.9}$$

Hence the most general perturbation metric in linear theory may be written,

$$\delta g_{\mu\nu} = a^2 \begin{pmatrix} -2\Psi & \partial_i B - J_i \\ \partial_j B - J_j & -2\Phi\delta_{ij} + 2\partial_i\partial_j E + \partial_j F_i + \partial_i F_j + h_{ij} \end{pmatrix}. \tag{2.10}$$

The perturbation metric constructed above incorporates a combination of four 3-scalars, two 3-vectors, and a symmetric 3-tensor. The constraints on these objects are that the 3-vectors F_i and J_i are divergence-free, (reducing each to have two degrees of freedom), and that the 3-tensor h_{ij} is transverse and traceless, (leaving it with only two degrees of freedom). This gives the description the ten degrees of freedom required for the ten independent components of the, (symmetric), perturbation metric tensor.

Only six of these are physical however, and the other four can be eliminated by choosing a particular 'gauge' to work in. The choice of gauge is essentially a choice of coordinates to be used for the perturbations relative to the background, (for which the coordinates remain the same in all gauges). Gauge choices are made by imposing certain gauge conditions such as setting parts of $\delta g_{\mu\nu}$ to be zero. The six physical degrees of freedom come from the two tensor degrees of freedom, (since they are gauge invariant), two vector degrees of freedom, (in the weak field limit these describe gravitomagnetism,

i.e. frame dragging and geodetic precession), and two scalar degrees of freedom, (describing Newtonian gravity and its GR corrections) [91].

Including the FLRW background gives the full perturbed metric tensor,

$$g_{\mu\nu} = a^2 \begin{pmatrix} -(1+2\Psi) & \partial_i B - J_i \\ \partial_j B - J_j & (1-2\Phi)\delta_{ij} + 2\partial_i\partial_j E + \partial_j F_i + \partial_i F_j + h_{ij} \end{pmatrix}, \tag{2.11}$$

and using $g_{\mu\nu}g^{\nu\lambda} = \delta^{\lambda}_{\mu}$ to first order its contravariant form may be found,

$$g^{\mu\nu} = a^{-2} \begin{pmatrix} -(1-2\Psi) & \partial^i B - J^i \\ \partial^j B - J^j & (1+2\Phi)\delta^{ij} - 2\partial^i\partial^j E - \partial^j F^i - \partial^i F^j - h^{ij} \end{pmatrix}. \tag{2.12}$$

The line element for a perturbed spacetime in linear theory can then be written,

$$\begin{aligned} \mathrm{d}s^2 = a^2\{ &-(1+2\Psi)\mathrm{d}\tau^2 + 2(\partial_i B - J_i)\mathrm{d}\tau\mathrm{d}x^i \\ &+ [(1-2\Phi)\delta_{ij} + 2\partial_i\partial_j E + \partial_j F_i + \partial_i F_j + h_{ij}]\mathrm{d}x^i\mathrm{d}x^j\}. \end{aligned} \tag{2.13}$$

2.2 Gauge Transformation

Having now introduced linear perturbations onto the FLRW background, the choice of coordinate system used for them has become important. Different sectionings of spacetime can be made through the choice of constant time hypersurfaces within it. This can greatly simplify analytical problems and speed up numerical calculations. A general small first order change of coordinates may be written as,

$$\tilde{\tau} = \tau + \xi^0(\tau, x^i), \qquad \tilde{x}^i = x^i + \partial^i\xi(\tau, x^i) + \hat{\xi}^i(\tau, x^i) \tag{2.14}$$

where ξ^0 is an arbitrary scalar field and defines constant-τ hypersurfaces, (slicing), while ξ and $\hat{\xi}$ are a scalar and a divergence free vector respectively which determine the spatial hypersurfaces, (threading). The total differen-

tials of these three functions at first order,

$$\mathrm{d}\xi^0 = \dot{\xi}^0 \mathrm{d}\tilde{\tau} + \partial_i \xi^0 \mathrm{d}\tilde{x}^i, \tag{2.15a}$$

$$\mathrm{d}\xi = \dot{\xi} \mathrm{d}\tilde{\tau} + \partial_j \xi \mathrm{d}\tilde{x}^j, \tag{2.15b}$$

$$\mathrm{d}\hat{\xi}^i = \dot{\hat{\xi}}^i \mathrm{d}\tilde{\tau} + \hat{\partial}_j \xi^i \mathrm{d}\tilde{x}^j, \tag{2.15c}$$

where dots denote derivatives with respect to conformal time τ, can be used with the transformation equation, (2.14) to obtain expressions for the coordinate differentials,

$$\mathrm{d}\tau = \mathrm{d}\tilde{\tau} - \dot{\xi}^0 \mathrm{d}\tilde{\tau} - \partial_i \xi^0 \mathrm{d}\tilde{x}^i, \tag{2.16a}$$

$$\mathrm{d}x^i = \mathrm{d}\tilde{x}^i - (\dot{\partial}^i \xi + \dot{\hat{\xi}}^i)\mathrm{d}\tilde{\tau} - (\partial^i \partial_j \xi + \hat{\partial}_j \xi^i)\mathrm{d}\tilde{x}^j, \tag{2.16b}$$

since $\xi^0(\tau, x^i) = \xi^0(\tilde{\tau}, \tilde{x}^i)$ and $\xi(\tau, x^i) = \xi(\tilde{\tau}, \tilde{x}^i)$ to first order. Using Eq. (2.14) and taking derivatives, the transformation of the scale factor can be found,

$$a(\tau) = a(\tilde{\tau}) - \xi^0 \dot{a}(\tilde{\tau}), \tag{2.17}$$

which can then be used with Eq. (2.16b) to obtain the line element of the spacetime incorporating the general gauge transformation to first order,

$$\begin{aligned} \mathrm{d}s^2 = a^2(\tilde{\tau}) \Big\{ & -\big[1 + 2(\Psi - \mathcal{H}\xi^0 - \dot{\xi}^0)\big]\mathrm{d}\tilde{\tau}^2 + 2\partial_i(B + \xi^0 - \dot{\xi})\mathrm{d}\tilde{\tau}\mathrm{d}\tilde{x}^i \\ & - 2(J_i + \dot{\hat{\xi}}_i)\mathrm{d}\tilde{\tau}\mathrm{d}\tilde{x}^i + \big[(1 - 2\Phi + 2\mathcal{H}\xi^0)\delta_{ij} + 2\partial_i\partial_j(E - \xi) \\ & + 2\partial_j(F_i - \hat{\xi}_i) + h_{ij}\big]\mathrm{d}\tilde{x}^i\mathrm{d}\tilde{x}^j \Big\}, \end{aligned} \tag{2.18}$$

where $\mathcal{H} \equiv \dot{a}/a$. Since the line element is an invariant in general relativity, this can be compared to the original version, Eq. (2.13) in order to identify expressions for the perturbations which include a general coordinate trans-

formation,

$$\tilde{\Psi} = \Psi - \mathcal{H}\xi^0 - \dot{\xi^0}, \tag{2.19a}$$

$$\tilde{\Phi} = \Phi + \mathcal{H}\xi^0, \tag{2.19b}$$

$$\tilde{B} = B + \xi^0 - \dot{\xi}, \tag{2.19c}$$

$$\tilde{E} = E - \xi, \tag{2.19d}$$

$$\tilde{F}_i = F_i - \hat{\xi}_i, \tag{2.19e}$$

$$\tilde{S}_i = S_i + \dot{\hat{\xi}}_i, \tag{2.19f}$$

while the tensor perturbation h_{ij} is gauge independent.

Physical scalar quantities such as the energy density, pressure, shear etc., (see Section 2.4), are 'spatially gauge invariant' in that they are defined with respect to the background, (which depends only on time), so they depend only on the choice of temporal gauge, or ξ^0 [81]. For example, the density perturbation $\delta\rho$ transforms at first order as,

$$\tilde{\delta\rho} = \delta\rho - \xi^0\dot{\rho}. \tag{2.20}$$

Quantities such as the velocity potential v however, relating to vectors derived from them via a spatial gradient $\partial_i v$, (see Section 2.4), are independent of time but depend on the choice of spatial hypersurfaces. This is because a different gauge choice is essentially a different choice of coordinates for the perturbations and if $\mathrm{d}x$ is altered, then so must $\mathrm{d}/\mathrm{d}x$ be. Spatial gradients are therefore not fixed with respect to the background in the same way as physical scalars and the velocity potential transforms as,

$$\tilde{v} = v + \dot{\xi}. \tag{2.21}$$

2.3 Gauge-Invariant Variables

In general the perturbations are altered by a gauge transformation. This can lead to the appearance of 'gauge relics', i.e. quantities that are simply artefacts of the transformation and may only be features of the particular

choice of gauge. These may be misinterpreted as having some real physical significance and in [88] it was stressed that 'only gauge-invariant quantities have any physical meaning'. The use of gauge-independent quantities enables the use of gauge-invariant equations, which do not contain the gauge transformation variables ξ^0, ξ and $\hat{\xi}$ and so are the same in all gauges. Gauge-independent variables can then be defined in different gauges and consistently mixed in the same equations.

There are many different combinations of the scalar perturbations which eliminate the gauge transformation variables and so there are essentially an infinite number of possible gauge-invariant variables resulting from them, since any linear combination can be taken to create a new one. Once defined however, only two independent gauge-invariant scalar quantities can be constructed using only the scalar metric perturbations. This is because there are four scalar perturbations Ψ, Φ, B and E, two of which can effectively be eliminated using the scalar gauge functions ξ^0 and ξ. For vector perturbations there are two vector functions in the metric, J and F, while only one is used in the gauge transformation $\hat{\xi}_i$. This means that there is one independent gauge-invariant vector quantity, which at first order is uniquely defined as,

$$\tilde{J}_i = \tilde{F}_i = J_i + \dot{F}_i. \tag{2.22}$$

Tensor perturbations are naturally gauge invariant with there being no tensor component to gauge transformations. Gauge-invariant variables can also be formed from quantities relating to matter allowing for example the construction of a gauge-invariant density function.

There are therefore two different approaches to eliminating the ambiguities of having gauge freedom. Either a specific gauge choice can be made and used consistently throughout or a system of gauge-independent variables and equations can be set up and worked with exclusively. The fixed gauge approach can allow for clear physical insight and easy application to particular problems, while the gauge-invariant approach may enable convenient choices of variables to be made, although it may not be so obvious what the physical

interpretation of some quantities may be.

2.4 Observables

Observable quantities must be defined with respect to the velocity of observers. For an exact FLRW universe this would simply be the Hubble flow, but at the level of the perturbations one must eventually make a choice of which velocity to consider fundamental as well as choosing which gauge to work in. For the moment we shall leave the equations general in these respects, although from here on, (and for the rest of the thesis), we shall consider only scalar perturbations. This is because only scalar modes source the density perturbations which lead to structures in the Universe, with which we are primarily concerned here, while vector and tensor modes are more important in for example CMB studies.

Observables are related to the metric perturbations via the perturbed total 4-velocity u^μ, normalised by,

$$u^\mu u_\mu \equiv 1. \tag{2.23}$$

There now remain three independent degrees of freedom in u^μ. These can be represented by the spatial derivative of the velocity potential v, (the choice of which remains to be specified), defined as,

$$\partial^i v \equiv \frac{u^i}{u^0}. \tag{2.24}$$

Using Eq. (2.23), Eq. (2.24) and the components of the metric Eq. (2.11), the components of u^μ can be found,

$$u^0 = a^{-1}(1-\Psi), \tag{2.25a}$$
$$u^i = a^{-1}\partial^i v, \tag{2.25b}$$
$$u_0 = -a(1+\Psi), \tag{2.25c}$$
$$u_i = a(\partial_i B + \partial_i v). \tag{2.25d}$$

Insight into the physical effects which combine to produce the total 4-velocity u^μ can be gained by decomposing its covariant derivative into irreducible parts [89],

$$\nabla_\nu u_\mu = \frac{1}{3}\Theta s_{\mu\nu} + r_{\mu\nu} + \sigma_{\mu\nu} - a_\mu u_\nu, \tag{2.26}$$

where,

$$\Theta \equiv \nabla_\mu u^\mu, \tag{2.27a}$$

$$s_{\mu\nu} \equiv g_{\mu\nu} + u_\mu u_\nu, \tag{2.27b}$$

$$r_{\mu\nu} \equiv s_\mu^{\ \alpha} s_\nu^{\ \beta}(\nabla_\beta u_\alpha - \nabla_\alpha u_\beta), \tag{2.27c}$$

$$\sigma_{\mu\nu} \equiv \frac{1}{2}s_\mu^{\ \alpha} s_\nu^{\ \beta}(\nabla_\beta u_\alpha + \nabla_\alpha u_\beta) - \frac{1}{3}\Theta s_{\mu\nu}, \tag{2.27d}$$

$$a_\mu \equiv u^\nu \nabla_\nu u_\mu, \tag{2.27e}$$

with $s_{\mu\nu}$ being a projection tensor which projects objects into the direction orthogonal to u^μ, while Θ, $r_{\mu\nu}$, $\sigma_{\mu\nu}$ and a_μ are the expansion scalar, rotation tensor, shear tensor and acceleration 4-vector respectively. The trace part of the decomposition is the expansion scalar, which in an unperturbed universe would be the only non-zero part and related to the Hubble factor by $\Theta = 3H$ with $H \equiv (1/a)(\mathrm{d}a/\mathrm{d}t)$. The rotation $r_{\mu\nu}$ is the antisymmetric part, (always zero for the scalar mode), while the shear $\sigma_{\mu\nu}$ is the symmetric trace-free part. Finally, the acceleration a_μ expresses the difference between the direction of u^μ and the direction of the vector field t^μ tangential to geodesics, for which $t^\nu \nabla_\nu t_\mu = 0$ by the geodesic equation. These observables can now be described in terms of geometrical quantities using Eq. (2.11) and Eq. (2.25), (see Section 2.6.2 for an example of this in a particular gauge).

2.5 Dynamics of the Metric

In Lagrangian mechanics the equations of motion governing a system are found by minimising the action,

$$S = \int L(\vartheta, \nabla_\mu \vartheta)\mathrm{d}^4 x, \tag{2.28}$$

where ϑ represents the dynamical variables of the system. The appropriate Euler-Lagrange equations by which this is achieved for a curved spacetime are,

$$\frac{\partial \hat{L}}{\partial \vartheta} - \nabla_\mu \left(\frac{\partial \hat{L}}{\partial(\nabla_\mu \vartheta)} \right) = 0, \tag{2.29}$$

where,

$$\hat{L} \equiv \frac{L}{\sqrt{-g}}. \tag{2.30}$$

These equations can be applied when the dynamical variable is for example a scalar field, but in GR the dynamical variable is the metric $g_{\mu\nu}$, the covariant derivatives of which vanish. It is therefore necessary to consider the behaviour of the action under small variations of the metric directly. The total action for a ΛCDM cosmology, (i.e. the Einstein-Hilbert action plus DM and a cosmological constant), can be written as,

$$S_{\Lambda\mathrm{CDM}} = \frac{1}{16\pi G} \int \mathrm{d}^4x \sqrt{-g}(R - 2\Lambda) + S_\mathrm{m}(g_{\mu\nu}, \varphi), \tag{2.31}$$

where S_m is the matter, (and energy), action, with φ representing the matter fields. Varying this action with respect to the metric we have,

$$\delta S_{\Lambda\mathrm{CDM}} = \delta S_1 + \delta S_2 + \delta S_3 + \delta S_\mathrm{m}, \tag{2.32}$$

where,

$$\delta S_1 = \frac{1}{16\pi G} \int \mathrm{d}^4x \sqrt{-g} g^{\mu\nu} \delta R_{\mu\nu}, \tag{2.33}$$

$$\delta S_2 = \frac{1}{16\pi G} \int \mathrm{d}^4x \sqrt{-g} R_{\mu\nu} \delta g^{\mu\nu}, \tag{2.34}$$

$$\delta S_3 = \frac{1}{16\pi G} \int \mathrm{d}^4x (R - 2\Lambda) \delta\sqrt{-g}. \tag{2.35}$$

The first of these, δS_1 is equivalent to a boundary term at infinity and can be set to zero, (see [82]), while for the third we must use,

$$\delta\sqrt{-g} = -\frac{1}{2}\sqrt{-g} g_{\mu\nu} \delta g^{\mu\nu}, \tag{2.36}$$

to find,

$$\delta S_3 = -\frac{1}{16\pi G} \int \mathrm{d}^4x \sqrt{-g} \frac{1}{2} g_{\mu\nu} (R - 2\Lambda) \delta g^{\mu\nu}. \tag{2.37}$$

We can now use the property of the action that,

$$\delta S = \int \mathrm{d}^4 x \frac{\delta S}{\delta g^{\mu\nu}} \delta g^{\mu\nu}, \tag{2.38}$$

and recombine the terms to write,

$$\frac{1}{\sqrt{-g}} \frac{\delta S_{\Lambda CDM}}{\delta g^{\mu\nu}} = \frac{1}{16\pi G}(R_{\mu\nu} - \frac{1}{2} g_{\mu\nu} R + g_{\mu\nu}\Lambda) + \frac{1}{\sqrt{-g}} \frac{\delta S_{\mathrm{m}}}{\delta g^{\mu\nu}}, \tag{2.39}$$

where we are interested in the stationary point $\delta S_{\Lambda\mathrm{CDM}}/\delta g^{\mu\nu} = 0$. Thus, by defining the stress-energy tensor as,

$$T_{\mu\nu} \equiv -\frac{2}{\sqrt{-g}} \frac{\delta S_m}{\delta g^{\mu\nu}}, \tag{2.40}$$

the particular form of S_m need not be specified and we arrive at the equations of motion for the metric, Einstein's field equations,

$$R_{\mu\nu} - \frac{1}{2} g_{\mu\nu} R + \Lambda = 8\pi G T_{\mu\nu}. \tag{2.41}$$

2.6 Specific Gauge Choices

There are many different choices of gauge which can be made for different purposes. Here we shall focus only on the two most commonly used gauges, the synchronous and Newtonian gauges, used often for numerical calculation and analytical interpretation respectively, (for a direct comparison of the two see [90]).

2.6.1 Synchronous

This is the gauge used in the seminal work of Lifshitz on cosmological perturbations [85] and is in fact a family of gauges for which $\Psi_{\mathrm{S}} = B_{\mathrm{S}} = 0$, where the subscript S stands for synchronous. Specifying $\Psi_{\mathrm{S}} = 0$ implies that the threading consists of geodesics, while $B_{\mathrm{S}} = 0$ means that the slicing is orthogonal to the threading, but there remains a residual gauge freedom since the threading is not unique. The synchronous gauge was used widely before the introduction of Bardeen's gauge-invariant formalism [88] and the gauge is

completely fixed by specifying the inital conditions of the system [92]. Subtleties involved in doing this historically led to confusion, but in this thesis we shall simply use the convention adopted in the Code for Anisotropies in the Microwave Background, (CAMB) [93], a numerical computation code used for evolving cosmological perturbations forward from the end of inflation which uses the synchronous gauge for computational efficiency. This means choosing a frame where the DM is initially at rest and indeed remains so for models without DM interactions.

2.6.2 Newtonian

This is the mathematically simplest gauge choice and has orthogonal slicing and threading. As well as the 'Conformal Newtonian' it is also known as the longitudinal gauge because it has both the longitudinal part of the vector mode and the doubly longitudinal part of the tensor mode set to zero. This means that the spatial part of the metric is isotropic and corresponds to a choice of spatial hypersurfaces such that the shear in the scalar mode is zero, making the Newtonian gauge is defined by,

$$\tilde{B}_{\rm N} = \tilde{E}_{\rm N} = \tilde{\sigma}_{\rm N} = 0, \tag{2.42}$$

where the subscript N stands for Newtonian. Comparing these conditions with Eq's. (2.19) shows the form of ξ and ξ^0 required to fix the gauge, thereby allowing expressions for the two remaining scalar perturbations to be found,

$$\Psi_{\rm N} = \Psi + \frac{1}{a}\frac{\mathrm{d}}{\mathrm{d}\tau}\left[a\left(B - \dot{E}\right)\right], \tag{2.43}$$

$$\Phi_{\rm N} = \Phi - \mathcal{H}\left(B - \dot{E}\right). \tag{2.44}$$

These are the independent gauge-invariant quantities chosen for use by Bardeen in [88]. The gauge also offers an intuitive understanding of the perturbations, as $\Psi_{\rm N}$ corresponds to a perturbation of the gravitational potential, while $\Phi_{\rm N}$ represents a curvature perturbation.

For the remainder of this chapter we shall drop the subscript N and work only in the Newtonian gauge. The line element in the Newtonian gauge can

be written as,

$$ds^2 = a^2\left[-(1+2\Psi)d\tau^2 + (1+2\Phi)\delta_{ij}dx^i dx^j\right]. \tag{2.45}$$

The metric tensor components are then,

$$g_{00} = -a^2(1+2\Psi), \tag{2.46}$$
$$g_{ij} = a^2(1+2\Phi)\delta_{ij}, \tag{2.47}$$
$$g^{00} = -a^{-2}(1-2\Psi), \tag{2.48}$$
$$g^{ij} = a^{-2}(1-2\Phi)\delta^{ij}, \tag{2.49}$$

which lead to the perturbed Christoffel symbols,

$$\Gamma^0_{00} = \mathcal{H} + \dot{\Psi}, \tag{2.50}$$
$$\Gamma^0_{0i} = \partial_i\Psi, \tag{2.51}$$
$$\Gamma^0_{ij} = [\mathcal{H} + 2\mathcal{H}(\Phi-\Psi) + \dot{\Phi}]\delta_{ij}, \tag{2.52}$$
$$\Gamma^i_{00} = \partial_j\Psi\delta^{ij}, \tag{2.53}$$
$$\Gamma^i_{j0} = \left(\mathcal{H} + \dot{\Phi}\right)\delta^i_j, \tag{2.54}$$
$$\Gamma^i_{jk} = \partial_j\Phi\delta^i_k + \partial_k\Phi\delta^i_j - \partial_l\Phi\delta^{li}\delta_{kj}, \tag{2.55}$$

The Ricci tensor components and Ricci scalar derived from the above are,

$$R_{00} = -3\frac{\ddot{a}}{a} + 3\mathcal{H}^2 - 3\ddot{\Phi} + \partial_i\partial^i\Psi - 3\mathcal{H}\dot{\Phi} + 3\mathcal{H}\dot{\Psi}, \tag{2.56}$$
$$R_{0i} = 2(\mathcal{H}\partial_i\Psi - \dot{\partial}_i\Phi), \tag{2.57}$$
$$\begin{aligned} R_{ij} = {} & [\frac{\ddot{a}}{a} + \mathcal{H}^2 + 2(\frac{\ddot{a}}{a} + \mathcal{H}^2)(\Phi-\Psi) + \ddot{\Phi} + 5\mathcal{H}\dot{\Phi} - \mathcal{H}\dot{\Psi}]\delta_{ij} \\ & - \partial_i\partial_j\Psi - \partial_i\partial_j\Phi - \partial^k\partial_k\Phi\delta_{ij}, \end{aligned} \tag{2.58}$$
$$\Rightarrow R = a^{-2}[6\frac{\ddot{a}}{a} + 6\ddot{\Phi} - 2\partial_i\partial^i\Psi - 4\partial_i\partial^i\Phi - 12\frac{\ddot{a}}{a}\Psi + 18\mathcal{H}\dot{\Phi} - 6\mathcal{H}\dot{\Psi}]. \tag{2.59}$$

We are now in a position to find expressions in the Newtonian gauge for the

scalar parts of the observable quantities described in Section 2.4,

$$\Theta = a^{-1}[\partial_i \partial^i v + 3\mathcal{H}(1-\Psi) + 3\dot{\Phi}], \tag{2.60}$$

$$r_{\mu\nu} = 0, \tag{2.61}$$

$$\sigma_{\mu\nu} = 0, \tag{2.62}$$

$$a_\mu = a_i = \partial_i \Psi + \partial_i \dot{v} + \mathcal{H}\partial_i v. \tag{2.63}$$

2.7 Dynamics of the fluid

The components of the stress-energy tensor $T_{\mu\nu}$ can be modelled as a perfect fluid,

$$T_{\mu\nu} = (\rho + p)u_\mu u_\nu + p g_{\mu\nu}, \tag{2.64}$$

where ρ is the energy density and p the pressure in the background. We can now define the perturbations in the fluid relative to this to be,

$$\bar{p} \equiv p + \delta p, \tag{2.65}$$

$$\bar{\rho} \equiv \rho + \delta\rho \equiv \rho(1+\delta), \tag{2.66}$$

leading to,

$$T^0_0 = -\rho(1+\delta), \tag{2.67a}$$

$$T^0_i = (\rho + p)\partial_i v, \tag{2.67b}$$

$$T^i_0 = -(\rho + p)\partial^i v, \tag{2.67c}$$

$$T^i_j = (p + \delta p)\delta^i_j + \pi^i_j, \tag{2.67d}$$

where the anisotropic stress π^i_j has been added by hand for generality and is trace-free, i.e. $\pi^i_i = 0$. The evolution equations for the fluid can be obtained using energy-momentum conservation, which follows from the Bianchi identity [83], (i.e. conservation of the left hand side of Eq. (2.41)),

$$\nabla_\mu T^{\mu\nu} = 0. \tag{2.68}$$

As an illustration of how to find equations for the growth of perturbations in the fluid, we shall now consider the simple case of a CDM universe not only

using the Newtonian gauge but also working in the Newtonian regime. In other words we shall consider only sub-horizon scales, (i.e. smaller than H_0^{-1}, but still large enough to be linear), so that overdensities have grown large relative to the metric perturbations, ($\delta \gg \Psi$). Furthermore we restrict ourselves to late times, where temporal derivatives of the metric perturbations are negligible relative to spatial ones and we can take $\dot{\Psi} = \dot{\Phi} = 0$.

The zeroth component of Eq. (2.68) can be split into the Euler equation for the background, which is always satisfied anyway,

$$\dot{\rho}_c + 3\mathcal{H}\rho_c = 0, \tag{2.69}$$

and an independent equation for its perturbation,

$$\dot{\rho}_c\delta_c + \rho_c\dot{\delta}_c + \rho_c\partial_i\partial^i v_c + 3\mathcal{H}\rho_c\delta_c = 0, \tag{2.70}$$

which may be rewritten using the velocity divergence $\theta_c = -k^2 v_c = \partial_i\partial^i v_c$, where k is the Fourier mode wavenumber, and the background equation (2.69) as,

$$\dot{\delta}_c = -\theta_c. \tag{2.71}$$

From the ith component of Eq. (2.68) we have,

$$\dot{\rho}_c\partial_i v_c + \rho_c(\partial_i\Psi + \partial_i\dot{v}_c + 4\mathcal{H}\partial_i v_c) = 0. \tag{2.72}$$

Taking a spatial derivative of this and again substituting for θ_c gives,

$$\dot{\theta}_c = -\mathcal{H}\theta_c - \partial_i\partial^i\Psi. \tag{2.73}$$

We can now use Eq. (2.71) and Eq. (2.73) to find a velocity independent second order equation for δ_c. Taking the time derivative of Eq. (2.71) and substituting for $\dot{\theta}_c$ using Eq. (2.73) gives,

$$\ddot{\delta}_c = -\mathcal{H}\dot{\delta}_c + \partial_i\partial^i\Psi. \tag{2.74}$$

This can be further simplified by replacing $\partial_i\partial^i\Psi$ using the GR 'Poisson' equation which can be found by first rewriting Eq. (2.41) as,

$$R_{\mu\nu} = 8\pi G\left(T_{\mu\nu} - \frac{1}{2}T g_{\mu\nu}\right), \tag{2.75}$$

then for the zeroth component of the right hand side of this we have from Eq's. (2.67),

$$T_{00} - \frac{1}{2}Tg_{00} = \frac{1}{2}a^2\rho_c(1 + \delta_c + 2\Psi), \tag{2.76}$$

while for the left hand side R_{00} is given by Eq. (2.56). We can now remove the background terms and take the limits described above, (i.e. $\delta \gg \Psi$ and $\dot{\Psi} = \dot{\Phi} = 0$), to end up with the 'Poisson' equation for Newtonian perturbations in GR,

$$\partial_i\partial^i\Psi = 4\pi G a^2\rho_c\delta_c. \tag{2.77}$$

Note that the Newtonian regime therefore demonstrably holds on scales smaller than the horizon at late times because by the Friedman equation, (the 00 component of Einstein's field equations, Eq. (2.41)), $4\pi G\rho_c a^2 = \mathcal{H}^2$, so we have,

$$k^2\Psi = \mathcal{H}^2\delta_c, \tag{2.78}$$

and remembering that at late times $\delta \gg \Psi$, implies that $k \gg \mathcal{H}$. Finally, plugging Eq. (2.77) into Eq. (2.74) we now have the CDM growth equation in its most convenient form,

$$\ddot{\delta}_c = -\mathcal{H}\dot{\delta}_c + 4\pi G a^2\rho_c\delta_c. \tag{2.79}$$

Chapter 3

IDE in the literature

This chapter serves as a summary review of IDE models and research. For the sake of brevity, unless otherwise of interest, only the latest observational constraints on the various couplings and parameterisations under consideration shall be reported. Section 3.1 defines what IDE models are and why they are studied, Section 3.2 frames IDE research in its historical context and Sections 3.3 to 3.5 summarise articles on the three most commonly studied forms of interaction types. Section 3.6 describes works on other forms of coupling, Section 3.7 looks at the wide range of IDE parameterisation studies, Section 3.8 lists a selection of other IDE related works and Section 3.9 contains a brief discussion of IDE topics.

3.1 An Overview of IDE

It is natural to expect some new physics in the dark sector given the richness of interactions between species in the standard model of particle physics [94]. Indeed taking dark sector interactions to be zero is an assumption of DE models. However modelling dark sector interactions is even more speculative that describing DE or DM themselves, with even less concrete guidance from particle physics, so studying interactions phenomenologically seems to be the most sensible approach. The caveat to this is that such studies should be

carried out in an intelligent way, so that the model does not exhibit behaviour caused by unphysical features of its design. Only then can light be shed on which types of model really might lead to unphysical behaviour and which are in best agreement with observations.

Motivation for IDE models has come from the fact that they can potentially address the cosmological constant and coincidence problems, (e.g. [95, 96]), as well as the fact that they affect structure formation in novel ways and provide a way to alleviate tensions between the standard non-interacting model and observations, (e.g. [97]). The extra degree of freedom obtained by admitting an interaction into the dark sector can however be both a blessing and a curse as it often causes instabilities in the perturbations which rule out some models completely.

The requirement resulting from the Bianchi identity that that the total energy-momentum tensor be conserved leads to an interaction term in the continuity equations of the DE, (subscript x), and CDM, (subscript c), fluids. Models of IDE are therefore characterised at the background level by the energy transfer rate Q,

$$\dot{\rho}_c = -3\mathcal{H}\rho_c - Q, \tag{3.1}$$

$$\dot{\rho}_x = -3\mathcal{H}(1+w)\rho_x + Q, \tag{3.2}$$

where dots denote derivatives with respect to conformal time τ, $\mathcal{H} = \mathrm{d}a/\mathrm{d}\tau$ and $w = p_x/\rho_x$ is the DE equation of state parameter. There are predominantly three forms of Q which have been studied in the literature;

$$Q \propto \dot{\psi}\rho_A, \tag{3.3}$$

$$Q \propto \mathcal{H}\rho_A, \tag{3.4}$$

$$Q = a\Gamma\rho_A, \tag{3.5}$$

where $A = x, c$ or total and Γ is a constant. From here on these shall generally be referred to as the $\dot{\psi}$, $\mathcal{H}$ and Γ couplings. The first of these defines a scalar field model of IDE, but note that in the literature this is generally denoted by ϕ, whereas here we use ψ because in later chapters ϕ is used to denote the

gravitational scalar field of MG theories. The other two have been studied in both scalar field and fluid models and in addition to the forms above all three have been studied using linear and quadratic combinations of the energy densities.

We can define an effective DE equation of state parameter to be that of a non-interacting DE with the same $\rho_x(a)$, i.e.,

$$w_{\text{eff}} = w - \frac{aQ}{3\mathcal{H}\rho_x}. \tag{3.6}$$

We can see from Eq (3.6) that w_{eff} can be dynamical even if w is a constant. Interestingly w_{eff} can be less than -1, or cross -1 during its evolution if $Q > 0$, even though w itself is always greater than -1.

Perturbations in multiple interacting fluids were first described in [89] and later developed in works such as [98], which detailed their evolution in different gauges and [99], which separated them into adiabatic and entropy parts as an aid to studying models of inflation. Interacting models can develop instabilities however and in particular there are two types of instability which present themselves in IDE. The first is a small scale, adiabatic instability restricted to the strong coupling regime [100, 101, 102, 103, 104], (originally noted in the context of coupled neutrinos [105, 106]), caused by a negative sound speed squared of the effective DM/DE fluid resulting in exponential growth. The second is large-scale, non-adiabatic and caused by a runaway DE velocity perturbation [107, 108, 109, 110, 111, 112]. The presence of this instability depends on the combined sign of the coupling strength and $1 + w$ and can be avoided in models with variable w.

3.2 Historical Context

Cosmological models with a coupling between matter and a scalar field arise naturally as alternative descriptions of MG theories such as Brans-Dicke theory [113, 114] and particle physics theories such as Kaluza-Klein theory [115, 116], (which was discussed by Jordan in relation to his precursor

to Brans-Dicke theory [117]). Both of these had already been studied for many years, and even proposed as solutions to the cosmological constant problem, long before the observation of an apparent late-time acceleration, e.g. [95, 118, 119]. Models such as these therefore soon became the focus of much research after 1998, especially due to the additional motivation for them as simply natural generalisations of the quintessence scalar field models which quickly grew in popularity [73].

Another source of inspiration for work on IDE was the inflation paradigm, first discussed in [120] but generally credited to [121] who demonstrated that it solves the flatness, horizon and monopole problems, although [122] points out that these were not pressing issues until a solution had been found for them, (much like the cosmological constant problem). By the late 90's this had led to a plethora of scalar field models being studied by cosmologists [123], including many interacting models, e.g. [124, 125], (see also [126] and refs. therein), again motivated by both MG and particle physics. The analytical techniques developed to study these models were all readily applicable to late-time acceleration and the theoretical cosmology community, by then experts in dealing with scalar fields, very quickly began to explore the possibilities that IDE had to offer.

Scalar field IDE models with a $Q \propto \dot{\psi}\rho_c$ coupling inspired by MG were soon under study [127, 128], as was a coupling of the form $Q \propto \mathcal{H}\rho_c$ [126, 96] along with other particle physics inspired couplings, e.g. [129]. Later however, the $Q \propto \mathcal{H}\rho_c$ coupling was criticised for being unnatural as a model of particle interactions due to the influence of the global parameter $\mathcal{H}$ on purely local physics [130]. An alternative coupling was therefore proposed where the interactions still varied with ρ_c but did not depend on $\mathcal{H}$ and were instead characterised only by a constant interaction rate parameter Γ, as had been previously applied in other particle interaction contexts.

With three different forms of coupling and two physical models, there was an enormous scope for the investigation of IDE. One could modify the dependence of the interactions on the fluid energy densities to include DE, or

consider quadratic terms, not to mention the fact that each particular choice of model and interaction could have different types of energy-momentum transfer at the level of the perturbations. As with the study of DE, the lack of knowledge about the form of IDE also made parameterisation studies a good way to gain insight into its evolution and relation to observations. The subject therefore blossomed and has received a great deal of attention over the years, although a comprehensive review of the topic remains to be undertaken.

3.3 Interactions Proportional to $\dot{\psi}$

In the MG representation a scalar field component of gravity is directly coupled to the metric and the gravitational equations can be very complex. A conformal transformation can be made however, to a new 'frame' where GR describes gravity but matter becomes coupled to the scalar field, (which is itself now rescaled and only minimally coupled to gravity). Couplings to gravity are also common in particle physics theories and the same transformation can equally well be made. The frame where the scalar field is coupled to gravity is known as the Jordan frame, (although interestingly both gravity and matter were coupled to the scalar field in Jordan's original theory [131]), while the frame where a scalar couples to matter is called the Einstein frame.

The obstacle to using this sort of model is that the conformal transformation from the Jordan frame to the Einstein frame usually means that the scalar field would be coupled to all matter [114], although since relativistic matter has $p = \rho/3$, its energy-momentum tensor is traceless and so it remains naturally decoupled, (c.f. Eq's (2.67) and (5.20)). A coupling to matter would rule out significant coupling strengths due to constraints from baryons [132, 133, 134, 135], but there are theories where species-dependent coupling may be natural [136, 137] and screening mechanisms can be invoked to deal with local gravity constraints [138, 139, 140].

In the rest of this Section the works discussed all employ some form of

scalar field model with a $\dot{\psi}$ term in the coupling between DE and DM. Many of these are motivated by theories in the Jordan frame, where a general STT action can be written as,

$$\begin{aligned} S_{STT} &= \frac{1}{16\pi G}\int d^4x\sqrt{-g}\left[f(\phi)R-\omega(\phi)(\nabla\phi)^2-U(\phi)\right] \\ &\quad +S_m(g_{\mu\nu},\varphi), \end{aligned} \tag{3.7}$$

where ϕ is the gravitational scalar field, $U(\phi)$ is its self interaction potential which may or may not be present and $f(\phi)$ and $\omega(\phi)$ are general functions determined by the particular theory in question, (see [141] for a detailed description of the most general second order STT action). Such models can then be translated to the Einstein frame by a conformal transformation, (see Chapter 5), where they become equivalent to coupled quintessence, which can broadly be described by the Einstein Hilbert action with a scalar field and coupled DM,

$$S_{IDE}=\frac{1}{16\pi G}\int d^4x\sqrt{-g}\left[R-\frac{1}{2}(\nabla\psi)^2-V(\psi)\right]+S_c(g_{\mu\nu},\psi,\varphi), \tag{3.8}$$

where $V(\psi)$ is the scalar field's potential, $S_c(g_{\mu\nu},\psi,\varphi)$ is the coupled CDM action and φ is the DM field. Varying this action then leads to equations of motion for the DE and DM backgrounds,

$$\ddot{\psi} = -2\mathcal{H}\dot{\psi}-a^2\frac{\partial V(\psi)}{\partial\psi}+\frac{1}{2}C(\psi)a^2\rho_c, \tag{3.9}$$

$$\dot{\rho}_c = -3\mathcal{H}\rho_c-\frac{1}{2}C(\psi)\rho_c\dot{\psi}, \tag{3.10}$$

where $C(\psi)$ determines the coupling strength and is variously taken as a constant or a variable function.

3.3.1 Early works

Early studies of $\dot{\psi}$ IDE, (post 1998), had a constant coupling strength parameter and many of these were by Luca Amendola. Indeed Amendola is an author on all of the early works below unless otherwise stated. His first IDE

paper [127] looked at scaling solutions where $\omega(\phi) \equiv 1$ and the dynamics depended only on the relation between $f(\phi)$ and $U(\phi)$ rather than their actual forms. This assumed a power law relation between them of the form,

$$V(\phi) = Af(\phi)^M, \tag{3.11}$$

which always led to an exponential potential in the Einstein frame as long as the coupling was strong enough that the kinetic terms of ϕ in the Lagrangian could be neglected. The background dynamics were studied but constraints on the effective time variation of G ruled out accelerated solutions in this strong coupling regime. Observational limits which applied in the case of the more general weak coupling case were later found in [142] using Boomerang CMB data and then [143] combined the newly released WMAP CMB data with SNIa data to find improved constraints on the coupling strength parameter.

Another early work by different authors [128] performed a phase plane analysis of a model motivated by STT, (Brans-Dicke plus a self interaction potential for the scalar field), in which power law potentials produce scaling solutions in the Jordan frame, (which are also automatically self similar in the Einstein frame). Unlike minimally coupled models it was shown to lead to late-time scaling solutions for $w \approx -1$, thus no finetuning was required. The setup again had $\omega(\phi) \equiv 1$ but $f(\phi) = \phi^2/8c$ with $c > -3/2$ in order to maintain a positive energy density for ψ in the Eistein frame. The constant c also determined the strength of the IDE coupling and it was again found that strong coupling, (in this case where $c \to -3/2$), needed to be approached in order to both evade BBN bounds and have a significant DE contribution at late times.

Around the same time Amendola also presented works on a model with the simple specification of an exponential potential. In [144] its perturbation equations were derived and used with CMB and matter power spectrum data in order to find constraints on the coupling strength. The effects on observables of viable solutions were discussed in [145] and the coupling strength was constrained using observations of the CMB and σ_8, (an observable measure

of structure growth). [146] looked at constant couplings with energy transfer from DE to DM which instead of having DM domination followed by acceleration had a short baryon dominated era followed by DM/DE scaling regardless of initial conditions. Uniquely this also provided an explanation for the relative abundances of baryons and DM but matter perturbations were shown to undergo too much growth during the accelerated regime to be compatible with both BBN and CMB constraints. A scaling cosmology which could avoid this problem was described in [147]. It was found by constructing a coupling function which switched between a low strength coupling initially, where structure formation is required, and high strength later, where scaling is desirable.

Amendola quantified the effect of coupling on structure growth and baryon bias for the exponential potential model in [148], investigating in particular the unusual property of structure growth during an accelerated phase. This would only happen for the DM however, since the baryons are not coupled, showing that baryon bias was potentially a useful test of IDE. Later [149] used SNIa to show that this model could fit observations with a much earlier transition to accelerated expansion, while another author showed in [150] that scaling solutions existed for the constant coupling strength model and performed a qualitative statefinder diagnosis, (involving the second and third derivatives of the scale factor).

In [151] Amendola derived first and second order perturbations using a variable coupling strength and a general potential, the motivation for which may have been [152] where he subsequently derived the most general Lagrangian which leads to scaling solutions. He showed that the non-existence of a matter dominated era is a generic feature of such models, thus ruling out all, (constant coupling strength plus scaling solutions), scalar field Lagrangians previously studied in the literature.

3.3.2 Later works

Recently the $\dot{\psi}$ coupling with a variable coupling strength which depends on the field value ψ, (from here on just called variable coupling), has begun to be investigated more widely. For example, [153] studied the dynamics of IDE with an exponential potential and a variable coupling, again related via a power law as in the early works, which included the particular case of an interaction proportional to the product of the energy densities. They showed a late-time stable accelerated attractor to be a generic feature of the model and constrained its parameters using CMB, BAO and SNIa data. They found no significant preference over the standard cosmological model but interestingly they did show that Weak Equivalence Principle constraints, (on cluster and galactic scales), were stronger than cosmological ones.

Another variable coupling study looked at the effects of IDE with exponential potential and coupling functions on CMB and matter power spectra [154]. Linear perturbations were developed and observational constraints were found, with BAO data being added in a later paper [155]. A coupling with an exponential function component was also looked at in the context of curved geometry in [156]. They found the best fit coupling and potential parameters from SNIa data, which in a flat universe led to a complex behaviour where the effective DE equation of state, Eq. (3.6), crossed the phantom divide twice in the past and once more in future.

Despite now being less well motivated due to its problems with structure formation, the $\dot{\psi}$ coupling with constant coupling strength, (from here on just called constant coupling), is still studied to this day. Indeed one could always consider it as simply an approximation to a more complex coupling function which is naturally suppressed at early times. It was still considered worth testing the model in the search for extra physics in the dark sector by [157], which used artificial CMB data with CAMB and CosmoMC [158], a Markov-Chain Monte-Carlo, (MCMC), likelihood distribution analysis program which is easily integrable with CAMB, to quantify how much bias neglecting an IDE coupling can introduce into parameter estimates, while [159]

performed a MCMC analysis to constrain the model using CMB, ISW, SNIa and BAO data, as well as future forecasts. [160] also studied the background dynamics of the model, motivated by the conformal transformation of $f(R)$ modified gravity theories.

A constant coupling was used in [161] to test the ability of cluster counts and future surveys to constrain $\dot{\psi}$ IDE. The analysis included non-interacting DM species and cluster scale inhomogeneities in the DE, both of which were shown to have significant effects. It was found that oscillations in cluster number counts at different redshifts could provide a signature of IDE and that future surveys may be able to detect such effects. A constant coupling was later used as an example to demonstrate a generic expression in terms of a model's coupling function which gives $w_{\rm eff}$ in [104]. They then also showed that the adiabatic instability in the perturbations was stabilised in the slow-roll regime of models with inverse power law potentials.

Constant couplings were employed in [162] to study the non-linear matter power spectrum, probably to make effects likely to be generic in IDE more amenable to analysis. They found a significant scale dependence to the baryon-DM bias, including around BAO scales, which future surveys could use to strongly constrain IDE. More recently [163] conducted a phase plane analysis of a constant coupling model and found an exact scaling solution. Presumably however, a study of perturbations in this model would rule it out on the basis of not having a matter dominated era to enable structure formation as discussed in [152].

A constant coupling was used for simplicity in [164] where constraints were forecast using a Fisher Matrix analysis for Planck CMB data combined with Euclid tomographic weak lensing, redshift space distortions and matter power spectrum results. They showed that a two orders of magnitude improvement on the coupling strength parameter β should be achievable. This finding tallies with [165] which used CMB, (including South Pole Telescope), SNIa, and BAO data and found a slight peak in the likelihood at $\beta = 0.041$, although $\beta = 0$ was still within the 1σ range. They used CAMB and Cos-

moMC to perform a likelihood analysis and were able to reduce previous constraints slightly to $\beta \leq 0.063(0.11)$ at 63%(95%) confidence level, whilst forecasting that Planck CMB data should be able to rule definitively on their finding of the marginal peak in the likelihood.

3.3.3 Particle theory

Couplings are a ubiquitous feature of particle physics and so a great deal of motivation for work on IDE has come from particle theory. Particle physics considerations for example led [166] to study coupled quintessence cosmologies in the context of DE being independently coupled to all species, also finding BBN constraints on the model. Another work [167] looked at cosmologies in a model where the DM is a particle with variable mass, first proposed in [168], studying the case of DM as the lightest supersymmetric particle. [169] also examined varying mass DM as a solution to the coincidence problem but found that extreme finetuning of the scalar field potential's present day value was needed to obtain viable cosmological parameters and that a typical age of the universe was around 15 Gyr, thus severely restricting the model's parameter space.

The dilaton field is motivated by Kaluza-Klein theory [115, 116] and resembles a STT. It can couple in a species dependent way and a cosmological constant in the 'string frame' can be shown to become a quintessence-like exponential potential in the physical frame [170]. A Kaluza-Klein theory inspired scenario, where DE is not only coupled to DM but also to an additional vector field, first considered in the context of inflation was also used to find scaling solutions in [171, 172].

In [173] and [174] the authors studied models of interactions in the dark sector using only scalar fields and considered the possibility of multiple DM fields. [175] placed observational constraints from CMB, BAO, lookback time to clusters, and SNIa on a similar model but with a tachyonic DE. A two scalar field model was also investigated in [176] where they employed a coupling in the scalar field potentials and generalised the model with a three

parameter quadratic polynomial part in the DM potential. This setup was motivated by string theory and they demonstrated the existence of solutions with transient accelerated expansion, while [100] studied perturbations in cosmologies containing uncoupled DM, baryons, radiation and interacting DM/DE, specialising to study the models of [174] and [170].

[177] modelled IDE with a fermionic field plus a scalar field using the 'First Order formalism' [178], which relates a scalar fields potential and the Hubble factor under certain assumptions, to find exact solutions to the equations of motion. Novel possibilities for producing a viable cosmology were found, including a scenario where the DM is massless and the DE alters in character from decelerating the universe at early times to accelerating it a late times.

Three-form fields can be motivated by string theory and [179] extended a model of three-form dark energy such that its scalar field component was covariantly coupled to DM. A dynamical analysis of the background was performed and the potential for observations to constrain its perturbations in the Newtonian regime was considered. Axions find motivation as solutions to finetuning issues in particle physics and [180] investigated coupled axion DE. An analysis of the model's dynamics to the level of perturbations was conducted and observational constraints with BAO, SN, growth rate and H_0 data were found, showing that the coupling allows greater deviation from $w = -1$ than in the uncoupled model.

String theory can motivate the existence of multiple DM species, but such theories also have the added justification for their study that we remain ignorant about dark sector particle physics, (assuming of course that a particle cause is to be found). The authors in [181] modelled interactions between a scalar field and multiple DM fluids with independent but constant coupling strengths and allowed for interactions of opposite signs. They found that the background evolution mimics a single fluid with a variable coupling parameter, but that multiple fluids should be distinguishable in the perturbations.

Multiple couplings can also serve to hide large coupling values, as was

highlighted in [182], where the specific case of two DM fluids with the same coupling strength but opposite signs was studied. The model then had the same number of free parameters as a single coupled DM fluid scenario and in [183] N-body simulations of such models were described which produced effects including 'mirror' cosmic structures in the two DM species. In [102] and [103] the authors considered multiple DM fluids while studying an adiabatic instability in coupled scalar field models. They showed that the instability originates from a negative sound speed squared of the effective DM/DE fluid resulting in exponential growth on small scales and that it can be avoided for sufficiently small coupling strengths.

3.3.4 Massive neutrinos

The detection of flavour oscillations in solar and atmospheric neutrinos implies that the particles must have mass. In the context of ΛCDM recent CMB+BAO limits on the sum of neutrino masses are $\Sigma m_\nu < 0.23\text{eV}$ (2σ) [32]. A Fisher Matrix analysis of current and forecast CMB and matter power spectrum data [184] has shown that constraints on neutrino masses are significantly weakened in the case of IDE with energy transfer from DM to DE and that in turn massive neutrinos can allow for higher coupling strengths than would otherwise be possible. This is all due to the fact that the two effects act in opposite directions on the amplitudes of the matter and CMB power spectra. It was then shown in [185] that uncoupled models with an inverse power law potential lay beyond 1σ limits when allowing for neutrinos to have mass. A peak in the likelihood was found for small DE/DM coupling and a neutrino mass of around 0.3eV. Supergravity-inspired quintessence potentials were more consistent with zero coupling however.

[186] used CMB, BAO, SNIa, BBN, H_0 and matter power spectrum data with CAMB and CosmoMC to study the interplay between neutrino mass and coupling strength further, whilst also considering constraints from future neutrino mass experiments. They assumed a neutrino mass of 0.3eV based on a claimed experimental lower limit of 0.2-0.6eV [187] and found a $7-8\sigma$

detection of non-zero coupling with energy transfer from DM to DE. They also stated that if the KATRIN neutrino mass experiment currently under construction, which will have a sensitivity down to 200meV (90% confidence limit) [188], confirms the result, then ΛCDM will be statistically ruled out. It is certainly clear that whatever the KATRIN result turns out to be it will be of significant importance for cosmology.

Later [189] looked at the ISW effect in IDE with massive neutrinos, including galaxy cross-correlation, and confronted theoretical predictions with observations, finding that current data could not distinguish between IDE and ΛCDM. They also showed however that tomographic analysis can improve the distinguishing power and that future surveys might be able to discriminate between the models.

3.3.5 Halo collapse

IDE introduces novel effects into the gravitational collapse of overdensities. The competition between background, perturbative and non-linear effects means that different processes occur at different scales, making the study of collapsed structures a powerful tool for testing the model. [190] studied clustering in IDE with energy transfer from DM to DE and found that as with uncoupled models DE underdensities can form on some scales in the presence of matter overdensities but that the coupling suppresses the DE fluctuations.

[97] modified CAMB and CosmoMC to study the halo mass function for a constant coupling strength model using different potentials. Observations of high-mass high-redshift clusters had been found to be in tension with ΛCDM and they showed that energy transfer from DM to DE could solve this problem. [191] also studied the effects of IDE on the halo mass function, showing significant effects at the high mass end which invalidate the use of standard fitting functions. Another interesting recent work on this topic was [192], which looked at the way in which DM and baryons separate out due to the interactions during gravitational collapse and showed how it was

even possible to discriminate between different scalar field potentials.

3.3.6 Simulations

N-body simulations are an important tool in modern cosmology and a number of high quality IDE simulations have now been performed, although the subtleties of energy-momentum transfer and how it is handled in the code can make some models easier to simulate than others. The Γ model, (detailed in Section 3.5), for example has so far proved prohibitively difficult to implement in existing N-body codes. The modifications which need to be made to N-body codes can be seen in Eq. (3.10) and Eq. (3.13). The first of these amounts to a variation of the DM particle mass or number density so that ρ_c scales as,

$$\rho_c = \rho_{c,0} a^{-3} \exp\left[-\frac{C}{2}(\psi - \psi_0)\right], \tag{3.12}$$

where C is a constant. Meanwhile the effects on the growth of structure, as determined by the growth equation, (derived later in Section 5.3.5),

$$\ddot{\delta}_c = -\left(\mathcal{H} - \frac{1}{2}C\dot{\psi}\right)\dot{\delta}_c + 4\pi G a^2 \rho_c \delta_c \left(1 + \frac{C^2}{16\pi G}\right), \tag{3.13}$$

can be accounted for by defining effective versions of the Hubble factor and Newton's constant,

$$\mathcal{H}_{\rm eff} \equiv \mathcal{H}\left(1 - \frac{C\dot{\psi}}{2\mathcal{H}}\right), \qquad G_{\rm eff} \equiv G\left(1 + \frac{C^2}{16\pi G}\right). \tag{3.14}$$

The first IDE N-body simulations to be performed were reported in [193], where a study of the halo mass function and density profiles in IDE with an inverse power law potential and a constant coupling strength were performed. They found that IDE was not able to resolve tensions between observations and the theoretically determined Navarro, Frenk and White halo profile [194]. Other early work on IDE simulations in [195] compared the dynamics of constant coupling IDE with STT. They described the models down to the level of the perturbations and determined the modifications to standard N-body codes which would be required in order to encompass them.

There are however two main authors who have produced large N-body simulations of IDE, one of whom is Baojiu Li. In [196] Li presented the formalism for a scalar field model with an exponential coupling strength and an inverse power law potential motivated by $f(R)$ theory. This was then implemented in a modified CAMB code and N-body simulations, with the effects of the model on CMB and matter power spectra being reported in [197]. It produced little effect on the CMB power spectrum and therefore required structure formation data to obtain useful observational constraints. A third paper in the series [198] focused on the species dependent effects of the coupling and how they show up in large scale and halo bias.

Three more papers by Li then built on these original works; [199] found amongst other things more high mass halos than for ΛCDM and showed that the inner density profile of halos is also relatively surpressed, [200] studied the properties of voids in models with different potentials and showed that voids generally develop earlier and end up being larger than in ΛCDM, while [201] considered the relative contributions of different IDE effects on structure formation.

The other author who has produced large N-body IDE simulations is Marco Baldi. In [202] he introduced the COupled Dark Energy Cosmological Simulations project, (CoDECS), a large set of N-body and hydrodynamical IDE simulations. These were based on the Gadget-2 code [203] and their development using less general models was described in [204, 205]. The introductory paper also looked at the effects of different couplings and potentials on DM-baryon bias and found that for the non-linear matter power spectrum the redshift evolution of its linear amplitude may be able to break the degeneracy between coupling strength and σ_8.

Following the release of the CODECS simulations Baldi has worked on a large number of papers investgating their properties. [206] discerned the effects of coupling on the high redshift inter-galactic medium, observations of which were used to constrain a constant coupling with competitive limits being found. [207] showed that baryons and DM are less preferentially aligned

in IDE than ΛCDM, alleviating tension with observations where a misalignment had been found [208]. [209] studied the spin alignment of galaxy pairs, and found that a Supergravity inspired potential, which leads to a 'bounce' off the $w = -1$ limit at recent times, creates such an alignment and could give a signature of IDE, although they found no such feature in SDSS data.

The CoDECS simulations were used in [210] to show that IDE can lead to high mass clusters at high redshifts and proposed their use as a test of the model. Then [211] studied the bouncing dark energy mentioned above as an explanation for the abundance of high mass clusters at high redshifts. The model was shown to be able to simultaneously account for this observation plus the standard abundance at the present day and the standard power spectrum normalisation at the CMB. [212] investigated whether different IDE models from the simulations could help explain the anomalously high speed of the bullet cluster by looking for analogous systems in the simulations. They found that the coupled models all had a higher probability of finding such a system than ΛCDM.

[213] used CoDECS to quantify the effect of coupling on the clustering of DM halos and gauge its effect on BAO measurements. BAO were found to be useful for breaking the degeneracy with σ_8 in clustering anisotropy measurements and the halo mass function. [214] then studied the effect of coupling on DM halo mass accretion and the resulting halo properties such as halo concentration and subhalo abundance. Recently [215] also used CoDECS to forecast weak lensing constraints on the model parameters for Euclid and the Dark Energy Survey and the simulations were employed in [216] to find the effect of coupling on DM clustering anisotropies and redshift space distortions. They found that at small scales the degeneracy with σ_8 can be broken and that future surveys should be able to place good constraints on IDE models.

The same N-body IDE code was used to study time varying couplings [217], where the effects on structure formation were found to be generally stronger than for constant couplings, while background effects were weaker. This was

confirmed by work disentangling linear and non-linear effects in [218], after some results had been found to be slightly at odds with [61]. This was shown to have been due to the implementation of different numerical analysis techniques in the codes. It was also used in [219] to consider $\dot{\psi}$ couplings with a time dependent part which is a power law of the scale factor. It was found that couplings where a sudden growth in coupling strength was present which would otherwise be indistinguishable from ΛCDM, can not fit the rotation curves of spiral galaxies.

3.4 Interactions Proportional to $\mathcal{H}$

The first work to consider the $\mathcal{H}$ coupling in an IDE context was [126], where it was partly motivated by analogy with dissipative fluids, such as those with bulk viscosity [220]. The authors compared its dynamics to those of the $\dot{\psi}$ coupling to show that other couplings could lead to scaling solutions. Conversely, Zimdahl, Chimento and Pavon in [96], (all of whom would later write a number of papers using the coupling), derived the $\mathcal{H}$ coupling by explicitly requiring the existence of a scaling solution.

Although it was originally only considered as a way to study solutions to the coincidence problem phenomenologically, the $\mathcal{H}$ coupling soon became widely used in a number of different contexts. This was no doubt largely because it allowed $\mathcal{H}$ in the fluid equations to be eliminated via a change of variable as in the uncoupled and $\dot{\psi}$ cases, making the system amenable to the same analyses. In addition it opened up the possibility of using barotropic fluid models of DE, although it can equally well be applied to scalar fields.

Perturbation studies using this coupling generally neglect perturbations in $\mathcal{H}$. Such models are not gauge invariant but it was shown in [221] that the effect of neglecting perturbations in $\mathcal{H}$ did not significantly change the observational constraints on the model. To this end they employed perturbations in the expansion rate of the total fluid, although they noted that this choice was not unique.

3.4.1 Constant coupling

Initially only constant couplings were studied, in the same way as for the $\dot{\psi}$ coupling. [222] extended the original analysis of [96] to include separate dissipative effects in the DM and constrained the model's parameters with SNIa and BBN data. They also noted that they assumed the coupling to be negligible during BBN and commented that this could be achieved by simple addition of an exponential dependence on $\mathcal{H}$ to the coupling. Later [223] also derived statefinder parameters for the model.

A general $\mathcal{H}$ coupling which is a linear combination of both the DE and DM energy densities is often employed in IDE studies. It was used for example in [224] to find the conditions required for transition to $w < -1$ for scalar field models that give the correct present day DM/DE ratio. [225] used it to show that the coincidence problem can be alleviated from a finetuning of 96 orders of magnitude in uncoupled DE to 6 orders of magnitude for IDE using it and pointed out that the coupling leads to standard matter domination, unlike the $\dot{\psi}$ coupling. Finetuning and the coincidence problem were looked at with the linear $\mathcal{H}$ coupling in [226] where it was shown that they could at best only be alleviated and that solutions of the coincidence problem led to negative energy densities at early times, (which it was noted however can be a feature of MG theories), whilst more recently [227] found scaling solutions and constrained the model using SNIa data.

Adiabatic instabilities of perturbations, (see also Section 3.4.6), in the general linear $\mathcal{H}$ coupling, (although as mentioned above perturbations of $\mathcal{H}$ are generally neglected), were analysed in [110], finding that $Q \propto \rho_x$ versions suffered slightly less severely than the $Q \propto \rho_c$ case. [109] also studied the issue and demonstrated that for models with energy transfer from DE to DM and $Q \propto \rho_x$ the curvature perturbation was stable for $w < -1$ and with a suitably small coupling strength for $w > -1$. This was then followed up in [228] which looked at the stability of density perturbations and found that for a stable model with $w > -1$, the effects of interactions could nevertheless overwhelm the effects of DE perturbations on structure growth.

The general linear $\mathcal{H}$ coupling was extended to include a constant term in order to replicate more general couplings at late times in [229]. Using an MCMC analysis they found that $Q \propto \rho_x$ couplings were most favoured, phantom models prefer energy transfer from DM to DE and non-phantom DE disfavoured non-coupled models. [230] included generalised non-linear $\mathcal{H}$ couplings in their analysis, as well as the Γ coupling, showing that only the $\mathcal{H}\rho_c$ case can solve the coincidence problem and even then only in a small area of the parameter space. [231] also used a general linear combination of the constant $\mathcal{H}$ coupling to study the general dynamical behaviour of interacting two-fluid cosmologies, both for uni-directional and bi-directional energy transfers.

3.4.2 Variable coupling

Given the need for negligible coupling during BBN it was natural for [232] to extend the $\mathcal{H}$ coupling to include a time dependent free function, (again designed to produce scaling solutions), and compare it to the simpler case. They found best fit parameters using $H(z)$ data and studied the behaviour of both cosmologies. These couplings were also studied in [233] where they used SNIa, $H(z)$, cluster X-ray gas mass fraction, BAO and CMB data to get observational constraints and found that the variable function case preferred energy transfer from DE to DM whilst the opposite was true when the free function was taken as constant.

Constant and variable couplings were again compared in [234] using SNIa, CMB and BAO data. They found a slight preference for phantom models with energy transfer from DM to DE in both cases but with ΛCDM still within 1σ limits. Then more recently the variable coupling was employed in the context of DM with a bulk viscosity in [235] where $H(z)$ data was used to constrain the parameters of the model before its behaviour was compared to the non-viscous case.

An alternative approach was taken to studying the background cosmology of models where the coupling is generalised to admit a time dependent

coupling strength in [236]. They considered the case of it being a power law of the scale factor as well as a case where a time derivative of the energy density was included in addition. Another method was also used in [237] where they generalised the usual coupling constant in the $\mathcal{H}$ model to vary with time according to two parameters in the same way as the Chevallier-Polarski-Linder, (CPL), parameterisation of w [238, 239]. Different forms of parameterisation for w itself were then tested using SNIa, BAO, CMB, $H(z)$ and x-ray gas mass fraction data. They found $w \approx -1$ with energy transfer from DM to DE during matter domination and DE to DM at late times gave the best fit.

In [240] the authors parameterised the interaction term in order to derive an analytically soluble toy model designed to exhibit transient acceleration, motivated by evidence that the acceleration may have peaked in the past [241]. They used observations of SNIa to find constraints on the model's parameters when two specific cases of $Q \propto \alpha \mathcal{H} \rho_x$ models with time-varying α were considered, but degeneracies between parameters did not allow for significant constraints. In a subsequent paper they tested perturbations in this model against growth rate data, by paramaterising the interaction perturbation and studying its effects quantitatively [242]. The model was found to be consistent with observations and then more recently it was shown that the model's DE perturbations are negligible on scales relevant for structure formation [243].

3.4.3 Observations

The original $\mathcal{H}$ coupling and its generalisation to include a linear dependence on both the DM and DE energy densities is still being confronted with observations today. In [244] SNIa data was used to constrain background cosmological parameters in constant and time-varying w models. The SNIa constraints were then compared to those from the CMB shift parameter, demonstrating a significant tension between the datasets which was only made worse by the coupling. Later, [245] also used the CMB shift parameter

in their analysis, along with BAO, SNIa and lookback time data, finding a preference for energy transfer from DE to DM. More recently [246] derived the perturbation equations, (neglecting perturbations of $\mathcal{H}$), for a coupling formed from a linear combination of the energy densities and found best fit parameters using CMB, BAO, SNIa and H_0. Some cases studied favoured energy transfer from DE to DM slightly but ΛCDM was always within 1σ.

The simple linear coupling model has been generalised in all manner of different ways. [247] for example placed observational constraints on linear $\mathcal{H}$ models as well as couplings proportional to the product of the energy densities. Both constant and time-varying w cases were considered in their MCMC analysis, which used SNIa, BAO and CMB data. Recently [248] also employed nonlinear, (and parameterised), forms of the $\mathcal{H}$ coupling to investigate limits on IDE models from the weak gravity conjecture. They found that in most cases the bounds are looser than those from observations, although in some cases the theoretically forbidden region does reduce the observationally allowed parameter space to some degree.

The added complexity of IDE models inevitably weakens constraints and leads to degeneracies. [249] studied the effect of admitting IDE on parameter constraints from the CMB experiments Planck and the European Photon Imaging Camera, (EPIC), onboard the European space Agency's X-ray Multi-Mirror Mission, XMM-Newton. They generated mock data and analysed it using MCMC techniques, finding that degeneracies led to errors which were an order of magnitude larger than when no coupling was considered. Recently [250] studied how to break parameter degeneracies in IDE using a simple fluid model with a $Q \propto \mathcal{H}\rho_c$ coupling and a time-varying w. They carried out a perturbation analysis but neglected perturbations in $\mathcal{H}$. They commented on the degeneracy between the coupling strength, w and Ω_c in CMB data then compared constraints from fitting to CMB, BAO and SNIa data.

In recent years GRB's have begun to be usable as an observational probe and [251] investigated the ability of GRB's to constrain couplings in the dark

sector. They found them to be better than BAO alone but much worse than the combination of CMB and SNIa data due to the small GRB sample size available at the time. Using mock GRB data they showed however that they could be a useful probe of IDE couplings in the future as sample size increases, not least because the are complementary to CMB constraints in a similar way to SNIa data. More recently [252] used SNIa, CMB, BAO and new GRB data to constrain a fluid $\mathcal{H}$ coupling model's parameters via an MCMC method, reporting marginalised 1σ constraints of $\Omega_m = 0.2886 \pm 0.0135$ and $w_x = -1.0658 \pm 0.0564$, with the constant coupling strength parameter where $Q = -\alpha \mathcal{H} \rho_c$ found $\alpha = -0.0047 \pm 0.0046$. This showed a slight preference for energy transfer from DM to DE and they noted that the GRB data had helped to eliminate some parameter degeneracies.

3.4.4 Clusters

As has already been mentioned, the study of gravitationally collapsed objects is a powerful tool for testing and constraining IDE. [253] for example compared coupled quintessence and Chaplygin Gas models to observations of cluster Abell 586. Chaplygin gases have an unusual equation of state such that they behave like matter at early times and a cosmological constant at late times. They can also be decomposed into an effective two fluid description of DM decaying into a $w = -1$ DE. They found a model independent suggestion of interactions due to an apparent violation of the equivalence principle. This implies a time-varying DM-baryon bias, which should be observable in large cluster surveys. Recently A1689 was also included in an analysis of different density profile models [254], with no evidence for interaction being found, although this may have be because they had to allow for large errors.

[255] also found a small preference for energy transfer from DE to DM from a study of 33 cluster masses. Since the coupling affects DM and not baryons, comparison of mass estimates from x-rays and weak lensing allowed constraints on the coupling to be found. It was recognised however that

unknown systematic errors in the data may be an issue. More clusters were later added [256], bringing the total to 100, and a 14σ deviation from zero coupling was found.

The novel features of collapse in IDE are often worthy of study for their own sake and [257] has studied the qualitative and quantitative effects of IDE on cluster collapse in different linear $\mathcal{H}$ couplings. More recently, [258] studied the alignment of baryons and DM in clusters for a toy model with a $Q \propto \mathcal{H}\rho_{\text{total}}$ coupling and used data from [259] to constrain its parameters.

3.4.5 Applications

The $\mathcal{H}$ coupling has been used to extend almost every cosmological model there is, but in the case of DE motivated by the holographic principle [260] this has been justified from thermodynamical considerations as being a reasonable approximation, given the accuracy of constraints from SNIa [261]. An early paper on the subject identified the infra-red cutoff of the theory with the Hubble factor [262], thus suggesting DE of the form $\rho_x = 3c^2\mathcal{H}^2/(8\pi G)$, where c is a constant. Applying this leads to the conclusion any coupling at all provides scaling solutions and w is just a function of the scaling ratio and the coupling function. It was then shown that a typical $\mathcal{H}$ coupling could result in a transition of the DE to the phantom regime [263]. The CMB shift parameter was used along with SN and BAO data to find constraints on the model in [264], with H_0 data later also being included in the analysis [265]. More recently a study of the background dynamics for a tachyonic model of holographic DE was also investigated in [266].

[267] carried out a dynamical analysis of generalised linear and non-linear $\mathcal{H}$ couplings in a Loop Quantum Cosmology framework and [268] compared the linear $\mathcal{H}$ coupling model with the $\Gamma\rho_c$ coupling in both classical and Loop Quantum Cosmology settings, highlighting generic features of the different systems by means of a phase space analysis. In [269] a fluid model with the $\mathcal{H}$ coupling was applied in a fractal cosmology setting (which leads to additional pressure terms in the fluids) and novel behaviours were found such

as solutions which oscillate between acceleration and deceleration. They also studied holographic and scalar field models in the fractal context and found stable accelerated solutions to be ubiquitous to all three models, although none of these were scaling solutions.

[270] extended a QCD motivated 'Ghost Dark Energy' model to include interactions and placed observational constraints on cosmological parameters with SN, CMB and BAO data. Later [271] carried out a statefinder diagnosis including testing a best fit model found using SNIa, $H(z)$, BAO and CMB data. A similar study was then undertaken in [272] to investigate the crossing of the model to the phantom regime. [273] studied the background dynamics of a model with a coupling proportional to the sum of the energy densities and an unusual equation of state for the DE motivated by wormhole physics and similar to a Chaplygin gas. More recently, [274] looked at cosmologies with $\mathcal{H}$ coupling between DE and viscous DM, also allowing for curvature, and found evidence for a crossing of the phantom divide from below for the effective DE equation of state.

3.4.6 Theory

Thanks to its mathematical simplicity, systems with an $\mathcal{H}$ coupling have been widely used in theoretical works. They are not without their share of problems however and like all IDE models can suffer from instabilities at the level of their perturbations. In [275, 276] this was unfortunately overlooked due to an interaction term being omitted in the pressure perturbation evolution equation, as pointed out in a work on the same effects in the Γ model [107], (the error in the equations had also been previously noticed in [100]).

These instabilities were properly categorised in [108, 277, 111] where they studied perturbations in the general $\mathcal{H}$ coupling model with constant w and defined the 'doom' factor,

$$\mathrm{d} = \frac{Q}{3\mathcal{H}\rho_x(1+w)}, \tag{3.15}$$

which characterises whether they are subject to non-adiabatic large scale

instabilities at early times. The instability is caused by the effect of coupling on pressure waves in the DE and the 'doom' factor shows up in the pressure perturbation for constant w models as,

$$\frac{\delta p_x}{\delta \rho_x} = 1 + 3(1-w)(1+w)(1+\mathrm{d})\frac{\mathcal{H}\theta_x}{k^2\delta_x}, \tag{3.16}$$

where $\mathrm{d} > 1$ leads to the instability [108]. They also used CAMB and CosmoMC with SNIa, CMB, H_0 and $H(z)$ data to show that the best fit case when $Q \propto \rho_x$ has $\mathrm{d} < 0$ and so is free from instabilities. The analysis of this model was then repeated with updated CMB data in [221] where they included pertubations of $\mathcal{H}$, which had previously been neglected, and then [278] forecast parameter constraints for Planck and Euclid. In a novel analysis for IDE [279] constrained $Q \propto \rho_c$ and $Q \propto \rho_x$ models with different parameterisations of w by assuming only a small change in the DE scalar field. A caveat to the conclusions of this work however is that DE is not necessarily constrained by slow-roll conditions [280, 281, 282, 283].

Some of the most interesting works on IDE are when realistic physical descriptions are used to model its behaviour. One attempt to do this was [284], which used thermodynamics to argue that if an interaction is present in the dark sector and DE is amenable to a fluid description with a well defined temperature not far from equilibrium, then the energy transfer must be from DE to DM, thus supporting the work of [285], (see Section 3.7.2). In contrast [286] showed that thermodynamics would favour decay from DM to DE if one of the fluids had a non-zero chemical potential. They then used the $Q \propto \alpha\mathcal{H}\rho_x$ model to study observational constraints from BAO, CMB and SNIa and found the decay of DM to DE to be favoured when including both directions of decay in the analysis, although $\alpha = 0$ was still within 1σ. Another study of IDE physics was also carried out in [287, 288], which studied the nature of singularities in coupled fluids.

A more phenomenological work was reported in [289] for a $Q \propto \mathcal{H}\rho_c$ coupling where the evolution of the scale factor was taken to be an exponential function. It was shown that while only open and flat universes can cross $w = -1$ for the uncoupled case, all three geometries permit $w = -1$ crossing

in IDE. Later, [290] modelled DM decaying into a scalar field in a closed universe parameterised by a power law evolution of the scale factor. They used CMB, SNIa and BAO data to constrain the parameters of a model with a coupling strength found previously in [234]. Then more recently, [291] studied a scalar field model with a complex form of potential that gave transient acceleration and tried to use the coupling to achieve a standard matter era as required, but found that the DE still always dominated at early times.

3.5 Interactions Proportional to Γ

In order to provide a more physically realistic model of IDE, a model was proposed with interactions in the background of the form $\Gamma\rho_c$, where Γ is constant. This had also been used to describe particle decays in other contexts, namely; the decay of DM to radiation [292, 293], the decay of the curvaton field from inflation to radiation [99] and the decay of super-heavy DM to a quintessence field [294]. The difference from models with interactions affected by the global expansion rate $\mathcal{H}$, is that the physics of the interaction is only determined locally.

Roy Maartens has been an author on most of the papers which use the Γ coupling and a number of comparative studies with other couplings have been carried out. This section shall detail works on the Γ model as a foundation for an investigation into a particular version of it in the following chapter.

3.5.1 Introducing the Γ model

The 'Γ' model was first introduced in [130], where a comparative study was performed on the background dynamics of all three of the different interaction types; $\dot{\psi}$, $\mathcal{H}$ and Γ taking $Q \propto \rho_c$. The IDE was modelled as a scalar field with an exponential potential and since only late-times were being considered the effects of radiation were neglected. The $\dot{\psi}$ and $\mathcal{H}$ models were studied using the same simple two-dimensional phase plane as that used for uncoupled models of quintessence, but the Γ model required the implementation of a

three-dimensional phase space because it is not possible to eliminate $\mathcal{H}$ from the continuity equations (3.1) and (3.2). This meant the introduction of the new variable $z = H_0/(H + H_0)$, which helpfully also compactified the phase space into a cylinder of unit height and radius, allowing an effective analysis to be performed.

The study found that while it did not display the accelerated scaling attractor solutions of the other two models, the Γ model permitted a ΛCDM-like accelerated attractor for the case of DM decaying to DE, something which was not present for the other two couplings. This presented a novel approach to alleviating the coincidence problem, as the model could contain no DE at early times yet lead to an accelerated universe independent of the initial conditions.

3.5.2 First constraints

Two follow-up papers to the initial study of its background dynamics [295, 296] aimed to confront the new Γ model of IDE with observations. The first [295] derived the equations governing the non-standard ISW effect using a simple fluid model of IDE with a CPL parameterisation of its equation of state parameter $w = w_0 + (1 - a)w_a$. This was possible without a comprehensive understanding of perturbations in the model because at linear order in the Newtonian regime, (i.e. where DE perturbations could be neglected), the only effects on the growth of structure for a model with $Q = a\Gamma\rho_c$ come from the modifications to its background. It was found that the interaction rate Γ was degenerate with both w and σ_8 and that strong constraints on Γ were not possible due to the weakness of the effect.

In the second paper [296] however the effects on weak-lensing bispectrum tomography were considered, which is a more sensitive observable measure. Forecasts were made on the possible sensitivity of the proposed Dark Universe Explorer, (DUNE), experiment, (now part of the EUCLID mission), using the same setup as before. The analysis showed that a DUNE-like experiment would be able to either detect or rule out production of the entire DE content

of the Universe within its age for cases where $w \approx -1$.

3.5.3 Instabilities

In order to better understand the dynamics of the new Γ model of interactions and place tighter observational constraints on its parameters, it was necessary to construct a covariant description of its perturbations. In the following chapter this shall be done for a Γ model with $Q \propto \rho_x$, but the method was presented for the first time in [107], where perturbations for constant-w fluid models with $Q \propto \rho_c$ were developed and a large-scale non-adiabatic instability in the perturbations was discovered.

The instability was different to those already known about in the $\dot{\psi}$ and $\mathcal{H}$ models which were small scale, adiabatic and restricted only to the strong coupling regime. In fact however it was found that this instability did also exist in the $Q \propto \mathcal{H}$ model but had been missed in previous works [275, 276] due to an incorrect handling of the energy-momentum transfer. The instability in both models led to a runaway blow-up of the dark energy velocity perturbation early in the radiation era and did not depend significantly on the choice of energy-momentum transfer four-vector. This could not be avoided by weakening the coupling as in other cases of IDE instabilities, but allowing w to vary was instead proposed as a solution.

3.5.4 Generalisation

The next paper to consider the Γ model was another comparative study [297], this time just with $Q \propto \mathcal{H}$ models and looking at a more general form of interaction where both DM and DE energy densities could play a role to a greater or lesser degree. It used a fluid model with a constant DE equation of state and whilst it was true that both of these models were known to exhibit the recently discovered instability in the perturbations, the work was still of interest because there were known to be ways around the instability. For example, the generalisation to a variable DE equation of state was expected

to avoid the problem, while it was also true that certain sign combinations of Γ and w could also be free from instabilities $w < -1$ models had not been considered in [107].

There were a number of findings in the paper, including analytical constraints on the parameters of the $Q \propto \mathcal{H}$ models. For the Γ model it was shown that with a non-zero $\Gamma_c \rho_c$ term with energy transfer from DE to DM was required in order to have positive ρ_x at early times. Furthermore, in cases with the interaction term $\Gamma_c \rho_c + \Gamma_x \rho_x$ it was shown to be necessary that the two interaction rates had opposite signs and $\Gamma_x > \Gamma_c$ in order to have a finite and positive DE-DM ratio at late times. It was therefore not possible to address the coincidence problem via production of DE from DM as had previously been hoped because the models were not well behaved at either early or late times.

The only way to avoid these problems in the background was shown to be to have $\Gamma_c = 0$ with the interactions being proportional to the DE energy density only. For $\Gamma_x < 0$ energy would pass from DM to DE and the DM energy density would again become negative at late times, but for $\Gamma_x > 0$ with energy transfer from DE to DM each fluid could be well behaved throughout. This would imply a transient period of DE domination and it was shown that the smaller the interaction rate, the larger the maximum value reached by the DE-DM ratio before entering a late-time matter dominated epoch. A study of its perturbations is used to place observational constraints on this model in Chapter 4.

The next work looking at the Γ model was a study of the effects of such interactions on structure growth and the weak lensing power spectrum [298]. Once again it considered both cases with interactions proportional to the DM energy density and those with interactions proportional to the DE energy density. In each case however the energy-momentum transfer four-vector in the perturbations was chosen to be parallel to the four-velocity of the DM, i.e. $Q^\mu = Q u_c^\mu$. One could therefore think of the interaction as a DM particle decaying and transferring its momentum to the DE. It was shown

that unlike the $\Gamma_x = 0$ case, the $\Gamma_c = 0$ produces direct modifications to the DM perturbation equations in addition to the effects from the modified background evolution. The qualitative effects on observations for each case were compared to the non-interacting case.

3.5.5 Classification

A useful classification of IDE models was made in the next article to consider the Γ model [299]. Three types of IDE model were identified, namely; those which in the Newtonian gauge and the Newtonian regime on sub-hubble scales leave the DM perturbation equations unchanged, those which modify the DM density perturbation equation and those which modify the DM velocity equation. Observational tests were then proposed which could could constrain these different types.

Firstly it was proposed that when interactions show up only in the background a combination of peculiar velocity and weak lensing measurements at multiple redshifts could be used to look for deviations from the standard $\rho_c \propto a^{-3}$ of DM in the non-interacting case. For the other two types it was shown that it should be possible to use combinations of weak lensing and peculiar velocity measurements to demonstrate that either the density perturbation or the velocity equation was being modified. It was also noted that the sorts of issues discussed in the paper might be helpful in distinguishing IDE from MG, since in MG standard DM perturbation equations apply and there is no apparent violation of the Weak Equivalence Principle.

[300] classified both linear Γ and $\mathcal{H}$ coupling models according to their energy density dependence and energy-momentum transfer type and found current and future constraints. They discussed the generic features of each class and separated out effects caused by modifications to the expansion history from those due to modifications of structure growth. They also discussed ways of observationally testing for and distinguishing between the different classes, as well as MG and $w(z)$ models.

3.5.6 Quadratic couplings

[301] studied the background dynamics of a model equivalent to the Γ coupling, (in fact well before the works discussed in this section), where the coupling was through a generalised interaction term $\rho_c^\alpha \rho_x^\beta$. The possibility of a cyclic DM/DE domination was found and discussed as a possible remedy for the coincidence problem. [302] studied the same coupling in a two fluid model where one of the fluids was warm DM. They performed a dynamical analysis of the background and used SNIa and $H(z)$ data to constrain the model parameters, finding a phantom DE with energy transfer from DE to DM and an interaction of the form $\rho_c \rho_x$ to be the best fit.

The coupling was also modelled as being proportional to the product of the DM and DE energy densities in [303]. The background dynamics of cases where $w = -1$ and $w =$ constant were looked at and for a constant $w < -1$ case bounded periodic solutions were found, which provide a natural mechanism by which the DE might have a small value at the present day. It was noted however that while the baryon density decreases as usual, the DM density is periodically increased and remains at a roughly constant level over multiple cycles. Perturbations in a model with a coupling proportional to the product of the energy densities and a constant coupling strength were looked at in [112]. An instability was found but shown to be avoided if $w > -1/3$ during radiation domination.

Another interesting paper studied the background dynamics of a coupled quintessence model with an exponential potential using the Γ model notation [304]. This pointed out that from a physical standpoint it might be more natural for the interactions to be quadratic in the energy densities and so considered the general case with $Q = A\rho_x^2 + B\rho_c^2 + C\rho_x\rho_c$. It found that accelerated critical points were possible as long as the potential was flat enough, but that again no scaling solutions existed. It also found that models with a ρ_c^2 term do not admit a suitable matter dominated era as required.

3.5.7 Improved constraints

With the perturbation formalism in place a pair of papers were published [305, 306] aimed at placing better constraints on the $\Gamma\rho_c$ version of the model with a DE equation of state parameterised via the CPL parameterisation. The first of these was a study of the initial conditions on the perturbations [305] and performed a complex matrix calculation method previously developed for non-interacting DE models with variable w [307]. The follow up paper [306] then implemented these initial conditions in a comprehensive study of the model's cosmological parameters using a modified version of CAMB and CosmoMC. It used SNIa, BAO and CMB data in a MCMC analysis to place observational constraints on the model's parameters, including Γ, for which a 95% confidence limit of $-0.23 < \Gamma/\mathcal{H}_0 < 0.15$ was found.

The same covariant framework for the description of the perturbations was later employed in [308] to study DM decay, DE decay and a scalar field model with the $\dot{\psi}$ coupling. An analysis of the effect on the matter power spectrum and the ISW was examined and shown to be more subtle than expected from results found elsewhere using parameterisation methods.

3.6 Other Forms of Couplings

Beyond the three most commonly studied couplings discussed above there are of course a wide variety of other forms which appear in the literature. Each of these however are either motivated by some underlying physical theory or designed with some particular purpose in mind and examples of these two types of study are given below.

3.6.1 Motivated by theory

Interactions between DE and DM have been studied in the context of QCD inspired 'New Agegraphic Dark Energy' [309]. This was later shown to be equivalent to an interacting polytropic gas model of DE [310], which itself

had a statefinder diagnosis performed on it in [311]. Interactions between scalar fields and also tachyon fields were studied using generalised couplings derived using Noether symmetry considerations in [312].

[313] studied a coupling motivated by supersymmetry and equivalent to a particular choice of $f(R)$ gravity model, where the DE scalar field can decay into hot and cold DM, thus alleviating the coincidence problem. Also, the general behaviour of a coupling containing an additional $\dot{\rho}$ term motivated by string theory has recently been studied [314].

3.6.2 Designed for a purpose

In [315] a complex coupling was derived by requiring that the DE/DM ratio varies slowly with time around the present day. They assumed energy transfer from DE to DM and studied both quintessence and tachyonic models. They found that their models could be compatible with SNIa data but that the tachyon model then led to excessively high values of $\Omega_{\rm m}$. They then repeated the analysis in [316], this time including baryons and phantom quintessence and found that ΛCDM is favoured by statistical measures.

A recent study of fluid IDE with different parameterisations of w found evidence for a change of sign of the interactions [317]. They performed a piecewise split of a constant $\mathcal{H}$ coupling into different redshift bins and constrained each one with SNIa, BAO, CMB and $H(z)$ data in an MCMC analysis. Data with $z > 0.5$ preferred energy transfer from DE to DM, whilst below $z = 0.5$ the interaction's sign seemed to oscillate. They argued therefore that more flexible parameterisations should be considered and in [318] a new coupling motivated by this study and designed to change its sign with the onset of acceleration was proposed,

$$Q = q(\alpha\dot{\rho}_A + 3\beta\mathcal{H}\rho_A), \tag{3.17}$$

where α and β are constants and q is the deceleration parameter. An analysis of this system's critical points was then performed, finding a complex dynamics which includes scaling solutions. The cosmological constraints on

the parameters of this model from SNIa, BAO and CMB data were then found in [319] and it was shown that ΛCDM is still more likely according to a number of statistical measures. [320] also constructed a coupling designed to change sign as the universe enters late-time acceleration. They showed that it is consistent with the second law of thermodynamics, (though it was not derived from an action), and that it can satisfy the CMB shift parameter constraints.

An extremely general coupling which could include linear and non-linear terms up to the second time derivative of the energy densities was shown to be describable as a single fluid in order to demonstrate a correspondence of IDE with Chaplygin gas models in [321]. More recently the authors also analytically studied the stability of scaling solutions in this framework [322]. A condition on couplings which avoid adiabatic instabilities was derived in [101] and found to infer an effective $w < -1$.

[323] studied a three-form field DE coupled to DM and considered each of the three common coupling types, (note however that [179] later pointed out that these could only be considered phenomenological in this context as they were not derived from a covariant Lagrangian). They compared the background dynamics of each case but found that none of them could address the coincidence problem in this framework and so proposed a new scalar field type coupling with an additional term linear in the field value which leads a scaling solution.

3.7 Parameterisations of Interactions

Due to the speculative nature of physically motivated forms for IDE couplings there has been a large amount of work carried out using parameterisations of the model. There are two main types of parameterisation used in the literature, works on which are discussed below and referred to by their notation as the ξ and ϵ parameterisations, before other forms in the literature are also reviewed.

3.7.1 The ξ parameterisation

In order to study IDE as a solution to the coincidence problem, the authors of [324] parameterised the relation between the DE and DM energy densities,

$$\rho_x \propto \rho_c a^{\xi}, \tag{3.18}$$

where ξ is a constant parameter. The special cases $\xi = 3$ and $\xi = 0$ correspond to ΛCDM and the self-similar solution with no coincidence problem respectively, so $0 < \xi < 3$ would reduce the severity of the coincidence problem. The work forecast the ability of high redshift SNIa observations, the application of the Alcock-Paczynski test to quasar pairs, and cluster evolution to constrain this parameter. They found in particular that the SNAP mission, (now part of the Joint Dark Energy Mission), should provide particularly definitive results.

This same power-law parameterisation was used in [325], where they implemented a new technique developed in [326, 327] of using the lookback time to clusters of galaxies as an observational constraint and found limits on ξ and w. About the same time [328] specifically implemented the $\mathcal{H}$ coupling in the ξ parameterisation in order to find scaling solutions and analytically integrated the case of $\xi = 1, w = -1$ showing that it could alleviate the coincidence problem.

Soon after this CMB constraints were placed on ξ [329], but the current constraints on the ξ parameterisation from SNIa, CMB and BAO observations were found in [330]. They found that ΛCDM was within 1σ of the best-fit in the w-ξ plane with $\xi = 3.06 \pm 0.35$ at 68.3% confidence limit. They also presented a theoretical constraint on the redshift at which the transition to acceleration occurs, showing that in the parameterised ξ model $z(\ddot{a} = 0) > 0.73$ would require interactions. Although not referred to by the authors, it is interesting to note that work showing that the acceleration may be slowing also shows that the transition redshift may indeed be slightly higher than this value [241].

3.7.2 The ϵ parameterisation

In [331] the authors proposed a parameterisation of decaying vacuum models with $w = -1$ via their deviations from the standard background evolution of CDM,

$$\rho_c = \rho_{c,0} a^{-3+\epsilon}, \tag{3.19}$$

where epsilon was taken to be a small positive constant, (since they studied DE decaying to DM). They found that it was not possible to address the cosmological constant problem in this model and put constraints on ϵ from SNIa, CMB and growth rate data.

It was later demonstrated in [285] that in a particle decay context decay from DE to DM is thermodynamically favoured when both fluids have zero chemical potential. They then used the ϵ parameterisation to find constraints from SNIa, CMB and cluster gas mass fraction observations, finding a best fit of $\epsilon = 0.11 \pm 0.12$ at 94.5% confidence limit, (1.5σ deviation from zero), although they only considered the range $\epsilon > 0$. From then on most studies using the ϵ parameterisation only considered $\epsilon \geq 0$, although [332] used a scalar field model with SNIa, BAO, and $H(z)$ data to constrain ϵ, finding a very slight preference for energy transfer from DM to DE, ($\epsilon < 0$).

[333] performed a joint statistical analysis of CMB, BAO and SNIa data, (considering only energy transfer from DE to DM), finding $\epsilon \leq 0.09$ at 3σ. However [334] put observational constraints on the same model from SNIa and BAO data, finding a χ^2 best fit of $\epsilon \approx 0.5$, (although with little statistical significance). They also performed a statefinder diagnosis and found an earlier transition to acceleration than for uncoupled models. In [335] the growth of overdensities was studied using the ϵ parameterisation. They showed that coupling leads to a suppression of the growth rate by a constant amount and considered the effect on redshift-space distortions and ISW observations leading to a wrongly inferred growth index $\gamma > 0.55$. The ϵ parameterisation was also used recently in [336] to assess the ability of future $H(z)$ data to constrain the parameter within the range -0.2 to 0.2 using both numerical and analytical methods. An accuracy of 1% in $H(z)$ was found to be required

in order to potentially detect an interaction using $H(z)$ data alone.

3.7.3 Other forms of parameterisation

In [337] solutions to a model with a parameterised coupling between DM and a tachyonic field which required the ratio of the densities to be constant at late times were found, while [338] rewrote a Chaplygin Gas model as a parameterised IDE model when discussing its observable effects on structure formation. Recently, [339] used a simple parameterisation of the coupling in order to investigate the potential effect of wrongly assuming that observations caused by IDE are produced by normal DE and highlighted the ability of IDE models to exhibit phantom-like effective DE equations of state.

The ϵ parameterisation was extended in [340] to allow for time-varying ϵ. They performed an analysis using CMB, BAO and SNIa observations and found no significant evidence of any deviation from $\epsilon = 0$, with both signs being equally likely, thereby favouring ΛCDM. [341] further generalised the ϵ and ξ parameterisations to include a wide variety of functional forms, placing observational constraints on them from SNIa, CMB and BAO data. They also performed three different statistical tests and in each case found ΛCDM to be preferred.

3.8 Other Works

3.8.1 Reconstruction of the coupling

[342] reconstructed the interaction term from Chebyshev polynomials, which are a complete set of orthonormal functions, using SNIa data and found a preference for a recent change in sign so that there is an energy transfer from DE to DM at early times and an energy transfer from DM to DE at late times. They then confirmed their findings by repeating the analysis using not only SNIa but also BAO, CMB, $H(z)$ and X-ray gas mass fraction data [343].

In a slightly different vein, [344] matched an IDE model to a MG cos-

mology by constructing the IDE potential and coupling functions to match the MG model's expansion and growth histories in order to highlight the difficulty of distinguishing between the two. An extension of this work is the subject of Chapter 6.

3.8.2 Particle theory

In [345] an IDE model was proposed where DM is uncoupled but coexists with a coupled particle whose mass grows as a function of time, taken to be neutrinos. They found viable cosmologies but with only small deviations from ΛCDM which would be difficult to measure. Interactions with standard model particles are among the topics studied in [346], while other results include that in addition to the degeneracy of an uncoupled DE+DM system with a single dark fluid, coupled systems can also be completely degenerate with a single fluid if the total adiabatic sound speed is equal to zero.

It was proved in [347] that the generalised second law of thermodynamics holds in a model where DE interacts with both DM and radiation, while [348] studied interactions in the framework of open systems with irreversible thermodynamics due to matter creation/annihilation. They described a coupling independent method for dealing with pressures arising from particle creation and decay and demonstrated its application to two particular examples. [349] studied coupled dilaton/DM scalar fields and realistic cosmologies with effects on galactic substructure were shown to be possible. A $\Gamma\rho_x$ coupling was applied to a k-essence model, (quintessence fields with a non-canonical kinetic term), inspired by Yang-Mills theory in [350] and it was found that smooth $w = -1$ crossing was possible but non-coupled models were favoured by statistical measures.

[351] showed that elastic scattering in the dark sector could be several orders of magnitude stronger than Thompson scattering as there should be no effect on background observations and structure formation is only weakly effected. More recently, [352] considered the effect on CMB anisotropies of a dark sector coupling analogous to Thompson scattering. They found that

constraints on the scattering cross section from CMB data, assuming a proton mass DM particle, are tighter for phantom DE than for cases where $w > -1$ but when $w = -1$ no constraints are possible.

3.8.3 Vacuum decay

There have been a large number of works published on the subject of vacuum decay and it is beyond the scope of this review to cover them all, (see e.g. refs. in [231]). Instead, a flavour of some of the recent topics of study is given below.

[353] looked at interacting vacuum energy and showed that thermodynamics restricts the energy transfer to being from the vacuum to DM. They then constrained the model's parameters using the ϵ parameterisation with SNIa BAO and CMB data. A similar study looked at a parameterisation of vacuum decay using a power series of $\mathcal{H}$ [354], where they also described an equivalent coupled quintessence model.

[355] recently developed a model of inhomogeneous vacuum energy, which due to the inhomegeneity necessarily interacts with matter. They showed its ability to describe any dark energy cosmology and gave the explicit example of a Chaplygin gas. [356] meanwhile modelled an interacting vacuum term using a power law of the DE energy density and found observational constraints from SNIa, GRB, CMB, BAO and $H(z)$ data. They found that observations disfavoured regions of the parameter space where the coincidence or cosmological constant problems are alleviated.

3.9 Discussion

The above list shows the wide scope and transferability of IDE models and techniques in modern cosmology. The rich phenomenology that they provide can seem like a panacea for any symptom that ΛCDM might display, but the temptation to overdose on cooked-up medicines should probably be resisted and holding too much store in the low significance results typical

Ref.	Coupling/ parameterisation	Result
[237]	$[b_0 a + b_e(1-a)]\, H_0(\rho_{x,0} + \rho_{c,0})$	early - DM $\rightarrow$ DE, late - DE $\rightarrow$ DM, $w \approx -1$, $(< 1\sigma)$
[246]	$\mathcal{H}\rho_c$, $\mathcal{H}(\rho_c + \rho_x)$	DE $\rightarrow$ DM, $(< 1\sigma)$
[252]	$\mathcal{H}\rho_c$	DM $\rightarrow$ DE, $w < -1$, (1σ)
[285]	ϵ	DE $\rightarrow$ DM, (1.5σ)
[286]	$\mathcal{H}\rho_x$	DM $\rightarrow$ DE, $(< 1\sigma)$
[306]	$\Gamma\rho_c$	DE $\rightarrow$ DM, $(< 1\sigma)$
[330]	ξ	DM $\rightarrow$ DE, $(< 1\sigma)$
[332]	ϵ	DM $\rightarrow$ DE, $(< 1\sigma)$
[343]	reconstruction	early - DE $\rightarrow$ DM, late - DM $\rightarrow$ DE, $w \approx -1$, $(< 1\sigma)$

Table 3.1: Observational constraints on the direction of energy transfer from a selection of simple models which might be hoped to display a trend.

of IDE studies is likely just as bad. That said, there are a couple of high significance results which one could point to, namely the massive neutrino study which found a $7-8\sigma$ detection of non-zero coupling using neutrino mass constraints [186] and the study of baryon to DM mass ratios of clusters which found a 14σ deviation from zero coupling [256]. Unfortunately however, the directions of energy transfer in these two findings are contradictory. This is probably no surprise really as they are both such anomalously high significance results, albeit from novel sources of constraint. Their novelty could of course also be seen as a reason to distrust them though, with one from an unconfirmed particle physics result and the other using techniques, (weak lensing and cluster modelling), which are notoriously difficult to implement. Whilst observational constraints are weakened by the addition of new parameters, it doesn't seem unreasonable to hope that as a first approximation a preferred direction of energy transfer might be hinted at by the

data. Table 3.1 summarises some of the observational constraints on different IDE models and highlights the variability of results. There are conflicting results even for the same couplings/parameterisations, doubtless in part due to the inability of data to constrain the model. After over a decade of work on the subject there are no trends across different analyses and the two most significant findings in Table 3.1 are both contradicted by other works using the same couplings. One might wonder if this is due to a change in the sign of the coupling in the past and the use of different data sets, but the two variable sign models are again contradictory and most works just use SNIa, CMB and BAO as standard anyway.

Ultimately one is forced to return to the issue of the ability of current data to constrain the model and the fact that as mentioned in Chapter 1, there are expected to be systematic problems with SNIa and H_0 measurements compare to CMB and BAO data [32]. The question does arise of whether IDE could give rise to this tension, but the disagreement in Table 3.1 is not encouraging and for H_0 at least, the cosmological effects of IDE are minimal out to the measurement's typical redshifts used of $z \approx 0.04$ [357].

Theoretical works on instabilities ruled out many early versions [102, 111], but each way around the problems weakened the testability of the model. The coincidence problem, (real or otherwise), does not seem as easily soluble with IDE as had originally been hoped. Scaling solutions seem too disfavoured now [110] and they may not be representative of whatever real physics underlies the IDE. The best IDE can do then perhaps is to alleviate the problem, but the trade off for extra complexity may well not be worth it.

Since 1998 a clear understanding of IDE models has been gained. The hope now must be that Stage 3 and 4 DE experiments will provide more definitive observations and that H_0 measurements are improved in conjunction with them. Probes such as studies of clusters and DM halos, which exploit the novel effects that IDE has on structure formation and ground based results regarding neutrino mass also offer the prospect of producing useful findings, but at present the results are contradictory.

Chapter 4

Constraining a Model of Interacting Dark Energy

This chapter is a study of perturbations in the $Q \propto \Gamma\rho_x$ model of IDE. The background cosmology of this model has previously been studied in [297], while the growth rate and weak lensing signals for a particular version of it were studied in [298]. In this work the model is studied more generally, with CAMB and CosmoMC being used to place constraints on its parameters by employing a combination of different observational probes. Section 4.1 is concerned with theoretical issues surrounding the model itself, including the derivation of its perturbation equations. Section 4.2 describes the numerical analysis and Section 4.3 presents its results, with conclusions then being drawn in Section 4.4.

4.1 Model Development

In this section issues surrounding the model's background are discussed, its perturbation equations are developed and the initial conditions for the model are determined.

4.1.1 IDE in the background

For convenience we present again the background continuity equations for an IDE model characterized by the energy transfer rate $Q_x = -Q_c$:

$$\dot{\rho}_c = -3\mathcal{H}\rho_c + aQ_c, \tag{4.1}$$

$$\dot{\rho}_x = -3\mathcal{H}(1+w)\rho_x + aQ_x, \tag{4.2}$$

where dots denote derivatives with respect to conformal time τ, $\mathcal{H} = d\ln a/d\tau$ and $w = p_x/\rho_x$. A simple model for Q_x is a linear function in the dark sector energy densities. IDE with $Q_x \propto \rho_c$ has been studied in the greatest detail [130, 295, 296, 107, 297, 298, 299, 305, 306]. However, for constant w the model suffers from an instability in the perturbations [107]. This instability arises because the model of DE as a fluid with constant w is non-adiabatic and can be cured by allowing w to vary in time [305].

Here we study the version with $Q_x \propto \rho_x$,

$$Q_x = -Q_c = \Gamma\rho_x, \tag{4.3}$$

where Γ is a constant transfer rate. The strength of the interaction is measured by $|\Gamma|/H_0$. $\Gamma > 0$ corresponds to energy transfer from DM→DE. This appears somewhat unnatural, since the energy transfer is proportional to ρ_x. For $\Gamma < 0$, the interaction can be seen in the background as a decay of DE into DM, which is a more natural model. The solution of Eq. (4.2) is [297],

$$\rho_x = \rho_{x0}a^{-3(1+w)}\exp\left[\Gamma(t-t_0)\right], \tag{4.4}$$

which shows that $\Gamma > 0$ leads to exponential growth of DE. By Eq. (4.1), it follows that ρ_c eventually becomes negative. The model breaks down if this happens before the current time, which is possible for large Γ/H_0. Observational constraints require $\Gamma/H_0 \lesssim 1$, so that typically the DM density only becomes negative in the future. In this case, we can treat the model as a viable approximation, for the past history of the Universe, to some more complicated interaction that avoids the blow-up of DE in the future. The DE→DM decay model, with $\Gamma < 0$, does not have this problem: both energy

densities remain positive at all times when evolving forward from physical initial conditions [297]. Furthermore, the $\Gamma < 0$ case includes the possibility of beginning with no DM present and having it created entirely from the decay of DE.

We use a phenomenological fluid model for DE, in which we treat w and the soundspeed c_s as arbitrary parameters. This is a commonly used model for non-interacting DE, where the model is known as wCDM. We impose the condition $w \geq -1$ to avoid 'phantom' instabilities that can arise in scalar field models of DE [358, 359]. The limiting case $w = -1$ is admitted by the background equations, but the perturbation equations have singularities (see below). Therefore we assume,

$$w > -1, \quad w = \text{const.} \tag{4.5}$$

For completeness, we consider also the $w \leq -1$ case in Section 4.2.3. In the background, the $\Gamma < 0$ case appears to be better motivated. However, the analysis of perturbations (see below) shows that these models suffer from an instability when $w > -1$. The $\Gamma > 0$ models avoid this instability.

4.1.2 IDE in the perturbations

The critical difference between the background and perturbed IDE is that there is nonzero momentum transfer in the perturbed universe. As emphasised in [107], a model for energy and momentum transfer does not follow from the background model and a covariant and gauge-invariant approach is essential to construct a physically consistent model for energy-momentum transfer.

General IDE

We give a brief summary of the general discussion in [107]. The Friedmann metric with scalar perturbations in a general gauge is,

$$\begin{aligned} ds^2 &= a^2\big\{-\big(1+2\Psi\big)d\tau^2 + 2\partial_i B d\tau dx^i \\ &\quad + \big[\big(1-2\Phi\big)\delta_{ij} + 2\partial_i\partial_j E\big]dx^i dx^j\big\}. \end{aligned} \tag{4.6}$$

Each fluid A satisfies an energy-momentum balance equation,

$$\nabla_\nu T^{\mu\nu}_A = \bar{Q}^\mu_A, \quad \Sigma_A \bar{Q}^\mu_A = 0, \tag{4.7}$$

where bars denote physical values, (i.e. the sum of the background plus the perturbation parts). The second condition expresses conservation of the total energy-momentum tensor. For dark sector interactions, the energy-momentum transfer four-vectors satisfy,

$$\bar{Q}^\mu_x = -\bar{Q}^\mu_c. \tag{4.8}$$

We split $\bar{Q}^\mu_A$ relative to the total four-velocity u^μ, so that,

$$\bar{Q}^\mu_A = \bar{Q}_A u^\mu + F^\mu_A, \quad \bar{Q}_A = Q_A + \delta Q_A, \quad u_\mu F^\mu_A = 0, \tag{4.9}$$

where $\bar{Q}_A$ is the energy density transfer rate relative to u^μ and F^μ_A is the momentum density transfer rate relative to u^μ. To first order,

$$F^\mu_A = a^{-1}\big(0, \partial^i f_A\big), \tag{4.10}$$

where f_A is the (gauge-invariant) momentum transfer potential.

We choose each u^μ_A and the total u^μ as the unique four-velocity with zero momentum density, i.e.,

$$T^\mu_{A\nu} u^\nu_A = -\bar{\rho}_A u^\mu_A, \quad T^\mu_\nu u^\nu = -\bar{\rho} u^\mu, \tag{4.11}$$

$$\bar{\rho}_A = \rho_A + \delta\rho_A, \quad \bar{\rho} \equiv \Sigma_A \rho_A = \rho + \delta\rho. \tag{4.12}$$

Then we have,

$$u^\mu_A = a^{-1}\big(1 - \Psi, \partial^i v_A\big), \quad u^\mu = a^{-1}\big(1 - \Psi, \partial^i v\big), \tag{4.13}$$

$$\big(\Sigma_A \bar{\rho}_A + \Sigma_A \bar{p}_A\big) v = \Sigma_A \big(\bar{\rho}_A + \bar{p}_A\big) v_A, \tag{4.14}$$

where v_A, v are the peculiar velocity potentials. Equations (4.9) and (4.13) imply that,

$$\bar{Q}^A_0 = -a\Big[Q_A\big(1 + \Psi\big) + \delta Q_A\Big], \tag{4.15}$$

$$\bar{Q}^A_i = a\partial_i\Big[Q_A\big(v + B\big) + f_A\Big]. \tag{4.16}$$

The evolution equations for $\delta_A \equiv \delta\rho_A/\rho_A$ and the velocity perturbation $\theta_A = -k^2(v_A + B)$ are [107]:

$$\begin{aligned}
&\dot{\delta}_A + 3\mathcal{H}(c_{sA}^2 - w_A)\delta_A + (1+w_A)\theta_A \\
&\quad + 9\mathcal{H}^2(1+w_A)(c_{sA}^2 - c_{aA}^2)\frac{\theta_A}{k^2} \\
&\quad - 3(1+w_A)\dot{\Phi} + (1+w_A)k^2(B - \dot{E}) \\
&\quad = \frac{aQ_A}{\rho_A}\left[\Psi - \delta_A + 3\mathcal{H}(c_{sA}^2 - c_{aA}^2)\frac{\theta_A}{k^2}\right] + \frac{a}{\rho_A}\delta Q_A,
\end{aligned} \tag{4.17}$$

$$\begin{aligned}
&\dot{\theta}_A + \mathcal{H}(1 - 3c_{sA}^2)\theta_A - \frac{c_{sA}^2}{(1+w_A)}k^2\delta_A - k^2\Psi \\
&\quad = \frac{a}{(1+w_A)\rho_A}\Big\{Q_A\big[\theta - (1+c_{sA}^2)\theta_A\big] - k^2 f_A\Big\}.
\end{aligned} \tag{4.18}$$

Here c_{sA} is the physical soundspeed and c_{aA} is the adiabatic soundspeed.

The physical soundspeed is gauge dependant, $c_{sA}^2 = (\delta p_A/\delta\rho_A)_{\text{restframe}}$. It is the fluid's phase speed and defines the speed at which pressure perturbations propagate through it [360]. The adiabatic soundspeed on the other hand is defined by $c_{aA}^2 \equiv \dot{p}_A/\dot{\rho}_A$ and for constant w_A we have $c_{aA}^2 = w_A$ [277]. For an adiabatic fluid, $c_{sc}^2 = c_{ac}^2$ because $\delta p/\dot{p} = \delta\rho/\dot{\rho}$ [361]. The DM fluid here for example has $c_{sc}^2 = c_{ac}^2 = w_c = 0$. By contrast the DE fluid is non-adiabatic because $c_{ax}^2 = w < 0$ is negative and so c_{ax} cannot be the physical soundspeed.

The physical soundspeed for the fluid DE model is instead a phenomenological parameter. It must be real and non-negative to avoid unphysical instabilities. We choose $c_{sx} = 1$, which is the soundspeed for quintessence (a self-consistent model of DE). The analysis is insensitive to the value of c_{sx}, as long as c_{sx} is close to one, so that DE does not cluster significantly on sub-Hubble scales, see [107] for more details.

DM-baryon bias from IDE

In IDE models, the DE exerts a drag on DM but not on baryons. This leads to a linear DM-baryon bias in the late-time density perturbations, and in

general also to a velocity difference [299]. For baryons after decoupling,

$$\dot{\delta}_b + \theta_b - 3\dot{\Phi} + k^2(B - \dot{E}) = 0, \qquad \dot{\theta}_b + \mathcal{H}\theta_b - k^2\Psi = 0. \tag{4.19}$$

Thus for non-interacting DE models,

$$\theta_c - \theta_b = (\theta_c - \theta_b)_{\rm i}\frac{a_{\rm i}}{a}, \tag{4.20}$$

where i stands for initial. We can choose $(\theta_b - \theta_c)_{\rm i} = 0$, so that,

$$\theta_c - \theta_b = 0, \quad \delta_c - \delta_b = (\delta_c - \delta_b)_{\rm i}. \tag{4.21}$$

Thus in standard DE models, there is no DM-baryon velocity difference, and any linear density perturbation difference is determined by initial conditions.

For IDE models, the interaction induces a non-constant difference between δ_c and δ_b – which is degenerate with the standard galaxy bias. The Euler equation for DM is (4.18), with $c_{sc}^2 = w_c = 0$. This differs from the standard Euler equation unless $k^2 f_c = Q(\theta - \theta_c)$, which follows only for $\bar{Q}_c^\mu = \bar{Q}_c u_c^\mu$, (see below for another version), regardless of the form of $\bar{Q}_c$ [299]. In those models that modify the Euler equation for DM, there will also be a velocity bias. Equations (4.17) and (4.18) imply,

$$\begin{aligned}(\dot{\delta}_c - \dot{\delta}_b) + \frac{aQ_c}{\rho_c}(\delta_c - \delta_b) + (\theta_c - \theta_b) \\ = \frac{a}{\rho_c}\Big[\delta Q_c + Q_c(\Psi - \delta_b)\Big],\end{aligned} \tag{4.22}$$

$$\begin{aligned}(\dot{\theta}_c - \dot{\theta}_b) + \Big(\mathcal{H} + \frac{aQ_c}{\rho_c}\Big)(\theta_c - \theta_b) \\ = \frac{a}{\rho_c}\Big[-k^2 f_c + Q_c(\theta - \theta_b)\Big].\end{aligned} \tag{4.23}$$

Thus there will be a velocity bias, unless $\bar{Q}_c^\mu = \bar{Q}_c u_c^\mu$.

Two Choices of Momentum Transfer

The preceding equations are completely general. A choice must now be made for the energy-momentum transfer in the dark sector. Firstly, the nature of the background energy transfer suggests that we take,

$$\bar{Q}_x = \Gamma\bar{\rho}_x = \Gamma\rho_x(1 + \delta_x) = -\bar{Q}_c. \tag{4.24}$$

Thus we are treating Γ as a universal constant. For the momentum transfer, the simplest physical choice is that there is no momentum transfer in the rest frame of either DM or DE [107, 299]. This leads to two types of model, with energy-momentum transfer four-vectors parallel to either the DM or the DE four-velocity:

$$\bar{Q}^{\mu}_{x} = \bar{Q}_{x}u^{\mu}_{c} = -\bar{Q}^{\mu}_{c} \quad \text{type: } Q\|u_{c}\ , \tag{4.25}$$

$$\bar{Q}^{\mu}_{x} = \bar{Q}_{x}u^{\mu}_{x} = -\bar{Q}^{\mu}_{c} \quad \text{type: } Q\|u_{x}\ . \tag{4.26}$$

Therefore we have,

$$\bar{Q}^{x}_{\mu} = a\Gamma\rho_{x}\big[1+\delta_{x}+\Psi,\, \partial_{i}(v_{A}+B)\big], \tag{4.27}$$

where $A = c, x$ for type $Q\|u_{c}$, $Q\|u_{x}$. By Eq. (4.16), the momentum transfer relative to the background frame is,

$$f_{x} = \Gamma\rho_{x}(v_{c}-v) = -f_{c} \quad \text{for } Q\|u_{c}\ , \tag{4.28}$$

$$f_{x} = \Gamma\rho_{x}(v_{x}-v) = -f_{c} \quad \text{for } Q\|u_{x}\ . \tag{4.29}$$

For both the $Q\|u_{c}$ and $Q\|u_{x}$ models, the density perturbation, (continuity), equation (4.17) reduces to,

$$\dot{\delta}_{c} + \theta_{c} - 3\dot{\Phi} + k^{2}(B-\dot{E}) = a\Gamma\frac{\rho_{x}}{\rho_{c}}(\delta_{c}-\delta_{x}-\Psi), \tag{4.30}$$

$$\begin{aligned}&\dot{\delta}_{x} + 3\mathcal{H}(1-w)\delta_{x} + (1+w)\theta_{x} + 9\mathcal{H}^{2}(1-w^{2})\frac{\theta_{x}}{k^{2}}\\ &\quad - 3(1+w)\dot{\Phi} + (1+w)k^{2}(B-\dot{E})\\ &\quad = a\Gamma\Big[\Psi + 3\mathcal{H}(1-w)\frac{\theta_{x}}{k^{2}}\Big].\end{aligned} \tag{4.31}$$

The velocity perturbation, (Euler), equations are however different. For the $Q\|u_{c}$ model, Eq. (4.18) gives,

$$\dot{\theta}_{c} + \mathcal{H}\theta_{c} - k^{2}\Psi = 0, \tag{4.32}$$

$$\dot{\theta}_{x} - 2\mathcal{H}\theta_{x} - \frac{k^{2}\delta_{x}}{(1+w)} - k^{2}\Psi = \frac{a\Gamma}{(1+w)}\big(\theta_{c}-2\theta_{x}\big). \tag{4.33}$$

For the $Q\|u_x$ model:

$$\dot{\theta}_c + \mathcal{H}\theta_c - k^2\Psi = a\Gamma\frac{\rho_x}{\rho_c}(\theta_c - \theta_x), \tag{4.34}$$

$$\dot{\theta}_x - 2\mathcal{H}\theta_x - \frac{k^2\delta_x}{(1+w)} - k^2\Psi = -\frac{a\Gamma\theta_x}{(1+w)}. \tag{4.35}$$

It follows that the Euler equation for DM in the $Q\|u_c$ model has the standard form, whereas it is modified in the $Q\|u_x$ model.

Instability

There is an obvious issue with the Euler equations for DE, (4.33) and (4.35), as $w \to -1$. Thus we must exclude the value $w = -1$. This is different from the problems associated with a dynamical DE model when w crosses -1, in which case the DE perturbation is well-defined, but at least one more degree of freedom is required, usually leading to its interpretation as a sign of modified gravity. Here though, the DE is not dynamical and the DE perturbation is ill-defined at $w = -1$, so here we must neglect the perturbations, treating it instead as an interacting vacuum.

These equations also reveal an instability for $w \neq -1$ in certain regions of parameter space. The underlying cause of this instability is the choice of $c_{sx}^2 = 1$, which means that the DE fluid is non-adiabatic, as discussed above. It is qualitatively similar to the instability first discovered for constant w IDE in [107], (see also [108, 109, 110, 277, 111] for the case of models with Γ replaced by αH). This is a DE velocity instability, which then drives an instability in the DE and DM density perturbations.

On large scales, we can drop the δ_x and Ψ terms in the DE Euler equations (4.33) and (4.35). In Eq. (4.33) we can also set $\theta_c = 0$ by Eq. (4.32). Then we can integrate to find that,

$$\frac{\theta_x}{\theta_x^{(\Gamma=0)}} = \exp\left[-\alpha\frac{\Gamma}{1+w}(t - t_0)\right], \tag{4.36}$$

where $\theta_x^{(\Gamma=0)}$ is the DE velocity in the non-interacting case, and $\alpha = 2, 1$ for

$Q\|u_c$, $Q\|u_x$. It follows that,

$$-\frac{\Gamma}{(1+w)} > 0 \quad \Rightarrow \quad \text{instability.} \tag{4.37}$$

Note that although one can choose a reference frame where $\theta_x \equiv 0$, the instability is still present in the velocity difference, which is gauge invariant. Given the assumption in Eq. (4.5), the stable models must have positive Γ, i.e.,

$$w > -1 \text{ and } \Gamma > 0 \quad \Rightarrow \quad \text{no instability,} \tag{4.38}$$

for both $Q\|u_c$ and $Q\|u_x$. This defines for us the physically acceptable models. In Section 4.2.3 we allow for any sign of Γ and $1+w$. In order for the instability to affect the perturbation evolution significantly by today, the time scale of growth of θ_x in Eq. (4.36) should be shorter than the Hubble time, i.e., the models with,

$$-\frac{\Gamma}{H_0(1+w)} \gtrsim \begin{cases} 1 & \text{for } Q\|u_c \ , \\ \\ 2 & \text{for } Q\|u_x \ . \end{cases} \tag{4.39}$$

may not be viable. This tallies with the findings in [108] and the results from the full parameter scan confirm this numerically (see the excluded wedges near to $w = -1$ in Fig. 4.8).

4.1.3 Initial conditions

In synchronous gauge, $\Psi = B = 0$ and ordinarily the residual gauge freedom is eliminated by setting $\theta_c = 0$. For the $Q\|u_x$ model the interaction term in the DM Euler equation (4.34) does not in general allow for $\theta_c = 0$. However, since $\Gamma \simeq \mathcal{H}_0 \ll \mathcal{H}$ in Eq's. (4.30)–(4.35), the interactions can be neglected at early times. Using $3\dot{\Phi} + k^2\dot{E} = -h/2$, where h is the synchronous gauge variable [90], the evolution equations used to find the initial conditions for

the dark sector are,

$$2\dot{\delta}_c + \dot{h} = 0, \quad \dot{\theta}_c = 0, \tag{4.40}$$

$$\dot{\delta}_x + 3\mathcal{H}(1-w)\delta_x + (1+w)\theta_x + 9\mathcal{H}^2(1-w^2)\frac{\theta_x}{k^2} + (1+w)\frac{\dot{h}}{2} = 0, \tag{4.41}$$

$$\dot{\theta}_x - 2\mathcal{H}\theta_x - \frac{k^2\delta_x}{(1+w)} = 0. \tag{4.42}$$

The dominant growing mode solution for h found in [90] leads to the standard adiabatic initial conditions for DM,

$$\delta_{c\,\mathrm{i}} = -\frac{1}{2}h = -\frac{1}{2}C(k\tau)^2, \quad \theta_{c\,\mathrm{i}} = 0. \tag{4.43}$$

For DE, we find the leading order solutions, in agreement with [205],

$$\delta_{x\,\mathrm{i}} = \frac{C(1+w)k^2\tau^2}{12w-14}, \quad \theta_{x\,\mathrm{i}} = \frac{Ck^4\tau^3}{12w-14}. \tag{4.44}$$

4.2 Coding for the Model

A number of different computational analysis techniques were employed in the study. Here we briefly describe how these were used to perform the necessary numerical calculations.

4.2.1 Modifying CAMB

The evolution of ΓwCDM models was computed numerically using a modified version of the CAMB Boltzmann code [93], including implementation of the initial conditions derived in Section 4.1.3. The code was adapted in three main ways; to allow for the non-standard background evolution caused by the interactions to evolve the DM velocity perturbation for the $Q \| u_x$ model, (which is ordinarily set to zero), and to suppress perturbations when $|1+w| < 0.01$ due to the blow up of terms in Eq's. (4.33) and (4.35) when $w \to -1$ because it was useful to include the $w = -1$ limit for comparison with ΛCDM.

The largest modification to the standard program was the additional coding required to solve the IDE Friedmann equation. In its standard form CAMB evolves the background using the usual scaling relations for each component in the Friedmann equation, e.g. $\rho_c \propto a^{-3}$. In the $Q \propto \rho_x$ model Eq. (4.4) describes solutions for $\rho_x(t)$ but there is no analytical solution for ρ_c and CAMB requires the energy densities to be functions of the scale factor a so that its time derivative can be found, thus requiring that the background was solved numerically.

This was achieved by using DVERK, the function for solving differential equations which was already used in CAMB. Normally CAMB solves the Friedmann equation every time the expansion rate is required, but this would be too computationally expensive in the non-standard case. Instead the entire background evolution is solved at a preliminary stage and a set of splines created which can be quickly and easily accessed to return the solutions for the dark sector energy densities at any time.

4.2.2 Maple checks

After coding for the new model in CAMB the output data was compared at late-times against a simulation of the same IDE cosmology in the Newtonian limit using the symbolic algebra program Maple. At late times the Newtonian and synchronous gauges are effectively equivalent, allowing a simple numerical check to be made on the novel coding implemented in the modified version of CAMB. Fig's. 4.1 and 4.2 shows two example plots comparing a numerically solved system written in Maple to CAMB output using the same input parameter values, with no deviation being detectable between the two results.

4.2.3 CosmoMC

Using CosmoMC [158] we explored the full parameter space of the ΓwCDM model, as illustrated in Fig. 4.6. The code was modified to vary the two new

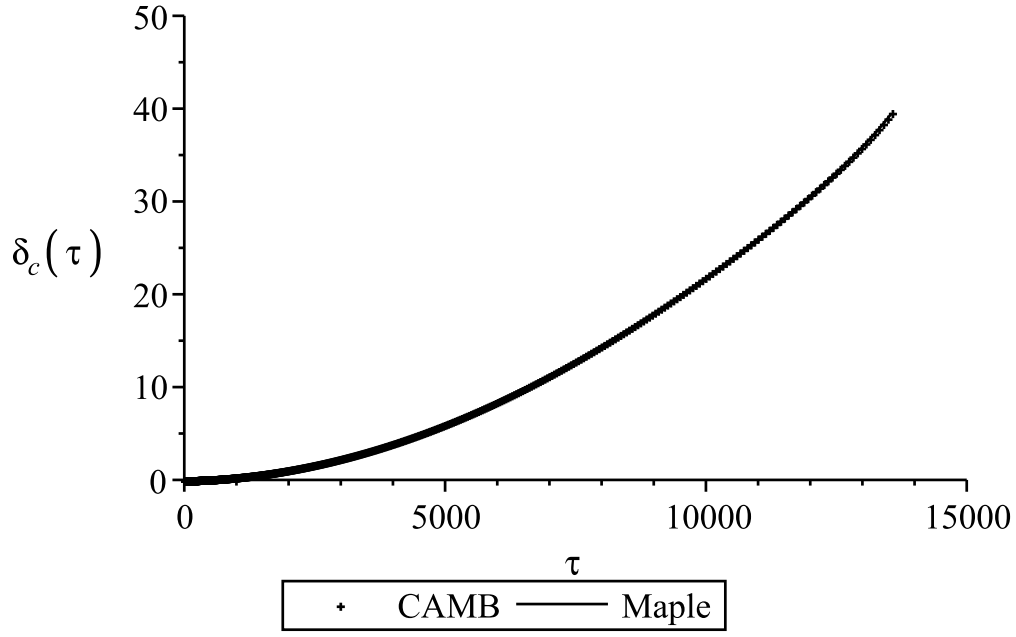

Figure 4.1: Comparison of δ_c for a numerically solved $Q \| u_c$ cosmology with $\Gamma/H_0 = 0.1$ and $w = -0.98$ written in Maple with output from CAMB demonstrating good agreement at late times in the Newtonian limit.

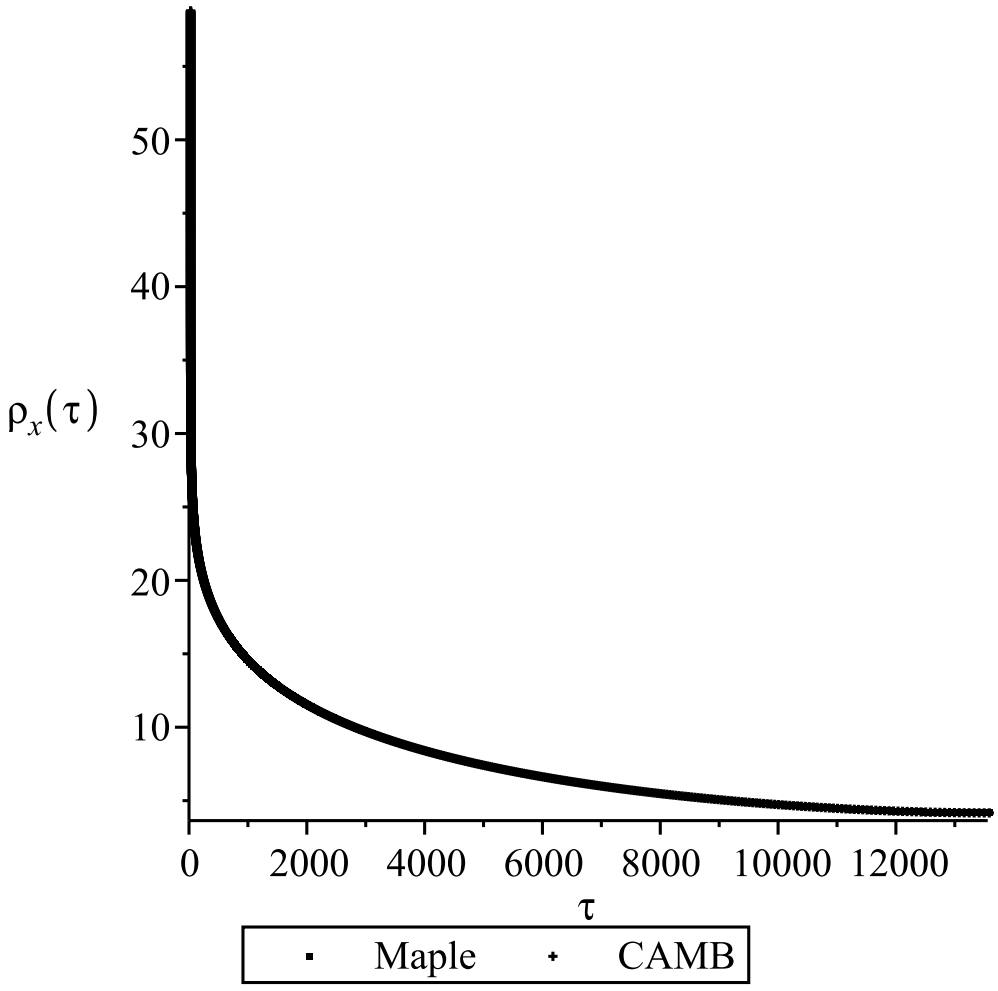

Figure 4.2: Comparison of ρ_x for a numerically solved $Q \| u_c$ cosmology with $\Gamma/H_0 = 0.1$ and $w = -0.98$ written in Maple with output from CAMB demonstrating good agreement at late times in the Newtonian limit.

parameters Γ and w and further coding was necessary to ensure that models with negative DM energy densities were rejected from the MCMC analysis. Another modification was made because CosmoMC varies a parameter $\theta =$ 100 times the ratio of the sound horizon to the angular diameter distance, in place of H_0, as it is more efficient. However the derivation of θ also assumes a standard background evolution. We therefore chose not to use θ, but to constrain H_0 directly instead.

The Hubble Space Telescope, (HST), prior on H_0 assumes a particular model of ΛCDM for evolving $H(z = 0.04)$ [357] up to the present day and so has a slight model dependence. Nevertheless, we neglected this effect due to the low redshift at which the measurement was made. For the BAO however, the scaling solution for the background used to find the redshift of the two data points was replaced by coding to take into account the non-standard background evolution of the IDE models. This was necessary because of the relatively high effective redshift of the BAO measurements, $(z = 0.2, 0.35)$ [362].

4.2.4 Using the SCIAMA supercomputer

Numerical computations were carried out on the SCIAMA High Performance Computer Cluster which is supported by the ICG, SEPNet and the University of Portsmouth. This comprises 1000 cores and enabled multiple MCMC chains to be run simultaneously, before later combining the results to achieve good statistical accuracy. The 'makefiles' of both CAMB and CosmoMC were adapted for use on SCIAMA and runs were submitted using its job queuing system. A full MCMC chain could take days to run, so the use of SCIAMA was invaluable in cutting down the results gathering time required from months to weeks.

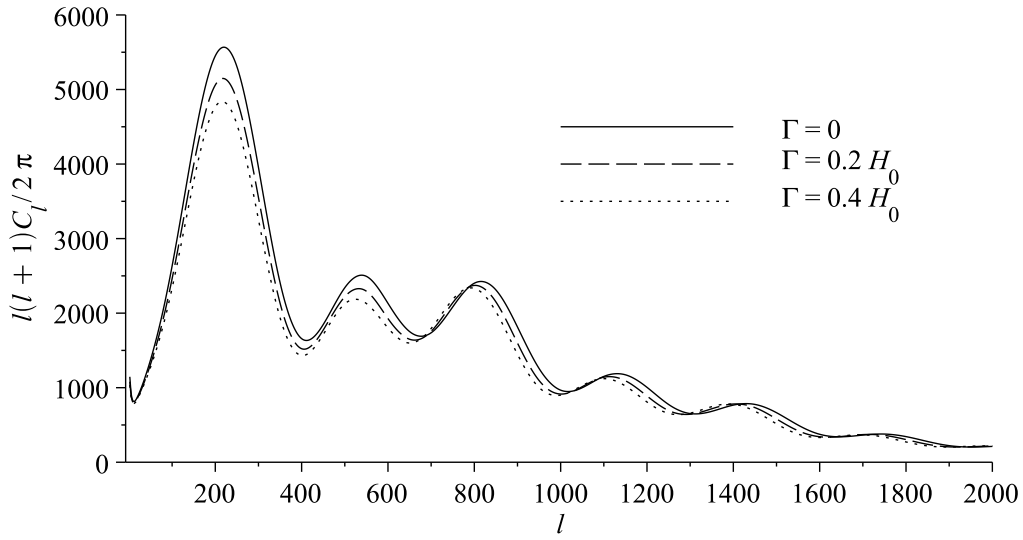

Figure 4.3: CMB power spectra from the modified CAMB code for 3 $Q\|u_c$ models with different values of Γ but identical values of their remaining parameters (see ΓwCDM A,B,C in Table 4.1).

4.3 Analysis

Here we describe the results of the numerical analysis, including qualitative effects on the CMB and matter power spectra, the final probability distribution, best-fit models and the growth of structure.

4.3.1 Effects on the CMB and matter power spectra

Insight into the physical implications of the interaction can be gained by running the modified CAMB code with fixed input parameters, varying only the interaction rate Γ. Figure 4.3 shows the CMB power spectrum for three values of Γ with all other cosmological parameters set to typical values (see Table 4.1 for details).

Positive Γ describes a transfer of energy from DM to DE, so with fixed Ω_c today, the DM energy density would have been correspondingly greater in the past than without interactions. Hence the amplitude of the CMB power

Model	$\bar{Q}^{\mu}_{A}$	$\Delta\chi^2$	Γ/H_0	w	H_0	$\Omega_b h^2$	$\Omega_c h^2$	n_s	A_s	τ_{rei}
ΛCDM best-fit	-	0	-	-1	69.8	0.0223	0.113	0.960	2.16×10^{-9}	0.0844
ΛCDM69	-	0.774	-	-1	69.0	0.0221	0.114	0.958	2.18×10^{-9}	0.0855
ΛCDM70	-	-0.0200	-	-1	70.0	0.0224	0.112	0.962	2.16×10^{-9}	0.0844
wCDM best-fit	-	-0.220	-	-1.03	70.7	0.0222	0.113	0.960	2.18×10^{-9}	0.0883
ΓwCDM A	$Q\|\|u_c$	-	0	-0.98	70.0	0.0226	0.112	0.960	2.10×10^{-9}	0.0900
ΓwCDM B	$Q\|\|u_c$	-	0.2	-0.98	70.0	0.0226	0.112	0.960	2.10×10^{-9}	0.0900
ΓwCDM C	$Q\|\|u_c$	-	0.4	-0.98	70.0	0.0226	0.112	0.960	2.10×10^{-9}	0.0900
ΓwCDM 1a	$Q\|\|u_c$	-0.00830	0.4	-0.95	70.9	0.0222	0.0702	0.961	2.16×10^{-9}	0.0816
ΓwCDM 1b	$Q\|\|u_c$	0.702	0.7	-0.85	70.0	0.0223	0.0311	0.963	2.15×10^{-9}	0.0832
ΓwCDM 2a	$Q\|\|u_x$	-0.236	0.4	-0.95	71.0	0.0224	0.0701	0.966	2.19×10^{-9}	0.0870
ΓwCDM 2b	$Q\|\|u_x$	-0.0420	0.7	-0.85	70.2	0.0224	0.0305	0.966	2.15×10^{-9}	0.0819
$\Gamma \geq 0, w \geq -1$ best-fit	$Q\|\|u_c$	-0.0522	0.366	-0.964	71.0	0.0224	0.0748	0.963	2.18×10^{-9}	0.0849
$\Gamma \geq 0, w \geq -1$ best-fit	$Q\|\|u_x$	-0.322	0.798	-0.851	70.4	0.0224	0.0194	0.965	2.18×10^{-9}	0.0870

Table 4.1: Cosmological parameters for IDE models with $w \geq -1$ and $\Gamma \geq 0$, (see Table 4.2 for more general constraints).

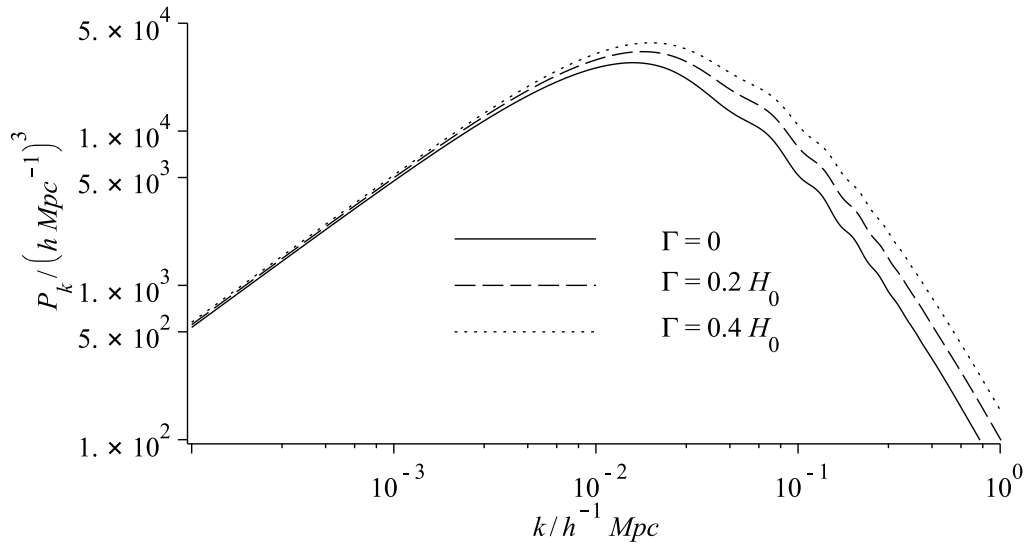

Figure 4.4: Total matter power spectra from the modified CAMB code for 3 $Q\|u_c$ models with different values of Γ but identical values of their remaining parameters (see ΓwCDM A,B,C in Table 4.1).

spectrum is decreased and the position of the peaks shifted, since a larger proportion of DM at early times implies a smaller amount of baryonic matter and therefore a more significant effect from photon driving before decoupling. The present-day matter power spectrum for these choices of Γ shows that a relative increase in the past DM density naturally leads to more structure formation and an increase in the amplitude of the matter power spectrum, as shown in Figure 4.4.

4.3.2 Likelihood analysis

The modified CAMB code was integrated into the CosmoMC MCMC code in order to explore the probability distribution for the parameter space. The data used in the MCMC analysis were; CMB, (WMAP7 [363]), BAO [362], HST [357], and SNIa, (SDSS [364]), data, as well as a prior on Ω_b from big-bang nucleosynthesis [365]. Figure 4.5 shows the 68% and 95% likelihood contours in the $w - \Gamma$ plane for the two different momentum transfer models

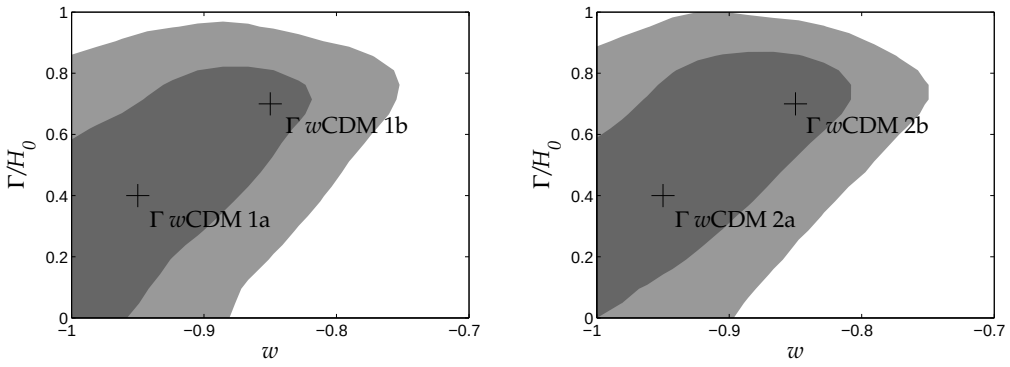

Figure 4.5: Smoothed 68% and 95% contours of the marginalised probability distribution for IDE model with $Q\|u_c$ (left) and $Q\|u_x$ (right) in the range of stability, $w > -1$ and $\Gamma \geq 0$. Crosses identify models chosen to be analysed in more detail (see Table I).

$Q\|u_c$ and $Q\|u_x$, where all other parameters have been marginalised over.

The likelihood regions are very similar for the two models since they differ only in their perturbations and the observations predominantly constrain the background evolution. The best-fit values for the $Q\|u_c$ and $Q\|u_x$ models are different due to the ISW effect on the CMB, and are shown in Table 4.1. For the $Q\|u_x$ model the best-fit value is a genuine global maximum. For the $Q\|u_c$ model however the mean likelihood function of w and Γ is essentially one-tailed, with the true global maximum lying outside of the region we consider physical. Indeed the χ^2 of this point is close to that of ΛCDM. This is because $Q\|u_c$ models in this region can closely mimic the ISW signature of ΛCDM.

There is a plane of degeneracy in the $\Gamma - w - \Omega_c$ parameter space which allows for an entire range of possibilities from zero DM at early times to zero DM at the present day – see Figs. 4.6 and 4.7. The cosmological parameters of the median and best-fit models from CosmoMC for $w = -1$ and when the entire parameter space is considered are shown in Table 4.2.

For $Q\|u_c$ models, the ISW creates a preference in the mean likelihood function for $\Gamma < 0$, as was found previously for the $\bar{Q}^\mu_c = \Gamma \bar{\rho}_c u^\mu_c$ models [306].

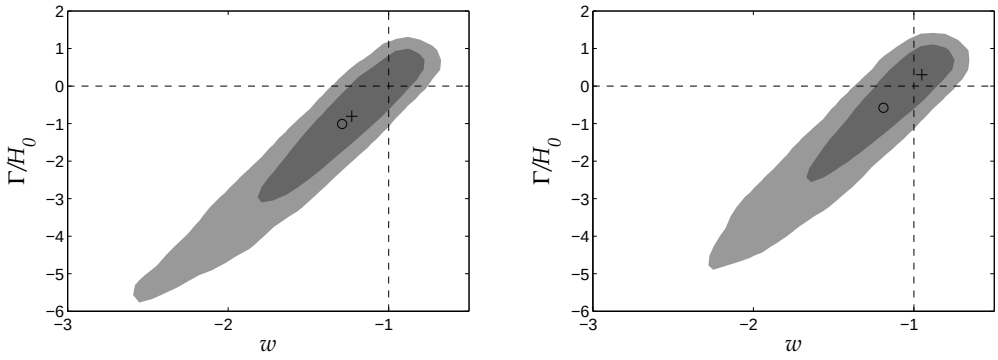

Figure 4.6: 68% and 95% contours of the marginalised probability distribution for the $Q\|u_c$ model (left) and $Q\|u_x$ model (right). The dashed lines cross at the position of ΛCDM, the crosses indicate the best-fits in each case and the circles indicate the median samples. Note that some areas appear only due to smoothing of the distributions (see Fig. 4.8).

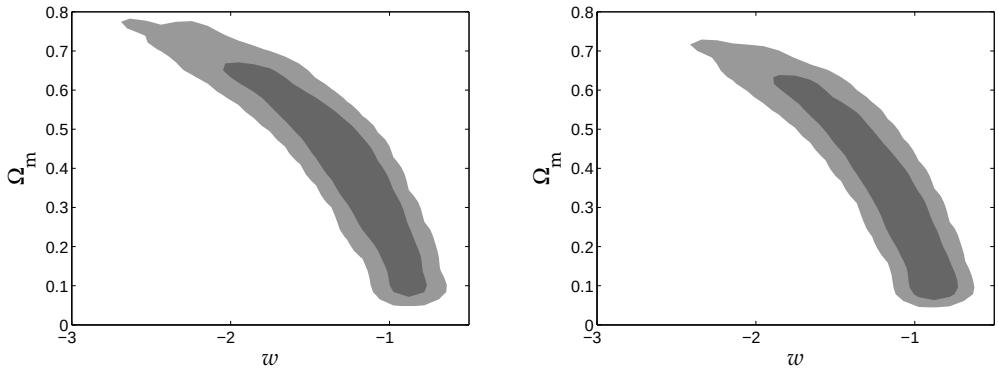

Figure 4.7: 68% and 95% contours of the marginalised probability distribution in the $\Omega_m - w$ plane for the $Q\|u_c$ model (left) and $Q\|u_x$ model (right).

Model	$\bar{Q}^{\mu}_{A}$	$\Delta\chi^2$	Γ/H_0	w	H_0	$\Omega_b h^2$	$\Omega_c h^2$	n_s	A_s	$\tau_{\rm rei}$
$w=-1$ ΓCDM best-fit	$Q\|\|u_c$	-0.146	0.154	-1	70.8	0.0222	0.0974	0.959	2.16×10^{-9}	0.0824
$w=-1$ ΓCDM best-fit	$Q\|\|u_x$	-0.0522	0.0916	-1	70.0	0.0222	0.105	0.959	2.18×10^{-9}	0.0852
all Γ, all w best-fit	$Q\|\|u_c$	-0.294	-0.806	-1.23	70.5	0.0222	0.180	0.956	2.17×10^{-9}	0.0822
all Γ, all w best-fit	$Q\|\|u_x$	-0.0879	0.302	-0.951	70.1	0.0222	0.0823	0.959	2.18×10^{-9}	0.0879
all Γ, all w median	$Q\|\|u_c$	-	-1.01	-1.29	70.7	0.0221	0.194	0.956	2.18×10^{-9}	0.0841
all Γ, all w median	$Q\|\|u_x$	-	-0.578	-1.19	70.7	0.0222	0.164	0.958	2.18×10^{-9}	0.0840

Table 4.2: Cosmological parameters of the median and best-fit samples from CosmoMC for $w=-1$ and when the entire parameter space is considered.

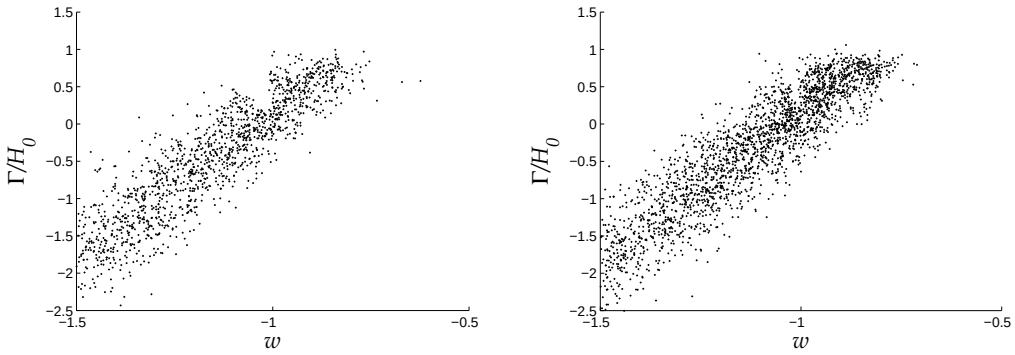

Figure 4.8: Distributions of accepted steps in the MCMC chains for the models with $Q\|u_c$ (left) and $Q\|u_x$ (right)

For $Q\|u_x$ models however, the best-fit has $\Gamma > 0$. This is because the $Q\|u_x$ model has a greater effect on structure growth than the $Q\|u_c$ model, (see Section 4.3.4 below for more details). Despite this the median samples have $\Gamma < 0$ and $w < -1$ for both the $Q\|u_c$ and $Q\|u_x$ models. The background data therefore shows a slight preference for values of $\Gamma < 0$ and $w < -1$. Both the best-fits and the median samples however are relatively close to ΛCDM, given the wide range of interaction strengths allowed.

The singularity in the perturbations at $w = -1$ leads us to impose $|1 + w| < 0.01$, so that we can explore the entire parameter space. The $w = -1$ results are included here to show the proximity of Γ to 0 for these models, in line with ΛCDM. The effect of the $w \neq -1$ instability (4.36) is illustrated in Fig. 4.8. The wedged gaps in the distribution of accepted MCMC chain steps are given by the boundaries of the instability region, defined by (4.39).

4.3.3 Analysis of the best-fit models

Models ΓwCDM 1a,1b,2a,2b (see Table 4.1) were selected for further study. CosmoMC was rerun with Γ and w fixed, to obtain the best-fit values of the other non-derived parameters for input back into CAMB, namely $\Omega_b h^2$, $\Omega_c h^2$, H_0, n_s, (scalar spectral index), A_s, (scalar amplitude), and $\tau_{\rm rei}$, (optical

depth of reionization).

The CMB data is best fit by a particular ISW signal, and the two momentum transfer models differ somewhat in their structure formation histories. DM in the $Q\|u_x$ model receives a change in momentum from the DE perturbations, as expressed by its modified Euler equation (4.32), leading to more structure growth relative to the $Q\|u_c$ model. This means that DE can be weaker for the $Q\|u_x$ model in order to give the same amount of ISW signal as the $Q\|u_c$ model.

Figure 4.9 shows the CMB power spectrum of the best-fit parameter sets for the chosen values of Γ and w. The only significant difference between the CMB spectra is in the ISW feature, although this is not very large because CosmoMC has fit them well to the data from WMAP7. By contrast, there are dramatic differences between the total matter power spectra at $z = 0$ for these models as shown in Fig. 4.10 (see also Fig. 4.11). We chose not to fit the matter power spectrum to observational data – because the modification to the growth of matter perturbations δ_m due to the interactions is degenerate with the galaxy-DM bias b in observations of galaxy number density fluctuations: $\delta_g = b\delta_m$. This degeneracy is governed by equations (4.22) and (4.23). Figure 4.10 does not include any bias.

Note that Ω_c can be very small in models with large Γ, since it can be compensated for by a higher w in order to obtain a sensible H_0. This explains the correlation in the $\Gamma - w$ plane shown in Fig. 4.5, so the late-time effect of the DM may be proportionately even greater than one might think at first glance.

In order to assess the relative merits of these models we have included the change in χ^2 from a ΛCDM baseline. To help put this quantity into context we have also included two best-fit ΛCDM models with H_0 fixed at 69 and 70 km/s/Mpc. The mean likelihoods of the samples vary little in the direction of the degeneracy in the $w - \Gamma$ plane. For example, the difference in $\Delta\chi^2$ between the $Q\|u_x$ best-fit and the ΛCDM best-fit is less than the difference between the two fixed-H_0 ΛCDM models (ΛCDM69 and ΛCDM70

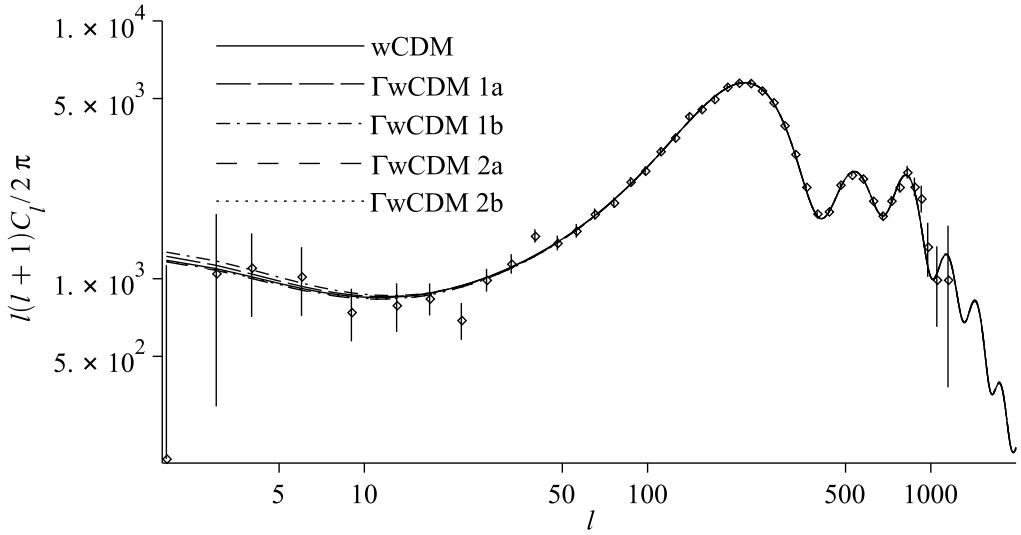

Figure 4.9: CMB power spectra from the modified CAMB code for the WMAP7 wCDM best-fit values and the ΓwCDM 1a,1b,2a,2b models chosen from the 95% confidence range for further analysis (see Table 4.1). The best-fit values of standard cosmological parameters were found using CosmoMC. Models 1a,1b have $\Gamma = 0.4H_0$ and $Q \| u_c$ while 2a,2b have $\Gamma = 0.7H_0$ and $Q \| u_x$.

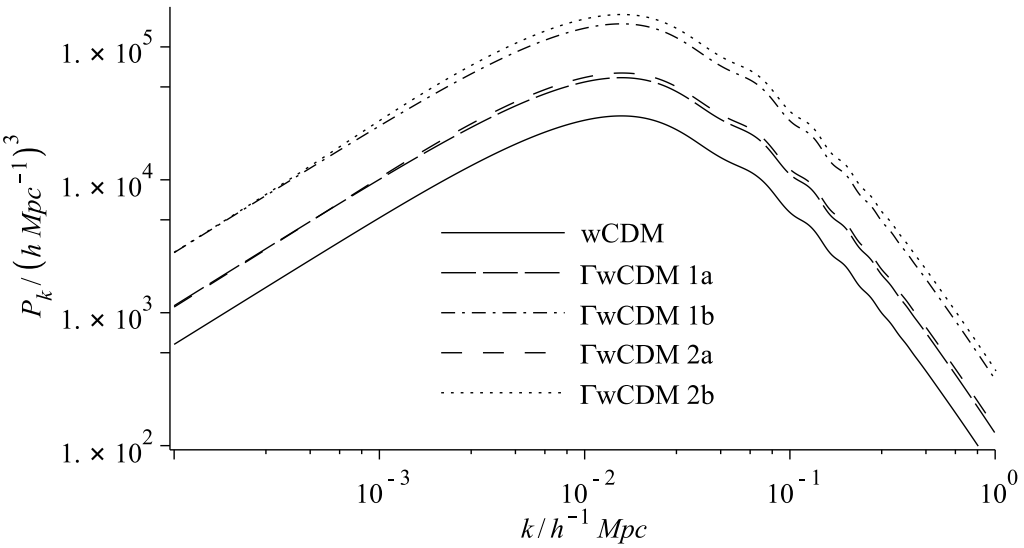

Figure 4.10: Total matter power spectra from the modified CAMB code for the WMAP7 wCDM best-fit values and the ΓwCDM 1a,1b,2a,2b models chosen from the 95% confidence range for further analysis (see Table 4.1). The best-fit values of standard cosmological parameters were found using CosmoMC. Models 1a,1b have $\Gamma = 0.4H_0$ and $Q \| u_c$ while 2a,2b have $\Gamma = 0.7H_0$ and $Q \| u_x$.

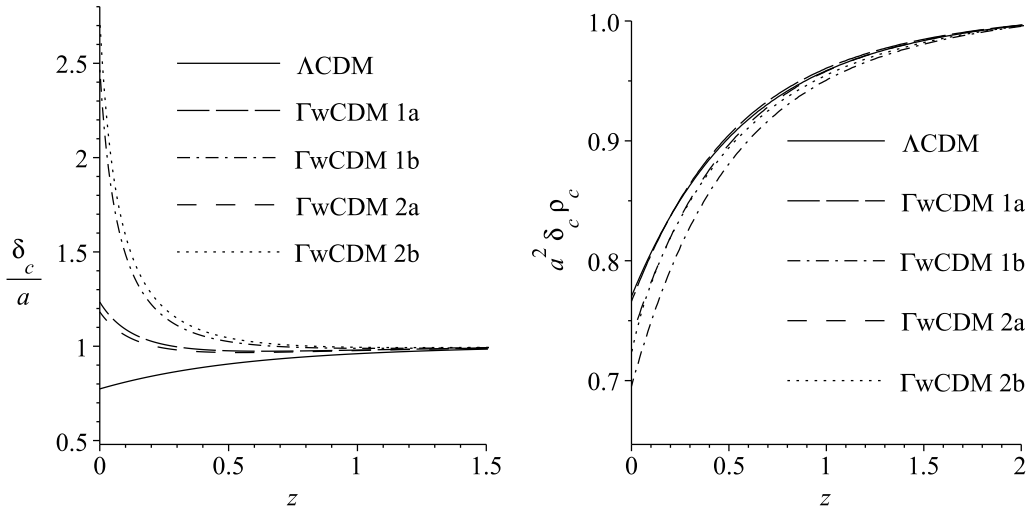

Figure 4.11: *Left:* Normalised growth rates for ΛCDM and the same best-fit models as in Fig's. 4.9 and 4.10. *Right:* The same models but showing a normalised combination of $a^2\rho_c\delta_c$ which is important for the ISW effect.

in Table 4.1).

In Fig. 4.12, we show the effective DE equation of state and the a^3-scaled energy density for DM for the selected models in comparison with ΛCDM. Interestingly, we find that the $w_{\rm eff}$ for the best-fit ΓwCDM models with $w = -0.85$ and -0.95 crosses -1 during its evolution, showing a quintom-like behaviour [366]. Note also that we have focused on the stable $\Gamma > 0$ models with $w > -1$. These models do have a problem of negative DM energy densities in the future, but we assume that this can be cured by a more realistic model to which the model is a good approximation where $\rho_c > 0$.

4.3.4 Growth of structure

The combination of similar ISW signatures and large differences in the growth of structure is unusual – in a ΛCDM cosmology for example, different growth rates lead to correspondingly dissimilar ISW signatures. The mechanisms behind this are clearest from the growth of DM perturbations in the Newtonian

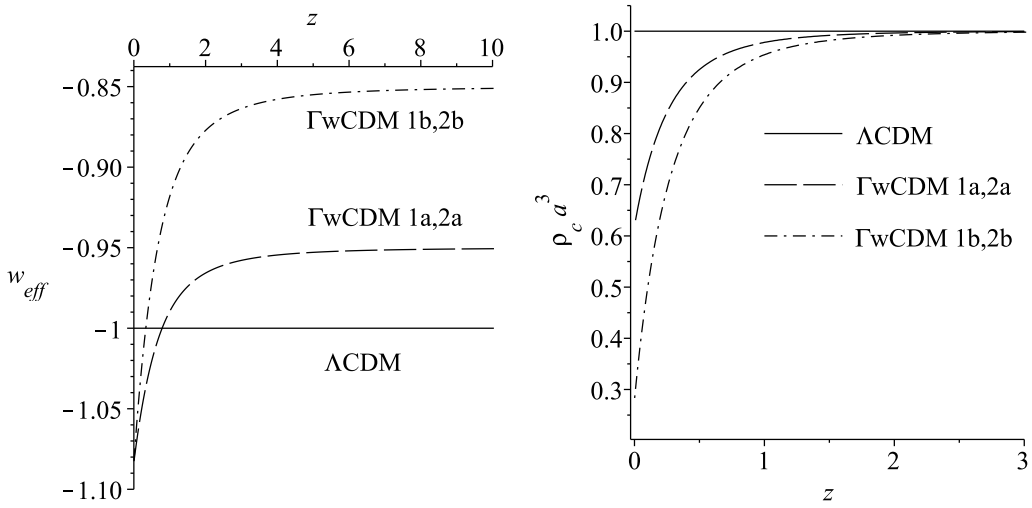

Figure 4.12: Comparison with ΛCDM of the effective DE equation of state (left) and the DM density (right), for the same best-fit models as in Fig's. 4.9 and 4.10.

limit: on sub-Hubble scales at late-times,

$$\delta_c \gg \Psi = \Phi, \quad \delta_x = \dot{\Psi} = \dot{\Phi} = 0, \tag{4.45}$$

in the Newtonian gauge, ($B = 0 = E$). The evolution of synchronous gauge density perturbations in CAMB matches that of perturbations in the Newtonian gauge. The ISW effect comes from gravitational potentials determined by the Poisson equation,

$$k^2\Psi = -4\pi G a^2(\rho_c\delta_c + \rho_b\delta_b), \tag{4.46}$$

and the left panel of Fig. 4.11 shows that there are indeed large differences between the models in their growth rates at late times. The reason the ISW effects can remain small for these models is that the non-standard background evolution, (see Fig. 4.12), can counteract the growth of δ_c in Eq. (4.46) and lead to relatively stable gravitational potentials. The right panel of Fig. 4.11 shows that the relevant combination, $a^2\rho_c\delta_c$, can remain comparable for models with very different structure formation histories such as those

considered here. Note how well the ΓwCDM 1a model mimics the ΛCDM behaviour of $a^2\rho_c\delta_c$, effectively leading to the same χ^2 (see Table I).

This important feature of IDE models has implications for any cosmological test which assumes a standard evolution of the DM energy density during matter domination, such as those for detecting deviations from GR. It may also be useful for distinguishing between IDE and modified gravity models [60], which have standard background evolutions.

Using Eq's. (4.1), (4.2), (4.30), (4.31), (4.32), (4.46) and the Friedmann equation, $\mathcal{H}^2 = 8\pi G a^2\rho/3$, a velocity independent equation of motion for δ_c can be derived for the $Q\|u_c$ model:

$$\ddot{\delta}_c + \mathcal{H}\Big(1 - \frac{a\Gamma}{\mathcal{H}}\frac{\rho_x}{\rho_c}\Big)\dot{\delta}_c = 4\pi G a^2\Big\{\rho_b\delta_b + \rho_c\delta_c\Big[1 + \frac{2\rho}{3\rho_c}\frac{a\Gamma}{\mathcal{H}}\frac{\rho_x}{\rho_c}\Big(2 - 3w + \frac{a\Gamma}{\mathcal{H}}\Big(1 + \frac{\rho_x}{\rho_c}\Big)\Big)\Big]\Big\}. \tag{4.47}$$

Thus the DM perturbations experience effectively different values of $\mathcal{H}$ and G due to the interactions:

$$\frac{\mathcal{H}_{\rm eff}}{\mathcal{H}} = 1 - \frac{a\Gamma}{\mathcal{H}}\frac{\rho_x}{\rho_c}, \tag{4.48}$$

$$\frac{G_{\rm eff}}{G} = 1 + \frac{2\rho}{3\rho_c}\frac{a\Gamma}{\mathcal{H}}\frac{\rho_x}{\rho_c}\left[2 - 3w + \frac{a\Gamma}{\mathcal{H}}\left(1 + \frac{\rho_x}{\rho_c}\right)\right]. \tag{4.49}$$

The $Q\|u_x$ model by contrast has a non-standard Euler equation (4.34), and there remains a term proportional to θ_x which can not in general be neglected:

$$\ddot{\delta}_c + \mathcal{H}\Big(1 - 2\frac{a\Gamma}{\mathcal{H}}\frac{\rho_x}{\rho_c}\Big)\dot{\delta}_c = 4\pi G a^2\Big\{\rho_b\delta_b + \rho_c\delta_c\Big[1 + \frac{2\rho}{3\rho_c}\frac{a\Gamma}{\mathcal{H}}\frac{\rho_x}{\rho_c}\Big(2 - 3w + \frac{a\Gamma}{\mathcal{H}}\Big)\Big]\Big\} + a\Gamma\frac{\rho_x}{\rho_c}\theta_x. \tag{4.50}$$

Nevertheless, for stable models θ_x remains small enough to be negligible and we can define the deviations from standard growth due to the interactions via,

$$\frac{\mathcal{H}_{\rm eff}}{\mathcal{H}} = 1 - 2\frac{a\Gamma}{\mathcal{H}}\frac{\rho_x}{\rho_c}, \tag{4.51}$$

$$\frac{G_{\rm eff}}{G} = 1 + \frac{2\rho}{3\rho_c}\frac{a\Gamma}{\mathcal{H}}\frac{\rho_x}{\rho_c}\left(2 - 3w + \frac{a\Gamma}{\mathcal{H}}\right). \tag{4.52}$$

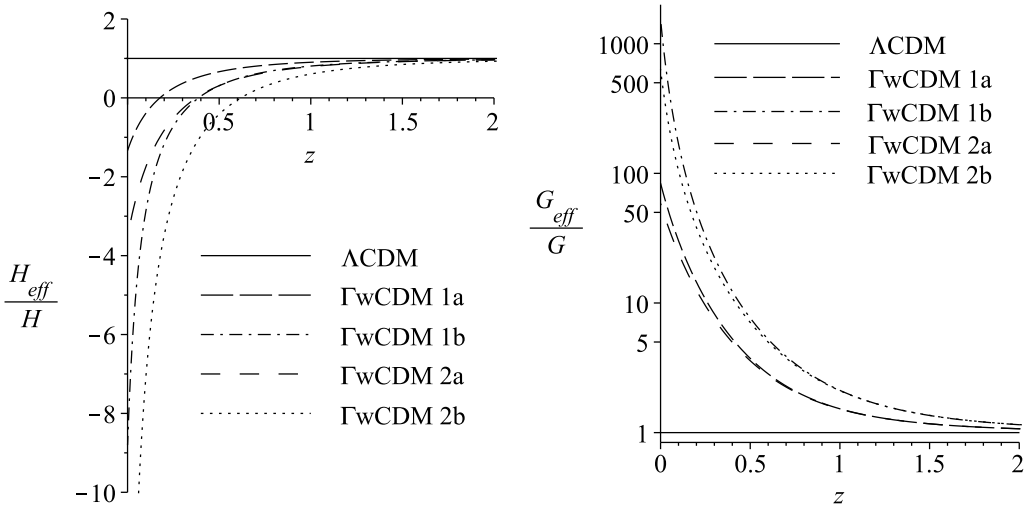

Figure 4.13: Deviations from ΛCDM of the effective Hubble parameter (left) and effective Newton constant for δ_c (right), for the same best-fit models as in Fig's. 4.9 and 4.10.

These equations show that the differences in momentum transfer lead to a greater modification to the growth via $\mathcal{H}_{\rm eff}$ for the $Q\|u_x$ model and via $G_{\rm eff}$ for the $Q\|u_c$ model, as can be seen in Fig. 4.13. It is clear that DM perturbations in the models with large couplings are already beginning to grow exponentially at the present day (compare [277, 111, 300, 210]). In models with $\bar{Q}^\mu_x = \Gamma\bar{\rho}_c u^\mu_c$, as studied in [107, 306, 305], there is no interaction source term in the synchronous gauge version of Eq. (4.30) and so the DM perturbations are stable.

4.4 Conclusions

We have studied a model of dark sector interactions with an energy transfer proportional to the DE energy density, and with momentum transfer vanishing either in the DM or the DE rest frame. We performed an MCMC analysis and found the best-fit parameters using a data compilation that predominantly constrains the background evolution. We found model con-

straints to which ΛCDM is a good fit, although parameter degeneracies do allow for significant interaction rates at the present day and even admit the two extreme cases of zero DM at early times and zero DM today.

We analysed the growth of structure in this model and found that the effects of large growth rates on the ISW signature in the CMB can be suppressed by the non-standard background evolution. We also showed that interactions can greatly enhance growth in these models via effective Hubble and Newton constants, in varying degrees depending on the momentum transfer.

There appears to be some tension between the background evolution and structure formation. The CMB, SNIa and BAO data slightly favour interactions, while the growth rate of DM perturbations likely rules out large interaction rates. There is a degeneracy with galaxy bias, which deserves further investigation. This would allow the use of the full range of large-scale structure data and would significantly improve the constraints on the IDE models considered here.

Interacting models are known to be degenerate with modified gravity models [64, 344, 299, 300, 335, 367]. It is important to break this degeneracy, in order to strengthen cosmological tests of GR – currently devised tests do not incorporate the possibility of a dark sector interaction. The key distinguishing features of IDE and MG occur in: (1) the late-time anisotropic stress, i.e. $\Psi - \Phi$; (2) the evolution of the background DM density, $\rho_c(1+z)^{-3}$; (3) the DM-baryon bias:

	MG	IDE
$\Psi - \Phi$	$\neq 0$	$= 0$
$\rho_c(1+z)^{-3}$	$=$ const	$\neq$ const
$\delta_b - \delta_c$	$=$ const	$\neq$ const
$\theta_b - \theta_c$	$= 0$	can be nonzero

These features are the basis for breaking the degeneracy. For example, any difference between the metric potentials can be tested via peculiar velocities, (a probe of Ψ), weak lensing and ISW, (both sensitive to $\Psi + \Phi$). Whether

or not it is possible to distinguish between IDE and MG using current observations is investigated in Chapter 6.

Chapter 5

Mathematically Equivalent Models of Interacting Dark Energy and Modified Gravity

In this chapter we develop the framework required for the study of IDE and MG which follows. After a brief introduction to conformal equivalence in Section 5.1 and the historical context in Section 5.2 we demonstrate the equivalence of the two descriptions mathematically, constructing the perturbation equations from two equivalent actions in Section 5.3. Finally the differences between the evolutions of quantities in the two models are looked at in Section 5.4

5.1 Conformal Equivalence

STT's contain an extra gravitational degree of freedom. They describe gravity using not only the metric tensor $g_{\mu\nu}$, but also a gravitational scalar field ϕ. These theories can however be described in terms of 'Einstein' gravity by making a suitable conformal transformation to what is known as the Einstein 'frame', while STT's are said to exist in the Jordan frame. The scalar gravitational component can then be recast as a physical scalar field coupled

to matter and GR is regained with the Einstein-Hilbert action.

5.2 Historical Context

An early example of a simple STT was proposed by Brans and Dicke in 1961 [113], (building on work by Jordan [117]). The equivalence to a coupled-matter system was later shown in [114] and it was noted that each description has certain advantages over the other. This is because in STT's the basic field equations such as the Friedmann equation are more complex than in GR, while the evolution equations for matter in the Jordan frame are simpler than in the coupled case.

Over the years there was much debate about the equivalence of these two frames, in particular their physical equivalence and which of the frames should be considered as physical, (see [368] for a comprehensive review). However recent works have explicitly shown the absolute physical equivalence of the Jordan and Einstein frames, (see [369] and references therein), demonstrating that they are equally valid as physical descriptions.

5.3 The Dual MG/IDE Descriptions

This section demonstrates the conformal equivalence of a STT and an IDE model by following their construction through from two equivalent actions to their perturbation equations. In MG theories all matter is generally free from couplings in the Jordan frame. The evolution of matter therefore simply obeys the standard evolution equations. This can be thought of as the distinguishing feature of the Jordan frame, while the distinguishing feature of the Einstein frame is that the gravity sector is described by GR through the Einstein-Hilbert action. In IDE however, only the DM couples to DE, so a transformation to its 'Jordan frame' not only removes the Einstein frame DM coupling, but it also introduces a baryon coupling which was not present in the Einstein frame.

This is the setup we shall consider here, the main purpose of which is to develop the equations for use in a study of the distinguishability of IDE and MG in Chapter 6, where we assume some sort of screening mechanism to be effective in the Jordan frame, thus negating baryon constraints. For the most part therefore we shall focus only on DM and not include the baryon equations of motion, although some description of points of interest which this framework presents is given initially.

The total action for the system may be written as,

$$S = S_{R+s} + S_c + S_b \tag{5.1}$$

where R, s, c and b stand for Ricci, scalar, CDM and baryons respectively. We can consider this action in two different representations of spacetime, the Einstein frame with metric $g_{\mu\nu}$ and the Jordan frame with metric $\tilde{g}_{\mu\nu}$, linked by a conformal transformation,

$$g_{\mu\nu} = G\phi\tilde{g}_{\mu\nu}, \quad \tilde{g}^{\mu\nu} = G\phi g^{\mu\nu}, \quad \sqrt{-g} = (G\phi)^2\sqrt{-\tilde{g}}, \tag{5.2}$$

with ϕ being a scalar field. The definitions of the separate actions for a generalised STT and its IDE counterpart are,

$$\begin{aligned}
S_{R+s} &= S_{EH} + S_\psi \\
&= \frac{1}{16\pi G}\int d^4x\sqrt{-g}R + \\
&\quad \int d^4x\sqrt{-g}\left[-\frac{1}{2}(\nabla\psi)^2 - V(\psi)\right] \\
&= S_{BD} + S_\phi \\
&= \int d^4x\sqrt{-\tilde{g}}\left[\phi\tilde{R} - \frac{\omega(\phi)}{\phi}(\tilde{\nabla}\phi)^2 - U(\phi)\right], \qquad (5.3) \\
S_c &\equiv S_c(\tilde{g}_{\mu\nu}, \zeta), \qquad (5.4) \\
S_b &\equiv S_b(g_{\mu\nu}, \varsigma), \qquad (5.5)
\end{aligned}$$

where BD stands for Brans-Dicke, EH stands for Einstein-Hilbert, ζ and ς denote the CDM and baryon matter fields, and ψ is a new, (non-gravitational), scalar field which exists in the Einstein frame and is related to ϕ by [370],

$$\phi(\psi) = e^{C(\psi)\psi}, \tag{5.6}$$

with the C/ω and V/U connections being [370],

$$C = \sqrt{\frac{16\pi G}{3+2\omega}}, \quad \text{and} \quad V = \frac{Ue^{-2C\psi}}{16\pi G}. \tag{5.7}$$

Note that the CDM and baryon actions S_c and S_b are each defined using the metric of the frame in which they are free from coupling to the scalar fields. As mentioned above, (and also shown below), the DM is free from coupling in the Jordan frame, whilst it couples to the DE ψ in the Einstein frame and the baryons are free from coupling in the Einstein frame, but couple directly to the gravitational scalar field in the Jordan frame.

The energy-momentum tensors for the various components must be defined in each frame and along with their transformation rules these are,

$$\tilde{T}^a_{\mu\nu} \equiv -\frac{2}{\sqrt{-\tilde{g}}}\frac{\delta S_a}{\delta \tilde{g}^{\mu\nu}} = \phi T^a_{\mu\nu}, \tag{5.8}$$

$$T^a_{\mu\nu} \equiv -\frac{2}{\sqrt{-g}}\frac{\delta S_a}{\delta g^{\mu\nu}} \tag{5.9}$$

$$\tilde{T}^{\mu\nu}_a = \phi^3 T^{\mu\nu}_a, \tag{5.10}$$

$$\tilde{T}_a = \phi^2 T_a, \tag{5.11}$$

$$T^{\mu\nu} = \sum_a T^{\mu\nu}_a, \tag{5.12}$$

where a can be ϕ, ψ, c or b.

5.3.1 Field equations

Varying the total action with respect to the metrics gives field equations for the Einstein frame,

$$R_{\mu\nu} - \frac{1}{2}g_{\mu\nu}R = 8\pi G T_{\mu\nu} \tag{5.13}$$

and for the Jordan frame

$$\begin{aligned}\tilde{R}_{\mu\nu} - \frac{1}{2}g_{\mu\nu}\tilde{R} &= \frac{8\pi G}{\phi}\tilde{T}_{\mu\nu} + \frac{1}{\phi}(\tilde{\nabla}_\mu\tilde{\nabla}_\nu\phi - \tilde{g}_{\mu\nu}\tilde{\Box}\phi) \\ &\quad + \frac{\omega(\phi)}{\phi^2}\left[\tilde{\nabla}_\mu\phi\tilde{\nabla}_\nu\phi - \frac{1}{2}\tilde{g}_{\mu\nu}(\tilde{\nabla}\phi)^2\right] \\ &\quad - \frac{1}{2\phi}\tilde{g}_{\mu\nu}U(\phi).\end{aligned} \tag{5.14}$$

The Euler-Lagrange equations can be used to find the equations of motion for the scalar fields, eg,

$$\frac{d\hat{L}}{d\psi} - \nabla_\mu \left(\frac{\partial \hat{L}}{\partial(\nabla_\mu \psi)} \right) = 0, \tag{5.15}$$

$$L \equiv \sqrt{-g}\hat{L}, \qquad S_\psi = \int d^4x L, \tag{5.16}$$

giving for ψ,

$$\Box\psi - \frac{\partial V}{\partial \psi} = \frac{1}{2} C(\psi) T_c, \tag{5.17}$$

and for ϕ

$$\tilde{R} + 2\frac{\omega(\phi)}{\phi}\tilde{\Box}\phi = -\left(\frac{1}{\phi}\frac{\partial \omega}{\partial \phi} - \frac{\omega}{\phi^2} \right) (\tilde{\nabla}\phi)^2 + \frac{\partial U}{\partial \phi} - \frac{8\pi G}{\phi}\tilde{T}_b, \tag{5.18}$$

where the baryon term has entered because its action, Eq. (5.5), depends on $g_{\mu\nu} = \phi\tilde{g}_{\mu\nu}$, whereas the DM action, Eq. (5.4), is independent of ϕ. Taking the trace of Eq. (5.14) and substituting the result into Eq. (5.18) then gives a new equation of motion for ϕ,

$$\tilde{\Box}\phi = \frac{1}{2\omega(\phi) + 3}\left[8\pi G\tilde{T}_c - \frac{\partial \omega}{\partial \phi}(\tilde{\nabla}\phi)^2 + \phi\frac{\partial U}{\partial \phi} - 2U(\phi) \right]. \tag{5.19}$$

Notice that this causes the baryon term to be cancelled, so the Jordan frame gravitational scalar field ϕ does not notice the baryons at all, (except indirectly through its own coupling to the metric). This makes perfect sense because the DM's relationship to ϕ is determined by its Einstein frame coupling to the DE ψ, whereas for the baryons no such coupling exists to get translated into the minimal Jordan frame coupling to ϕ that DM experiences. Instead the baryons couple to ϕ directly, as can be seen in the Bianchi identities,

$$\tilde{\nabla}_\mu \tilde{T}_c^{\mu\nu} = 0, \qquad \nabla_\mu T_c^{\mu\nu} = -\frac{1}{2}C(\psi)T_c\partial^\nu\psi = -\nabla_\mu T_\psi^{\mu\nu}, \tag{5.20}$$

$$\nabla_\mu T_b^{\mu\nu} = 0, \qquad \tilde{\nabla}_\mu \tilde{T}_b^{\mu\nu} = \frac{\partial^\nu \phi}{2\phi}\tilde{T}_b = -\tilde{\nabla}_\mu \tilde{T}_\phi^{\mu\nu}, \tag{5.21}$$

where we used a reduced equation of motion for ϕ, (i.e. not including the coupling to gravity). The baryons still appear in the Jordan frame field equations (5.14), so they still feel the same gravity as the DM, but in addition

they feel an extra force due to their direct interactions with the gravitational scalar field ϕ. This is clearly an unusual setup as the gravity, (spacetime), and matter, (energy), sectors would normally be completely distinct, even in theories of MG. Indeed the idea of an actual gravitational force is a Newtonian one and was superseded by the notion of curvature in GR. This setup therefore seems more like a particle physics theory, where the gravity sector is described in terms of particles.

There are tight observational constraints from the solar system on the coupling of baryons to other species [371, 133] and weaker constraints on cosmological scales, (see [372] and references therein). It should be possible to translate these into constraints on ϕ in this setup and subsequently also on ψ, but we leave this for other work. Finally, we note that the Jordan frame baryon coupling would effectively vary only with space in the 'quasi-static' approximation which is often used in MG analyses, (where temporal derivatives of ϕ are neglected with respect to spatial ones because the change in the effective value of Newton's constant is know to be small at late times).

5.3.2 Scalar field equations of motion

From here on in the derivations we shall not present the equations for baryons as they are not required for the work which follows in Chapter 6. Furthermore we shall now be concerned with the perturbations and so we shall use bars to distinguish physical quantities, (i.e. background plus perturbation parts), from their background averages. The IDE scalar field equation of motion (5.17) may be written as,

$$\Box\bar{\psi} - \frac{\partial\bar{V}}{\partial\psi} = \frac{1}{2}CT_c = -\frac{1}{2}C\rho_c(1+\delta_c). \tag{5.22}$$

For the D'Alembertian of $\bar{\psi} = \psi + \varphi$ in the Newtonian regime, ($\dot{\Psi} = \dot{\Phi} = 0$), we have,

$$\Box\bar{\psi} = a^{-2}(\partial_i\partial^i\varphi - \ddot{\psi} - \ddot{\varphi} + 2\Psi\ddot{\psi} - 2\mathcal{H}\dot{\psi} + 4\mathcal{H}\Psi\dot{\psi} - 2\mathcal{H}\dot{\varphi}), \tag{5.23}$$

while the scalar field potential is split up as,

$$\bar{V} = V + \frac{\partial V}{\partial \psi}\varphi, \quad \Rightarrow \quad \frac{\partial \bar{V}}{\partial \psi} = \frac{\partial V}{\partial \psi} + \frac{\partial^2 V}{\partial \psi^2}\varphi. \tag{5.24}$$

This gives us a background part to the EoM,

$$\ddot{\psi} = -2\mathcal{H}\dot{\psi} - a^2\frac{\partial V}{\partial \psi} + \frac{1}{2}Ca^2\rho_c, \tag{5.25}$$

and a perturbation part,

$$\partial_i\partial^i\varphi = -\frac{1}{2}Ca^2\rho_c\delta_c, \tag{5.26}$$

where we have neglected perturbations as small relative to δ_c and time derivatives as small relative to spatial ones.

For MG, the function $\omega(\phi)$ is now split into its background and a perturbation as,

$$\bar{\omega} = \omega + \frac{\partial \omega}{\partial \phi}\chi, \quad \Rightarrow \quad \frac{\partial \bar{\omega}}{\partial \phi} = \frac{\partial \omega}{\partial \phi} + \frac{\partial^2 \omega}{\partial \phi^2}\chi, \tag{5.27}$$

with the potential being split up in the same way,

$$\bar{U} = U + \frac{\partial U}{\partial \phi}\chi, \quad \Rightarrow \quad \frac{\partial \bar{U}}{\partial \phi} = \frac{\partial U}{\partial \phi} + \frac{\partial^2 U}{\partial \phi^2}\chi. \tag{5.28}$$

The D'Alembertian of $\bar{\phi} = \phi + \chi$ in Eq. (5.19), the equation of motion for the gravitational scalar field expands to,

$$\tilde{\Box}\bar{\phi} = a^{-2}(\partial_i\partial^i\chi - \ddot{\phi} - \ddot{\chi} + 2\Psi\ddot{\phi} - 2\mathcal{H}\dot{\phi} + 4\mathcal{H}\Psi\dot{\phi} - 2\mathcal{H}\dot{\chi}). \tag{5.29}$$

Substituting this in means that in the background we have,

$$\ddot{\phi} = -2\mathcal{H}\dot{\phi} + \frac{a^2}{2\omega+3}\left(8\pi G\rho_c - \frac{\dot{\phi}^2}{a^2}\frac{\partial \omega}{\partial \phi} - \phi\frac{\partial U}{\partial \phi} + 2U\right), \tag{5.30}$$

and in the perturbations we have,

$$\begin{aligned}\ddot{\chi} = \partial_i\partial^i\chi - 2\mathcal{H}\dot{\chi} + \frac{a^2}{2\omega+3}\Bigg[&8\pi G\rho_c\delta_c - \frac{\partial U}{\partial \phi}(2\Psi\phi - 3\chi) \\ &-\frac{2\dot{\phi}\dot{\chi}}{a^2}\frac{\partial \omega}{\partial \phi} - \frac{\dot{\phi}^2}{a^2}\frac{\partial^2 \omega}{\partial \phi^2}\chi - 4\Psi U + \phi\frac{\partial^2 U}{\partial \phi^2}\chi\Bigg].\end{aligned} \tag{5.31}$$

If we now apply the quasi-static approximation, $\dot{\chi} \ll \partial_i \partial^i \chi$, and neglect the terms containing Ψ and χ as being small relative to the δ_c term, since we shall only be concerned with late times, we end up with,

$$\partial_i \partial^i \chi \simeq -\frac{8\pi G}{2\omega + 3} a^2 \rho_c \delta_c. \tag{5.32}$$

5.3.3 Metric perturbations

The perturbed metric in the Newtonian regime may be written,

$$ds^2 = a^2[-(1+2\Psi)d\tau^2 + (1-2\Phi)\gamma_{ij}dx^i dx^j]. \tag{5.33}$$

The 00 component of the Jordan frame 'Einstein equations' Eq. (5.14) gives the background 'Friedmann equation',

$$\mathcal{H}^2 = \frac{8\pi G}{3\phi} a^2 \rho - \mathcal{H}\frac{\dot{\phi}}{\phi} + \frac{\omega}{6}\left(\frac{\dot{\phi}}{\phi}\right)^2 + \frac{a^2}{6\phi} U., \tag{5.34}$$

and combining this with the ii component we have the modified acceleration equation in the background,

$$\frac{\ddot{a}}{a} = -\frac{4\pi G}{3\phi} a^2 (3p - \rho) - \frac{\ddot{\phi}}{2\phi} - \frac{\omega}{6}\left(\frac{\dot{\phi}}{\phi}\right)^2 + \frac{a^2 U}{3\phi} - \mathcal{H}\frac{\dot{\phi}}{\phi}. \tag{5.35}$$

The perturbation equations for the modified Brans-Dicke system come from perturbing the four 'Einstein equations' (5.14). We shall here derive only the ii component as an informative example of how this is done and the demonstration of a sign error in previous works. To begin with we multiply the ij component of the Jordan frame field equations (5.14) by g^{ij},

$$\begin{aligned} g^{ij}(R_{ij} - \frac{1}{2}g_{ij}R) &= g^{ij}\left\{\frac{8\pi G}{\bar{\phi}}T_{ij} + \frac{1}{\bar{\phi}}(\nabla_i\nabla_j\bar{\phi} - g_{ij}\Box\bar{\phi})\right. \\ &\left. + \frac{\bar{\omega}}{\bar{\phi}^2}\left[\nabla_i\bar{\phi}\nabla_j\bar{\phi} - \frac{1}{2}g_{ij}(\nabla\bar{\phi})^2\right] - \frac{1}{2\bar{\phi}}g_{ij}\bar{U}\right\}. \end{aligned} \tag{5.36}$$

Taking each term in turn, we have for the left hand side,

$$\begin{aligned} g^{ij}\left(R_{ij} - \frac{1}{2}g_{ij}R\right) &= 6a^{-2}\left(\frac{1}{2}\mathcal{H}^2 - \frac{\ddot{a}}{a} + 2\frac{\ddot{a}}{a}\Psi - \mathcal{H}^2\Psi + \ddot{\Phi}\right. \\ &\left. + 2\mathcal{H}\dot{\Phi} + \mathcal{H}\dot{\Psi} + \frac{1}{3}\partial_i\partial^i\Psi - \frac{1}{3}\partial_i\partial^i\Phi\right), \end{aligned} \tag{5.37}$$

the first term on the right hand side,

$$\begin{aligned} g^{ij}\frac{8\pi G}{\bar{\phi}}T_{ij} &= g^{ij}\frac{8\pi G}{\bar{\phi}}g_{ik}T^k_j \\ &= \gamma^{ij}\frac{8\pi G}{\phi}\gamma_{ik}\left(1-\frac{\chi}{\phi}\right)\left[(p+\delta p)+\pi^k_j\right] \\ &= 3\frac{8\pi G}{\phi}\left(1-\frac{\chi}{\phi}\right)(p+\delta p). \end{aligned} \tag{5.38}$$

the second term on the right hand side,

$$\begin{aligned} g^{ij}\frac{1}{\bar{\phi}}\left(\nabla_i\nabla_j\bar{\phi}-g_{ij}\Box\bar{\phi}\right) &= \frac{1}{\bar{\phi}}\left(g^{ij}\nabla_i\partial_j\bar{\phi}-3g^{\mu\nu}\nabla_\mu\nabla_\nu\bar{\phi}\right) \\ &= \frac{1}{\bar{\phi}}\left[g^{ij}\nabla_i\partial_j\chi-3(g^{00}\nabla_0\partial_0\bar{\phi}-g^{ij}\nabla_i\partial_j\chi)\right] \\ &= \frac{1}{\phi}\left(1-\frac{\chi}{\phi}\right)\Big[-3g^{00}(\partial_0\partial_0\bar{\phi}-\Gamma^0_{00}\partial_0\bar{\phi}-\Gamma^i_{00}\partial_i\chi) \\ &\quad -2g^{ij}\left(\partial_i\partial_j\chi-\Gamma^0_{ij}\partial_0\chi-\Gamma^k_{ij}\partial_k\chi\right)\Big] \\ &= \frac{1}{\phi}\left(1-\frac{\chi}{\phi}\right)\Big\{3a^{-2}(1-2\Psi)\Big[\ddot{\phi}+\ddot{\chi} \\ &\quad -\left(\mathcal{H}+\dot{\Psi}\right)\left(\dot{\phi}+\dot{\chi}\right)\Big] \\ &\quad -2a^{-2}(1+2\Phi)\gamma^{ij}\{\partial_i\partial_j\chi \\ &\quad -[\mathcal{H}-2\mathcal{H}(\Phi+\Psi)-\dot{\Phi}]\gamma_{ij}\dot{\chi}\}\Big\} \\ &= \frac{3}{a^2\phi}\Big(1-\frac{\chi}{\phi}\Big)\Big(\ddot{\phi}+\ddot{\chi}-\mathcal{H}\dot{\phi}-\mathcal{H}\dot{\chi}- \\ &\quad \dot{\Psi}\dot{\phi}-2\Psi\ddot{\phi}+2\Psi\mathcal{H}\dot{\phi}-\frac{2}{3}\partial_i\partial^i\chi\Big), \end{aligned} \tag{5.39}$$

the third term on the right hand side,

$$\begin{aligned} g^{ij}\frac{\bar{\omega}}{\bar{\phi}^2}[\nabla_i\bar{\phi}\nabla_j\bar{\phi}-\frac{1}{2}g_{ij}(\nabla\bar{\phi})^2] &= \frac{\bar{\omega}}{\bar{\phi}^2}\Big[g^{ij}\nabla_i\chi\nabla_j\chi \\ &\quad -\frac{1}{2}g^{\mu\nu}(\nabla_\mu\bar{\phi})(\nabla_\nu\bar{\phi})\Big] \\ &= -\frac{3}{2}\frac{\omega+\chi\frac{d\omega}{d\phi}}{\bar{\phi}^2}g^{\mu\nu}\nabla_\mu\bar{\phi}\nabla\nu\bar{\phi} \\ &= \frac{3}{2}\frac{\omega}{\phi^2}\Big(1-2\frac{\chi}{\phi}\Big)\Big(\dot{\phi}^2+2\dot{\phi}\dot{\chi}-2\Psi\dot{\phi}^2\Big) \\ &\quad +\frac{3\chi}{2a^2}\frac{d\omega}{d\phi}\frac{\dot{\phi}^2}{\phi^2}, \end{aligned} \tag{5.40}$$

and the final term on the right hand side,

$$-g^{ij}g_{ij}\frac{1}{2\bar{\phi}}\bar{U} = -\frac{3}{2\phi}\left(1-\frac{\chi}{\phi}\right)\left(U+\frac{dU}{d\phi}\chi\right). \tag{5.41}$$

Within the complete equation lies the background equation,

$$\mathcal{H}^2 - 2\frac{\ddot{a}}{a} = \frac{8\pi G}{\phi}pa^2 + \frac{\ddot{\phi}}{\phi} - \mathcal{H}\frac{\dot{\phi}}{\phi} + \frac{\omega}{2}\frac{\dot{\phi}^2}{\phi^2} - \frac{a^2U}{2\phi}. \tag{5.42}$$

which can be removed immediately. Also, there are many terms proportional to χ/ϕ on the right hand side which can be eliminated, again using the background equation, namely,

$$\begin{aligned}\frac{\chi}{\phi}\Bigg[&-3\frac{8\pi G}{\phi} - \frac{3\ddot{\phi}}{a^2\phi} + \frac{3\mathcal{H}\dot{\phi}}{a^2\phi} \\ &-3\frac{\omega}{a^2}\left(\frac{\dot{\phi}}{\phi}\right)^2 + \frac{3U}{2\phi}\Bigg] \;=\; -\frac{3\mathcal{H}^2}{a^2}\frac{\chi}{\phi} + \frac{6\chi}{\phi a^2}\frac{\ddot{a}}{a} - \frac{3\omega}{2a^2}\frac{\chi}{\phi}\frac{\dot{\phi}^2}{\phi^2}.\end{aligned} \tag{5.43}$$

The final result therefore is,

$$\begin{aligned}2a^{-2}\Bigg(&2\frac{\ddot{a}}{a}\Psi - \mathcal{H}^2\Psi + \ddot{\Phi} + 2\mathcal{H}\dot{\Phi} \\ &+\mathcal{H}\dot{\Psi} + \frac{1}{3}\partial_i\partial^i\Psi - \frac{1}{3}\partial_i\partial^i\Phi\Bigg) \;=\; \frac{8\pi G}{\phi}\delta p \\ &+\frac{1}{a^2\phi}\Big(\ddot{\chi} - \mathcal{H}\dot{\chi} - \dot{\Psi}\dot{\phi} \\ &-2\Psi\ddot{\phi} + 2\Psi\mathcal{H}\dot{\phi} - \frac{2}{3}\partial_i\partial^i\chi\Big) \\ &+\frac{\omega}{\phi^2}\Big(\dot{\phi}\dot{\chi} - \Psi\dot{\phi}^2\Big) \\ &+\frac{\chi}{2a^2}\frac{d\omega}{d\phi}\frac{\dot{\phi}^2}{\phi^2} \\ &-\frac{1}{2\phi}\frac{dU}{d\phi}\chi \\ &-\frac{\mathcal{H}^2}{a^2}\frac{\chi}{\phi} + \frac{2\chi}{\phi a^2}\frac{\ddot{a}}{a} - \frac{\omega}{2a^2}\frac{\chi}{\phi}\frac{\dot{\phi}^2}{\phi^2},\end{aligned} \tag{5.44}$$

which on comparison with Eq. (52) of [373], where $\Psi_s = \Psi$, $\Phi_s = -\Phi$ and $X_s = \chi$ etc., shows that there is a sign error in their paper, (now also carried

forward into Eq. (146) of [77]), on the term,

$$-\frac{2\phi'}{a^2\phi}\frac{a'}{a}\Psi_s = -\frac{2\Psi\mathcal{H}\dot{\phi}}{a^2\phi}, \tag{5.45}$$

which should have positive sign.

Appropriate limits

In the Newtonian regime we can eliminate time derivatives of the metric potentials, the quasi-static approximation allows us to eliminate time derivatives of χ relative to its spatial derivatives and at late times overdensities have grown large relative to other perturbations, leading to a set of vastly simplified perturbation equations for the metric potentials,

$$\frac{2}{a^2}\partial_i\partial^i\Phi = \frac{8\pi G}{\phi}\delta\rho + \frac{\partial_i\partial^i\chi}{a^2\phi}, \tag{5.46}$$

$$\frac{2}{a^2}(\mathcal{H}\Psi_{,i}) = -\frac{8\pi G}{\phi}(\rho+p)v_i - \frac{\mathcal{H}\chi_{,i}}{\phi}, \tag{5.47}$$

$$-a^{-2}(\Psi-\Phi)_{,ij} = \frac{8\pi G}{\phi}\pi_{ij} + \frac{1}{a^2\phi}\partial_i\partial_j\chi, \tag{5.48}$$

$$\frac{2}{3a^2}\partial_i\partial^i(\Psi-\Phi) = \frac{8\pi G}{\phi}\delta p - \frac{1}{a^2\phi}\frac{2}{3}\partial_i\partial^i\chi. \tag{5.49}$$

From here on we explicitly do not include baryons such that $\delta \approx \delta_c$. In the Einstein frame we have $\Psi = \Phi$ and so the Poisson equation is simply,

$$\partial_i\partial^i\Psi = 4\pi G a^2\rho_c\delta_c \tag{5.50}$$

In the Jordan frame however we can combine the metric perturbation equations and the scalar field perturbation equation to get the Poisson equation's equivalent in MG,

$$\partial_i\partial^i\Psi = \frac{4\pi G}{\phi}a^2\rho_c\delta_c\left(1+\frac{1}{2\omega+3}\right). \tag{5.51}$$

For the Einstein frame we may also write the sum of the potentials as,

$$\partial_i\partial^i(\Psi+\Phi) = 8\pi G a^2\rho_c\delta_c, \tag{5.52}$$

while in the Jordan frame we find from the above equations,

$$\partial_i\partial^i(\Psi+\Phi) = \frac{8\pi G}{\phi}a^2\rho_c\delta_c. \tag{5.53}$$

5.3.4 Coupling terms

The covariant description of IDE CDM coupling is defined as,

$$\nabla_\nu T^\nu_{c\mu} = \bar{Q}_\mu = \bar{Q}_c u_\mu + F^c_\mu = (Q_c + \delta Q_c)u_\mu + a\partial_i f_c, \tag{5.54}$$

where u_μ is the total four-velocity, as opposed to u^c_μ, the CDM four-velocity perturbation, each of which may be written as,

$$u^\mu_c = a^{-1}(1-\Psi, \partial^i v_c), \quad u^\mu = a^{-1}(1-\Psi, \partial^i v), \tag{5.55}$$

where v and v_c are the total and CDM peculiar velocity potentials respectively. From the above equations we can write the components of the CDM energy-momentum transfer four-vector $\bar{Q}^c_\mu$ as,

$$\bar{Q}^c_0 = -a[Q_c(1+\Psi) + \delta Q_c], \quad \bar{Q}^c_i = a\partial_i[Q_c v + f_c], \tag{5.56}$$

In the IDE/MG model the covariant expression for the coupling is,

$$\begin{aligned} \nabla_\nu T^{\mu\nu}_c &= -\frac{1}{2}CT_c\partial^\mu\bar{\psi}, & (5.57)\\ &= \frac{1}{2}C(\rho_c\partial^\mu\psi + \rho_c\partial^\mu\varphi + \delta\rho_c\partial^\mu\psi), & (5.58) \end{aligned}$$

where C is the coupling function. The components of the energy-momentum transfer four-vector then turn out to be,

$$\begin{aligned} \bar{Q}^0_c &= -\frac{1}{2}Ca^{-2}\rho_c[(1+\delta_c)\dot{\psi} + \dot{\varphi}], & (5.59)\\ \bar{Q}^i_c &= \frac{1}{2}Ca^{-2}\rho_c\partial^i\varphi, & (5.60)\\ \bar{Q}^c_0 &= \frac{1}{2}C\rho_c[(1+\delta_c)\dot{\psi} + \dot{\varphi}], & (5.61)\\ \bar{Q}^c_i &= \frac{1}{2}C\rho_c\partial_i\varphi. & (5.62) \end{aligned}$$

where we have used $\partial^0\psi = g^{00}\dot{\psi}$. Now equating (5.56) and (5.61),

$$\begin{aligned} -a[Q_c(1+\Psi) + \delta Q_c] &= \frac{1}{2}C\rho_c[(1+\delta_c)\dot{\psi} + \dot{\varphi}], & (5.63)\\ &= \frac{1}{2}C\rho_c\dot{\psi}(1+\Psi)\\ &\quad + \frac{1}{2}C\rho_c(\dot{\varphi} - \dot{\psi}\Psi + \dot{\psi}\delta_c), & (5.64) \end{aligned}$$

$$\Rightarrow Q_c = -\frac{1}{2}Ca^{-1}\rho_c\dot{\psi}, \quad \delta Q_c = -\frac{1}{2}Ca^{-1}\rho_c(\varphi + \dot{\psi}\delta_c - \dot{\psi}\Psi). \tag{5.65}$$

In this model we have $\bar{Q}^\mu_c = \bar{Q}_c u^\mu_\psi$, the right hand side of which is,

$$(Q_c + \delta Q_c)u^\mu_\psi = -\frac{1}{2}Ca^{-2}\rho_c(\dot{\psi} + \dot{\varphi} + \dot{\psi}\delta_c - 2\dot{\psi}\Psi, \dot{\psi}\partial^i v_\psi). \tag{5.66}$$

Comparing Eq's. (5.60) and (5.66) we see that,

$$\frac{1}{2}Ca^{-2}\rho_c\partial^i\varphi = -\frac{1}{2}Ca^{-2}\rho_c\dot{\psi}\partial^i v_c, \tag{5.67}$$

$$\Rightarrow v_\psi = -\frac{\varphi}{\dot{\psi}}. \tag{5.68}$$

5.3.5 Growth equations

The IDE model CDM coupling terms are,

$$\bar{Q}^c_0 = \frac{1}{2}C\rho_c(\dot{\psi} + \delta_c\dot{\psi} + \dot{\varphi}), \tag{5.69}$$

$$\bar{Q}^c_i = \frac{1}{2}Ca^2\rho_c\partial_i\varphi, \tag{5.70}$$

and from energy-momentum conservation we have,

$$\nabla_\nu T^\nu_{c0} = \bar{Q}^c_0, \tag{5.71}$$

$$\nabla_\nu T^\nu_{ci} = \bar{Q}^c_i. \tag{5.72}$$

The first of these gives,

$$\dot{\rho}_c + \dot{\delta\rho}_c + \rho_c\partial_i\partial^i v_c + 3\mathcal{H}\rho_c(1 + \delta_c) = -\frac{1}{2}C\rho_c(\dot{\psi} + \delta_c\dot{\psi} + \dot{\varphi}). \tag{5.73}$$

This has a background part,

$$\dot{\rho}_c + 3\mathcal{H}\rho_c = -\frac{1}{2}C\rho_c\dot{\psi}, \tag{5.74}$$

and a perturbation part,

$$\dot{\delta\rho}_c + \rho_c\partial_i\partial^i v_c + 3\mathcal{H}\rho_c\delta_c = -\frac{1}{2}C\rho_c(\delta_c\dot{\psi} + \dot{\varphi}), \tag{5.75}$$

which may be written using $\theta_c = -k^2 v_c = \partial_i\partial^i v_c$ as,

$$\dot{\delta}_c = -\theta_c - \frac{1}{2}C\dot{\varphi}. \tag{5.76}$$

However the final term of this equation is suppressed by k^{-2} relative to the δ_c' term, as can be seen from the scalar field equation of motion, $\partial_i\partial^i\varphi = -\frac{1}{2}Ca^2\rho_c\delta_c$, thus giving us,

$$\dot{\delta}_c \simeq -\theta_c. \tag{5.77}$$

The ith component of energy-momentum conservation gives us,

$$\dot{\rho}_c\partial_i v_c + \rho_c(\partial\Psi + \partial_i\dot{v}_c + 4\mathcal{H}\partial_i v_c) = \frac{1}{2}C\rho_c\partial_i\varphi. \tag{5.78}$$

Taking a spatial derivative of this and again using $\theta_c = -k^2 v_c = \partial_i\partial^i v_c$ and $\partial_i\partial^i\varphi = -\frac{1}{2}Ca^2\rho_c\delta_c$ we find,

$$\dot{\theta}_c = -\mathcal{H}\theta_c - \partial_i\partial^i\Psi + \frac{1}{2}C\dot{\psi}\theta_c - \frac{1}{4}C^2a^2\rho_c\delta_c. \tag{5.79}$$

We can now use Eq's. (5.77) and (5.79) to find a velocity independent second order equation for δ_c. We first take the time derivative of Eq. (5.77) and substitute for $\dot{\theta}_c$ using Eq. (5.79) then use the Poisson equation $\partial_i\partial^i\Psi = 4\pi Ga^2\rho_c\delta_c$ to get the final answer,

$$\ddot{\delta}_c = -\left(\mathcal{H} - \frac{1}{2}C\dot{\psi}\right)\dot{\delta}_c + 4\pi Ga^2\rho_c\delta_c\left(1 + \frac{C^2}{16\pi G}\right). \tag{5.80}$$

5.4 Direct Comparison

It is interesting to consider the differences between the evolutions of quantities in equivalent IDE and MG models, as described by the preceding framework, (see also [195] for a detailed comparison of their dynamics). The degree to which a MG model differs from its IDE equivalent naturally depends on how much ϕ varies over time. This is governed primarily by the Brans-Dicke parameter ω but can be enhanced by the MG potential U.

The Jordan frame equivalent of ΛCDM has $\omega \to \infty$ so that $C = 0$ and $\phi = 1$ by Eq. (5.6). There are then no interactions, (again neglecting baryons), and a constant potential in both frames by Eq. (5.7). In this case there is no disparity between the models as ϕ does not evolve. If we allow for a non-zero constant IDE coupling parameter C however, the cosmology

evolves significantly differently to its MG counterpart, as shown in Fig. 5.1 for a MG model with $\omega = 36$, (or equivalently $C = 6.69 * 10^{-6}$). Here we can see that the expansion and the metric perturbations are different for the two models, while the energy density and its perturbation, whose evolutions do not directly depend on ϕ, remain quite similar.

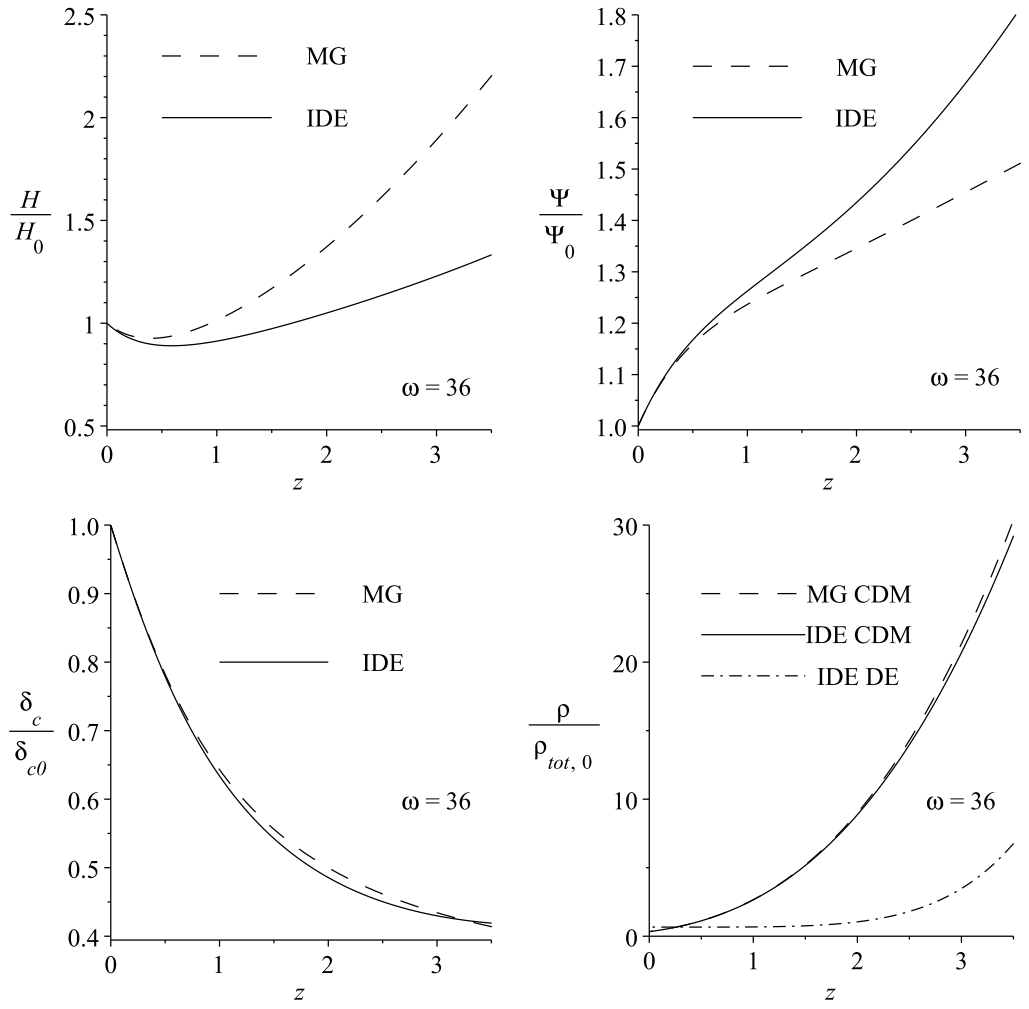

Figure 5.1: Evolution of quantities in equivalent IDE and MG models showing that quantities which depend on ϕ can be greatly altered.

Chapter 6

The Distinguishability of Interacting Dark Energy from Modified Gravity

In this chapter the question of whether it is possible to distinguish between models of IDE and MG using current observations is investigated. It was shown previously that the descriptions of these two alternative explanations for late-time acceleration can be conformally equivalent, but it is of course also possible for them to be considered separately, motivated by distinct physical theories. In this case the two models may appear similar observationally, so the question arises, is it always possible to tell them apart from each other?

6.1 Introduction

Whilst there have been many studies of ways in which to distinguish between DE and MG, the question of whether it is possible to tell IDE and MG apart has not been fully explored. To address this issue we employ the IDE and MG models derived in Chapter 5 to explore the potential distinguishability of scalar field IDE from different MG models for a range of parameter values.

6.1.1 Distinguishing DE and MG

It is always possible to find a DE model with a time varying equation of state parameter which produces a given expansion history [374, 375, 376], so in a worst-case scenario a DE model could exactly mimick a MG model's expansion history. To break this degeneracy it is necessary to take differences in the growth of structure into account and a great deal of effort has gone into distinguishing DE from MG [377, 378, 379, 380, 381, 382, 383, 384, 385, 386, 387, 388, 389, 390, 391, 392, 393, 394, 395, 396, 397, 7, 398, 335, 399, 400, 401, 367]. It has been argued that by finetuning the properties of a DE model its structure growth can also be made to mimick that of a given MG theory [402, 403, 404], but by employing suitable combinations of observables consistency tests can be made which should be able to distinguish between realistic models [405, 406].

6.1.2 Distinguishing IDE and MG

The works mentioned above focus on minimally coupled DE but they do not allow for the fact that observations permit significant interactions in the dark sector [407]. In [344] it was shown that it is possible to match the growth and expansion histories of MG cosmologies with those of IDE models. IDE models can look like modifications of GR [300], but they should deviate from GR+ΛCDM in a manner which is distinct to that of MG [408], so we might hope to be able to distinguish them observationally.

In the work that follows we revisit an example DGP [409] model from [344] to examine the observational distinguishability of matched IDE/DGP models, then extend the matching procedure used to a more general STT model and again consider whether the matched IDE models can be distinguished from their MG counterparts observationally. We assume the MG models in this chapter to be the large scale limit of models to which local constraints on the gravity theory [133] do not apply due to a screening mechanism such as the chameleon [138, 139, 140]. Also, the IDE interacts with DM only

and we are only interested in late-time effects. We therefore need only consider a simple system comprising a metric, scalar field and DM in each case, neglecting baryons and so from now on we drop the extraneous subscript c.

6.1.3 The IDE and MG models

We shall now rewrite the IDE and MG models from the previous chapter in terms of the independent variable $N \equiv \ln(a)$. Note however that these are no longer considered as formally equivalent descriptions of the same model, but are now independent of each other. This means that the ψ/ϕ, C/ω and U/V relations in Eq's. (5.6) and (5.7) no longer apply so that the scalar field potential V and the DE/DM coupling function C are now taken to be free functions.

To recap, a general action for a scalar field model of IDE may be written as,

$$\begin{aligned} S_{IDE} &= \int d^4x\sqrt{-g}\left[\frac{R}{16\pi G} - \frac{1}{2}(\nabla\psi)^2 - V(\psi)\right] \\ &\quad + S_m(g_{\mu\nu}, \psi, \eta), \end{aligned} \tag{6.1}$$

where $S_m(g_{\mu\nu}, \psi, \eta)$ is the matter action, with ψ and η being the IDE and matter fields respectively. The action for a STT model may be written as,

$$\begin{aligned} S_{STT} &= \int d^4x\sqrt{-g}\left[\phi R - \frac{\omega}{\phi}(\nabla\phi)^2 - U\right] \\ &\quad + S_m(g_{\mu\nu}, \eta), \end{aligned} \tag{6.2}$$

where in general ω and U can be functions of the gravitational scalar field ϕ, but for our purposes we take them to be constant. The action for the IDE model, Eq. (6.1), leads to its fluid, scalar field, Friedmann and density

perturbation equations,

$$\rho' = -3\rho - \frac{1}{2}C\rho\psi', \tag{6.3}$$

$$\psi'' = -\left(2 + \frac{\mathcal{H}'}{\mathcal{H}}\right)\psi' - \frac{a^2V'}{\mathcal{H}^2\psi'} + \frac{Ca^2\rho}{2\mathcal{H}^2}, \tag{6.4}$$

$$\mathcal{H}^2 = \frac{8\pi G}{3}a^2\left(\rho + \frac{\mathcal{H}^2\psi'}{2e^{2N}} + V\right), \tag{6.5}$$

$$\delta'' = -\left(1 + \frac{\mathcal{H}'}{\mathcal{H}} - \frac{1}{2}C\psi'\right)\delta' + \frac{3}{2}\Omega\delta\left(1 + \frac{C^2}{16\pi G}\right). \tag{6.6}$$

where primes denote derivatives with respect to N and $\Omega = 8\pi G/(3\mathcal{H}^2)$. The acceleration, scalar field and density perturbation equations derived from the STT action are,

$$\mathcal{H}' = -\frac{\mathcal{H}}{2}\left(\frac{\tilde{\Omega}}{\phi} + \frac{\mathcal{H}'}{\mathcal{H}}\frac{\phi'}{\phi} + \frac{\phi''}{\phi}\right) - \frac{\mathcal{H}\omega}{3}\left(\frac{\phi'}{\phi}\right)^2 + \frac{Ue^{2N}}{6\mathcal{H}\phi}, \tag{6.7}$$

$$\phi'' = -\left(2 + \frac{\mathcal{H}'}{\mathcal{H}}\right)\phi' + \frac{1}{2\omega + 3}\left(3\tilde{\Omega} + \frac{2Ue^{2N}}{\mathcal{H}^2}\right), \tag{6.8}$$

$$\delta'' = -\left(1 + \frac{\mathcal{H}'}{\mathcal{H}}\right)\delta' + \frac{3\tilde{\Omega}\delta}{2\phi}\left(1 + \frac{1}{2\omega + 3}\right), \tag{6.9}$$

where $\tilde{\Omega} = 8\pi G/(3\phi\mathcal{H}^2)$ and the final term in Eq. (6.9) could be interpreted as the standard case but with a time varying gravitational constant [410]. These equations determine the expansion and growth histories for both the STT and matched IDE models.

6.2 IDE/DGP

In [344] the authors matched a generalised IDE model to a particular choice of DGP model which had been fitted to observations. They used the IDE potential and coupling functions to match the DGP expansion and growth histories respectively. Essentially the evolution of the background CDM density ρ in the IDE model is determined by the matching of its perturbation $\delta \equiv \delta\rho/\rho$ to that of the DGP model. Below we replicate their results and extend the analysis to a range of initial conditions before considering the findings in the context of recent observations.

6.2.1 Matching

Matching here means constructing an IDE cosmology which has the same expansion and growth histories as a given MG cosmology. Only the self-accelerating branch of DGP is considered in [344], such that instead of Eq. (6.7), the expansion history on the MG side is given by,

$$\tilde{E} = \sqrt{\tilde{\Omega}_0 \exp[-3\ln(a)] + \tilde{\Omega}_{r_c}} + \sqrt{\tilde{\Omega}_{r_c}}, \tag{6.10}$$

where $\tilde{E} = \mathcal{H}/\mathcal{H}_0$ and $\tilde{\Omega}_{r_c}$ is a constant. It is clear from this equation that $\phi = 1 =$ constant, so $\tilde{\Omega}_{r_c}$ is the model's only free parameter, which we take as the best-fit value of 0.170 found from SN data used in [344]. The constraint $\tilde{E}(z=0) = 1$ also requires that,

$$\tilde{\Omega}_0 = 1 - 2\sqrt{\tilde{\Omega}_{r_c}}, \tag{6.11}$$

whilst the evolution of the matter is given by,

$$\tilde{\Omega} = \frac{\tilde{\Omega}_0 \exp[-3\ln(a)]}{\tilde{E}^2}. \tag{6.12}$$

To begin the matching process with we take the DGP version of Eq. (6.9) and compare it to the IDE equivalent Eq. (6.6) to find,

$$\kappa\frac{1}{2}C\psi'\delta' = \frac{3}{2}\delta\left[\left(1 + \frac{1}{2\omega+3}\right)\tilde{\Omega} - (1 + \frac{C^2}{16\pi G})\Omega\right], \tag{6.13}$$

where $\frac{1}{2}C$ and $\frac{1}{2\omega+3}$ are equivalent to κQ and $\frac{1}{3\beta}$ from [344], with the function $\beta = -(1+\tilde{\Omega}^2)/(1-\tilde{\Omega}^2)$ and the coupling function C is expressed by,

$$C^2 = 16\pi G\frac{\left(1 + \frac{\Omega'}{\Omega} + 2\frac{\mathcal{H}'}{\mathcal{H}}\right)^2}{1 - \frac{\mathcal{H}'}{\mathcal{H}} - \frac{3}{2}\Omega}. \tag{6.14}$$

From Eq. (6.3) we see that,

$$\frac{\Omega'}{\Omega} + 2\frac{\mathcal{H}'}{\mathcal{H}} + 1 = -\frac{1}{2}C\psi', \tag{6.15}$$

while taking the derivative of the Friedmann equation (6.5) and then also using Eq's. (6.3) and (6.4) gives,

$$\psi'^2 = \frac{1}{4\pi G}\left(1 - \frac{\mathcal{H}'}{\mathcal{H}} - \frac{3}{2}\Omega\right). \tag{6.16}$$

These last two equations now allow us to rewrite Eq. (6.13) as a differential equation for Ω,

$$\frac{1}{2}\left(1+\frac{\Omega'}{\Omega}+2\frac{\mathcal{H}'}{\mathcal{H}}\right)\delta' = -\frac{3}{2}\delta\left[\left(1+\frac{1}{2\omega+3}\right)\tilde{\Omega} - \left(1+\frac{C^2}{16\pi G}\right)\Omega\right]. \quad (6.17)$$

The entire system is now fixed and can be solved numerically to find the matched evolutions of the IDE and DGP models. Eq. (6.17) is quadratic in Ω' and so we choose the root which is typically negative initially, (the alternative branch typically leads to increasing Ω and the limits described below are reached before the present day). We can solve Eq. (6.9), along with the root of Eq. (6.17), to find Ω, $\mathcal{H}$, δ and δ' at any given N. In this way the freedom in the coupling function C is explicitly used to match the evolutions of the δ's, while the freedom in the scalar field potential V is used implicitly to match the expansion histories via the IDE Friedmann constraint, Eq. (6.5).

6.2.2 Comparison

Fig. 6.1 shows the evolution of δ and the different background evolutions of the IDE and DGP density parameters Ω and $\tilde{\Omega}$. Also plotted for comparison is a GR+ΛCDM model chosen to give $\Omega_0 \approx 0.227$, (subscript 0's denote present day quantities throughout), in line with recent constraints [363].

Initial conditions are set early in the matter dominated era at $z = 1000$ and the original example had an initial DGP energy density parameter $\tilde{\Omega}_i \approx 1$, (subscript i's denote initial values). The initial IDE density parameter used was $\Omega_i = 0.995$ and in addition to this solution we plot the result of choosing $\Omega_i = 0.996$ and $\Omega_i = 0.997$ in Fig. 6.1, but find that there are no solutions with $\Omega_i \gtrsim= 0.997$, (see below).

Eq. (6.13) is quadratic in Ω', so to solve it for Ω we must first solve it for Ω', but it is not always the case that real roots exist. Using the above initial conditions, the solutions are initially complex for $\Omega_i \simeq \tilde{\Omega}_i$. As Ω_i is decreased

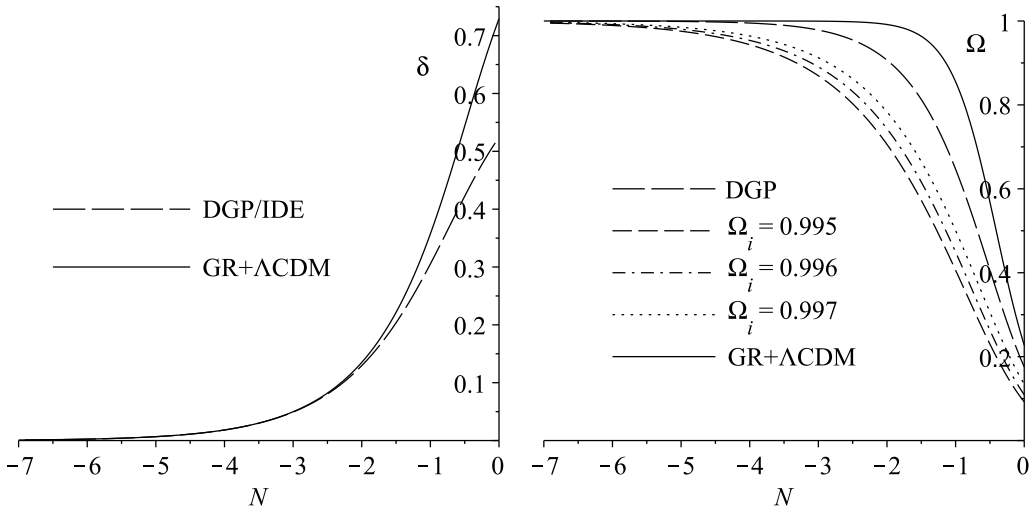

Figure 6.1: Evolution of the density perturbation (left) and the density parameters (right) for the matched DGP/IDE models, each with a different Ω_i, and a GR+ΛCDM model.

the solutions extend to later times but there are no solutions which reach the present day for $\Omega_i \gtrsim 0.997$, so there is a limit on how close Ω_i can be set to $\tilde{\Omega}_i$. This can be seen in Fig. 6.2 where solutions for values of Ω_i either side of this limit are plotted.

This means that there is a limit on how closely one can hope to match the evolution of the IDE/DGP densities through the choice of the boundary conditions on Ω. This difference should be evident in any quantity which depends on the CDM density, for example the sum of the metric potentials. The perturbed metric in the Newtonian regime may be written,

$$ds^2 = a^2[-(1+2\Psi)d\tau^2 + (1-2\Phi)\gamma_{ij}dx^i dx^j]. \tag{6.18}$$

The Poisson equations are for the DGP and IDE models respectively,

$$\partial_i\partial^i\Psi = 4\pi G a^2\tilde{\Omega}\delta\left(1+\frac{1}{3\beta}\right), \qquad \partial_i\partial^i\Psi = 4\pi G a^2\Omega\delta, \tag{6.19}$$

while both the DGP and IDE models obey the same evolution equation for the sum of the metric potentials Ψ and Φ,

$$\partial_i\partial^i(\Psi+\Phi) = 8\pi G a^2\tilde{\rho}\delta, \qquad \partial_i\partial^i(\Psi+\Phi) = 8\pi G a^2\rho\delta. \tag{6.20}$$

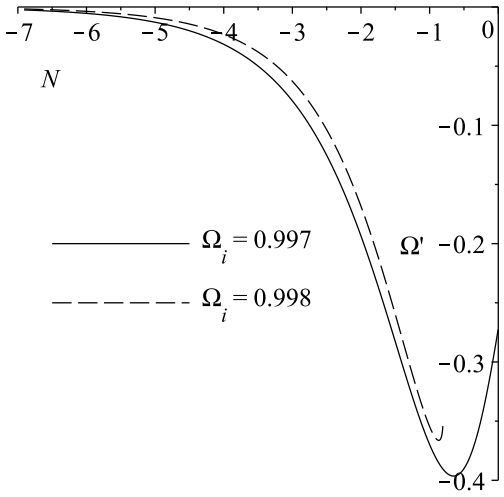

Figure 6.2: Solutions of Ω' in the IDE/DGP setup with initial conditions either side of the limit in Ω_i.

This quantity is plotted in the left-hand panel of Fig. 6.3 as a function of redshift at late times, making clear the significant distinction arising between the IDE and DGP models from the restriction on the boundary conditions for Ω.

6.2.3 Distinguishability

One way of testing for these differences is to parameterise deviations from the GR+ΛCDM case in Eq's. (6.19-6.20). One such parameterisation is the $\mu - \Sigma$ parameterisation [408], (see [412, 413, 414] for discussions of parameterisations of MG), defined by,

$$\partial_i \partial^i \Psi = 4\pi G a^2 \mu \hat{\rho} \delta, \tag{6.21}$$

$$\partial_i \partial^i (\Psi + \Phi) = 8\pi G a^2 \Sigma \hat{\rho} \delta, \tag{6.22}$$

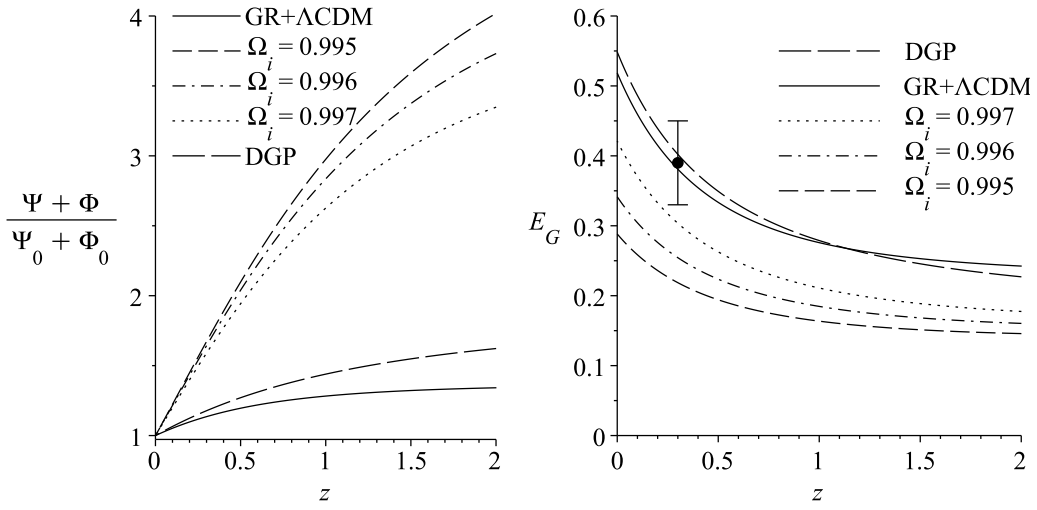

Figure 6.3: Evolution of the sum of the metric potentials normalised at the present day (left) and the E_G parameter (right) for the matched DGP/IDE models, each with a different Ω_i, and a GR+ΛCDM model. The observational measurement is $E_G = 0.39 \pm 0.06(1\sigma)$ at an effective redshift of $z = 0.3$ [411].

where $\hat{\rho} = \hat{\rho}_0 a^{-3}$ is the standard non-interacting CDM density solution. Comparing Eq's. (6.19-6.20) and (6.21-6.22) therefore we have,

$$\mu_{IDE} = \Sigma_{IDE} = \frac{\rho}{\hat{\rho}}, \tag{6.23}$$

$$\mu_{DGP} = \left(1 + \frac{1}{3\beta}\right), \qquad \Sigma_{DGP} = 1. \tag{6.24}$$

Fig. 6.4 shows results in the $\mu - \Sigma$ plane for the DGP and matched IDE models, (see [415] for observational constraints on μ and Σ with respect to the comoving density perturbation Δ at these two redshifts).

In [416] a bias-free measure of deviations from GR+ΛCDM was constructed. This is known as the E_G prameter and is defined by,

$$E_G \equiv \left[\frac{\partial_i \partial^i (\Psi + \Phi)}{-3\mathcal{H}_0^2 a^{-1}\theta}\right]_z, \tag{6.25}$$

where in the Newtonian regime $\theta = -\delta'$. Note however that this relation does not hold for all IDE models, e.g. the model studied in Chapter 4 [407]. The

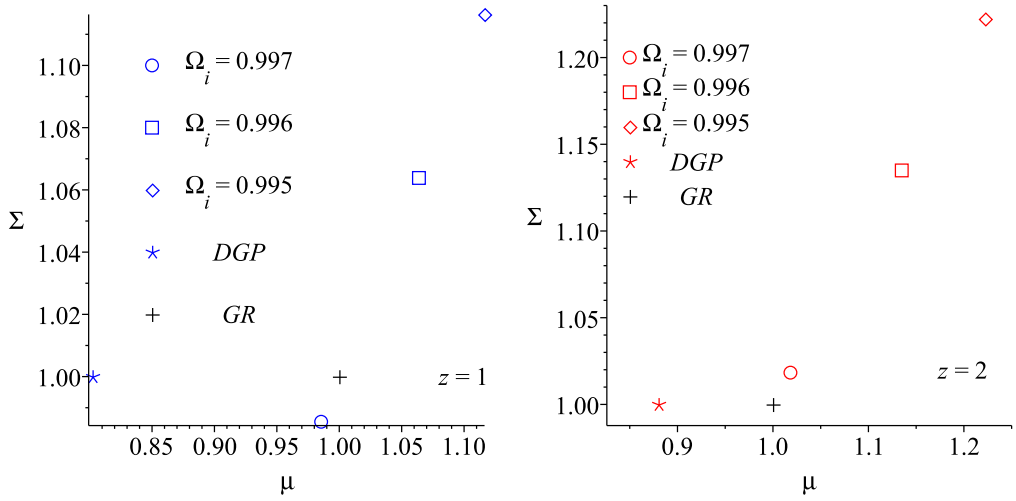

Figure 6.4: Results in the $\mu - \Sigma$ plane for the three IDE cases and the DGP cosmology at two different redshifts.

numerator in Eq. (6.25) can be measured from weak lensing observations, while the denominator can be found from peculiar velocity measurements and for the models studied here we have,

$$E_G^{DGP} = \frac{\tilde{\Omega}_0 \delta}{\delta'}, \tag{6.26}$$

$$E_G^{IDE} = \frac{a\mathcal{H}^2 \Omega \delta}{\mathcal{H}_0^2 \delta'}. \tag{6.27}$$

The right-hand panel of Fig. 6.3 shows E_G at late times for the DGP, IDE and GR+ΛCDM models along with some recent observational constraints [411]. We can see that although the DGP model is a good fit, even the worst-case IDE model with boundary conditions as close as possible to those of the DGP model is disfavoured by observations.

6.3 IDE/STT

Using the same procedure as in the previous section, we can repeat the analysis for the simple STT model. We consider scenarios where the two

cosmologies are as closely matched as possible for different parameter values and then assess their observational distinguishability.

6.3.1 Matching

We solve Eq's (6.7-6.9) numerically, along with the root of Eq. (6.17), to find Ω, $\mathcal{H}$, δ, δ', ϕ and ϕ' at any given N. The initial conditions used are,

$$\begin{aligned} N_i = -7, \quad \phi_i = 1, \quad \phi_i' = 0, \\ \mathcal{H}_i = 1, \quad \delta_i = a_i, \quad \delta_i' = a_i. \end{aligned} \tag{6.28}$$

$\tilde{\Omega}_i$ is chosen so that $\tilde{\Omega}_0$ is the same as the previously mentioned GR+ΛCDM model's present day density parameter when $\omega \to \infty$, while U_i is determined by the choice of $\tilde{\Omega}_i$ due to the 'Friedmann' constraint,

$$U_i = \frac{6\mathcal{H}_i^2}{a_i^2}\left(\phi_i - \tilde{\Omega}_i + \phi_i' - \frac{\omega\phi_i'^2}{6\phi_i}\right). \tag{6.29}$$

As in the case of the earlier DGP example there is a limit on how close Ω_i can be to $\tilde{\Omega}_i$. The solutions of the quadratic Eq. (6.17) are not initially complex for $\Omega_i \simeq \tilde{\Omega}_i$ as they are for Eq. (6.13) of the DGP setup discussed above. A similar solution limit on how close Ω_i can be set to $\tilde{\Omega}_i$ does exist however and depends on ω. In addition there is a physical limit which is reached before this solution limit and prevents the existence of physical IDE counterparts for those STT cases which deviate most greatly from GR. Similar problems have also been found in studies of parameterised STT models [380, 399].

The denominator in Eq. (6.14) can be shown to equal ψ'^2 using Eq's. (6.3-6.5). This decreases and reaches zero when the universe begins to accelerate and the $\frac{\mathcal{H}'}{\mathcal{H}}$ term grows faster than the Ω term decreases. It can then become negative, which would require ψ' to be complex and so we take this as a physical limit. The left hand panel of Fig. 6.5 shows this happening before the present day for a particular choice of ω and Ω_i, while the right hand panel shows that at the same time solutions for $\tilde{\Omega}'$ still exist.

We plot both the ψ' and Ω' limits in Fig. 6.6, showing that the smaller the value of ω, (and so the greater the deviation from GR), the farther Ω_i

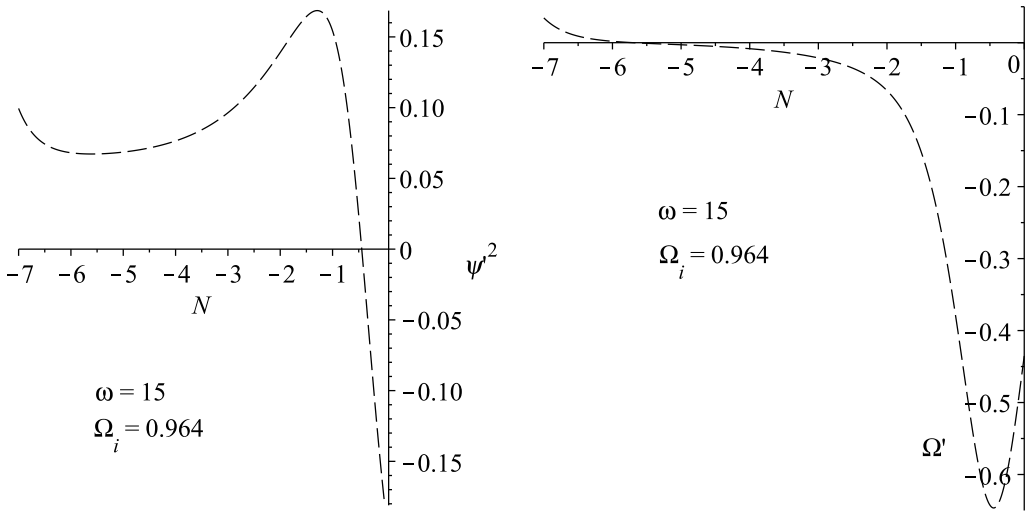

Figure 6.5: Left: an example of ψ'^2 becoming negative before the present day in the IDE/STT setup. Right: solutions of Ω' in the IDE/STT setup continuing beyond the present day, before which ψ'^2 has become negative.

has to be from $\tilde{\Omega}_i$. The limit beyond which ψ' becomes complex shows that it is not possible to find a matched IDE/STT system for $\omega \lesssim 10$, contrary to the statement in [344] that for any given MG model it is always possible to construct a matched IDE model.

Note that it is possible to finetune ϕ_i' to be very small and negative so that the ψ' limit is avoided, (too much and the STT universe contracts at late-times). Conversely, taking ϕ_i' small and positive shifts the limit to much larger ω making it impossible to find a physical IDE counterpart for cases with any noticable deviation from GR at all.

The reason that the derivative of the IDE scalar field does not become complex for the DGP model can be seen from the 'Friedmann' equation of [344] where they define,

$$E \equiv \frac{H}{H_0} = \sqrt{\tilde{\Omega}_0 e^{-3N} + \tilde{\Omega}_{r_c}} + \sqrt{\tilde{\Omega}_{r_c}}, \tag{6.30}$$

with $\tilde{\Omega}_{r_c} = 0.170$. Differentiating this with respect to N and using $\tilde{\Omega} =$

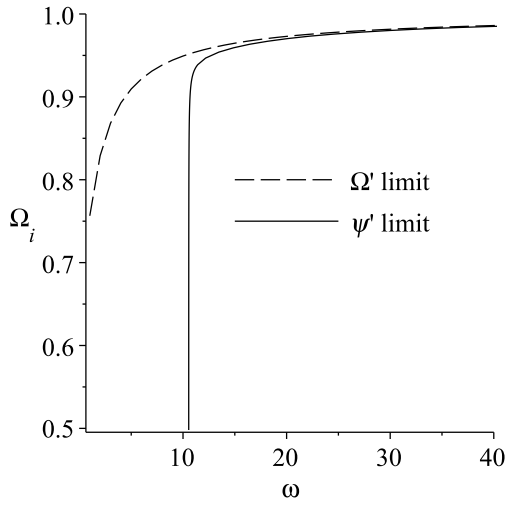

Figure 6.6: ψ' and Ω' limits on Ω_i as a function of ω for the IDE/STT system.

$\tilde{\Omega}_0 e^{-3N} E^{-2}$ leads to,

$$\frac{E'}{E} = \frac{H'}{H} = -\frac{1.5\tilde{\Omega}}{1 - \frac{\sqrt{\tilde{\Omega}_{rc}}}{E}}. \tag{6.31}$$

This quantity varies from about $-1.5\tilde{\Omega}_m$ at early times when E is large, to roughly $-2.5\tilde{\Omega}$ at late times as $E \to 1$. Since $\Omega_m < \tilde{\Omega}$ at all times we therefore find a condition which is true at all times in the IDE/DGP setup,

$$(\kappa\phi')^2 = -3\Omega_m - 2\frac{H'}{H} > 0. \tag{6.32}$$

6.3.2 Comparison

Fig. 6.7 shows results for three different values of ω where in each case Ω_i has been chosen to be as close as possible to $\tilde{\Omega}_i$ in the spirit of representing a worst-case scenario for distinguishing between the IDE/STT models.

The STT Poisson equation reads,

$$\partial_i \partial^i \Psi = \frac{4\pi\tilde{G}}{\phi} a^2 \tilde{\rho}\delta \left(1 + \frac{1}{2\omega + 3}\right), \tag{6.33}$$

while the evolution equation for the sum of the metric potentials in the STT

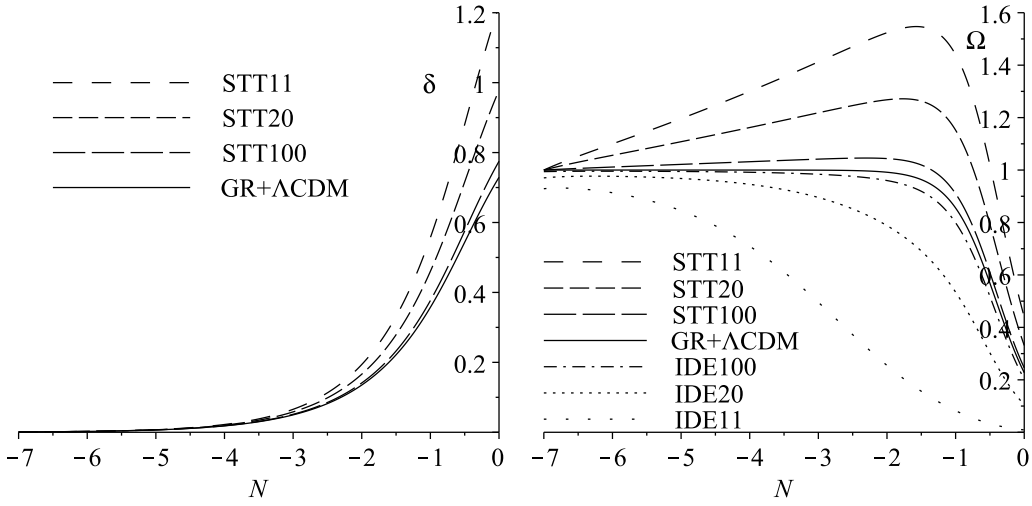

Figure 6.7: Evolution of the density perturbation (left) and the density parameters (right) for the matched STT/IDE models and a GR+ΛCDM model. The models STT11, STT20 and STT100 have $\omega = 11$, $\omega = 20$ and $\omega = 100$ respectively, with IDE11, IDE20 and IDE100 being their matched IDE counterparts. Note that including ϕ in the definition of $\tilde{\Omega}$ would bring the STT models on the right much closer to the GR+ΛCDM Ω curve. Even then however $\tilde{\Omega} > 1$ is still possible despite the spacetime being flat because the sum of the gravitational scalar field terms in the STT 'Friedmann' equation can be negative.

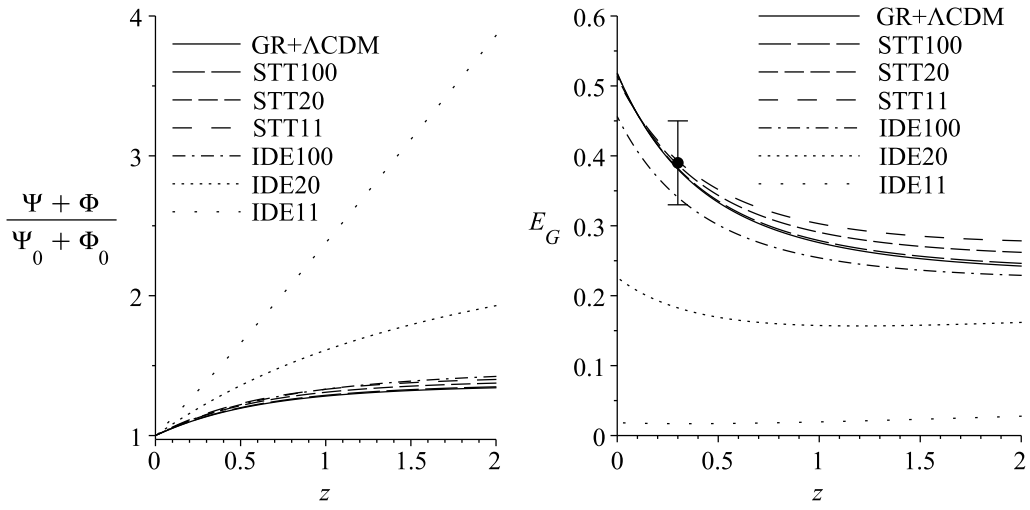

Figure 6.8: Evolution of the sum of the metric potentials normalised at the present day (left) and the E_G parameter (right) for the matched STT/IDE models, each with a different Ω_i, and a GR+ΛCDM model. The models STT11, STT20 and STT100 have $\omega = 11$, $\omega = 20$ and $\omega = 100$ respectively, with IDE11, IDE20 and IDE100 being their matched IDE counterparts. The observational measurement is $E_G = 0.39 \pm 0.06(1\sigma)$ at an effective redshift of $z = 0.3$ [411].

model is,

$$\partial_i \partial^i (\Psi + \Phi) = \frac{8\pi \tilde{G}}{\phi} a^2 \tilde{\rho} \delta, \tag{6.34}$$

where $\tilde{G} = G\phi_0$. This quantity is plotted in the left-hand panel of Fig. 6.8.

6.3.3 Distinguishability

For the STT the $\mu - \Sigma$ parameterisation gives,

$$\mu_{STT} = \frac{\phi_0}{\phi}\left(1 + \frac{1}{2\omega + 3}\right), \tag{6.35}$$

$$\Sigma_{STT} = \frac{\phi_0}{\phi}, \tag{6.36}$$

while for the IDE model it is the same as in Eq's. (6.23-6.24).

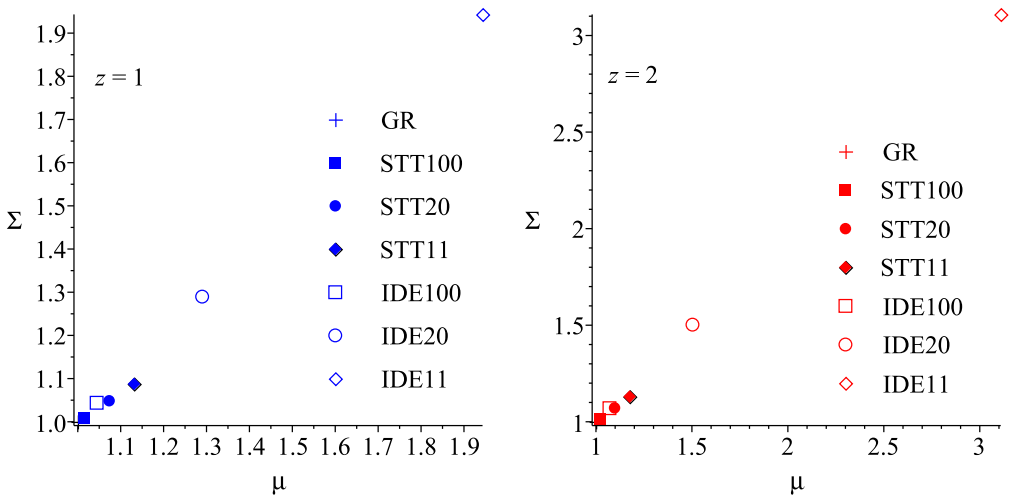

Figure 6.9: Results in the $\mu - \Sigma$ plane for the three STT cases and their matched IDE counterparts at two different redshifts.

Fig. 6.9 shows $\mu - \Sigma$ values for the IDE/ST models. For STT we also have,

$$E_G^{STT} = \frac{\tilde{\Omega}_0 \delta}{\phi \delta'}, \tag{6.37}$$

with the IDE expression as before in Eq. (6.27). The right-hand panel of Fig. 6.8 shows $\Psi + \Phi$ and E_G as functions of z at late times for the STT models and their matched IDE counterparts. Once again the IDE models lie much farther from the GR+ΛCDM case than their MG counterparts, with all but that matched to the $\omega = 100$ STT model lying outside of the observational constraints on E_G.

In [417] it was shown that constraints on STT models from cosmic microwave background, matter power spectrum and local gravity measurements could be avoided using a chameleon mechanism, leading to only a weak bound of $\omega > -1.28$. As stated earlier, the model here is considered only as an effective description on large scales of some underlying physical theory incorporating screening of the baryons. Fig. 6.8 shows that such models are distinguishable from IDE for sufficiently low values of ω.

However, the model is also essentially a Brans-Dicke theory [113] plus a

cosmological constant, for which lower bounds of $\omega > 120(2\sigma)$ [418], $\omega > 97.8(2\sigma)$ [419] and most recently $\omega > 177(2\sigma)$ [372] have been found, (Note that [420] give a lower bound of $\omega > 1000(2\sigma)$, but see discussions in [418, 419] and the possible sign error reported in Chapter 5). Fig. 6.8 then shows that such models which satisfy these constraints can not be distinguished by the observations.

The addition of supernova data would significantly improve constraints on ω, but account would need to be taken of local [421] and temporal [422] variation in the gravitational scalar field ϕ. In [423] a recovery of GR at late-times sufficient to allow the use of supernova data was assumed and bounds of $\omega > 500 - 1000$ from future data were forecast. If these constraints can be achieved it will not be possible to distinguish between the matched STT/IDE models with the E_G results we use here, although with new data of course the E_G constraints could also be tightened.

6.4 Conclusions

We have shown that although it is possible to construct an IDE model which matches the growth and expansion histories of a DGP model fitted to observations, even in the worst-case scenario, where their density evolutions are as close as theoretically possible, the matched IDE model can be distinguished by observations.

For the simple STT model and its matched IDE counterpart we have calculated a limit on how similar the initial matter densities can be. This limit depends on the strength of deviation from GR and we find that in cases which differ significantly from GR+ΛCDM even the worst-case matched IDE model can be distinguished by observations.

We have also shown that it is not always possible to construct a physical IDE model which matches the growth and expansion histories of the STT models and that there is a limit on the deviation from GR, beyond which the time derivative of the IDE scalar field becomes complex before the present.

Chapter 7

Conclusions

This thesis has been part of the ongoing endeavour to test ΛCDM and improve our understanding of the Universe. Over the last 15 years Λ has stood up to the scrutiny of increasingly accurate observational data. CDM has maintained its consensus of support for even longer, but both of these phenomena shall soon face definitive tests of their true natures. In the case of the cosmological constant, another decade of work should see Stage 4 experiments pass final judgement on the value of w, while for DM new direct detection experiments will test the current theoretical paradigm to its limits.

The articles contained within this thesis are just two among hundreds of published papers on IDE and contribute to a greater understanding of the model, serving also as templates for future studies. Addressing the coincidence problem has been the motivation for most work on IDE for example. In many cases the simplest IDE models have been ruled out on theoretical grounds alone, while observational constraints have shrunk the model space still further. The viable IDE models that remain, along with parameterisations and reconstructions show no trends or compelling features to recommend them over models with fewer degrees of freedom.

The $Q \propto \rho_x$ model had not been studied is detail before, despite being one of the simplest models of IDE which remains theoretically viable, (and also one which could potentially describe a real physical system). The placing of

observational constraints on the model provided a useful map of the models range of viability. It also demonstrated however the difficulty in constraining IDE given current data and the gaps in our theoretical understanding, in particular our lack of knowledge about DM-baryon bias, which prevents us from reliably using a fully complimentary range of observational probes. A better understanding of DM-baryon bias will break the degeneracy with σ_8 and accurate measurements of neutrino masses will also go some way toward helping with that. Ultimately perhaps weak-lensing surveys will produce accurate enough DM maps for us to really get a handle on its relation to baryons.

An interesting question which has arisen recently and is related to this piece of work is whether IDE could ease the tension of ΛCDM with the low-multipole anomaly in the CMB temperature anisotropy power spectrum, recently confirmed by Planck [32]. IDE can in theory drastically alter the slope of the ISW plateau, but the best-fit models shown in Fig. 4.9 demonstrate that this may not be possible when fitted to observations. Nevertheless, the degeneracy of Γ with other parameters seems likely to be able to provide a significant reduction in the power spectrum at low multipoles while still retaining virtually the same χ^2 as best-fit models with smaller Γ. Furthermore, given the tensions between CMB/BAO and SNIa/H_0 data highlighted by Planck, it would be interesting to undertake a comparative study of different observational probes which looked into all these issues further.

The second paper to come out of this thesis was a more abstract but nevertheless useful study and led to a couple of particularly interesting findings. The first noteworthy result was that contrary to what had previously been stated in the literature, it is not always possible to find an IDE model to fit a given MG model. The second was that some STT models should be distinguishable from IDE even in a worst case scenario where their expansion and growth histories are identical.

The long term future of theoretical cosmology seems to be in a return to 'classical' methods. A proper understanding of the effects of inhomogeneities

will be important for any cosmological model, as observations map our Universe in ever greater detail. The model space will no doubt continue to be explored and gaps in the literature do need to be filled so that a fully comprehensive picture is available for the Stage 4 era. It seems however that until then at least, there is no reason to believe that the expansion of the Universe is being driven by anything other than the CC mentioned by Einstein as a footnote in his original paper on GR nearly 100 years ago [15].

Bibliography

[1] **Supernova Search Team** Collaboration, A. G. Riess *et al.*, "Observational evidence from supernovae for an accelerating universe and a cosmological constant," *Astron.J.* **116** (1998) 1009–1038, arXiv:astro-ph/9805201 [astro-ph].

[2] **Supernova Cosmology Project** Collaboration, S. Perlmutter *et al.*, "Measurements of Omega and Lambda from 42 high redshift supernovae," *Astrophys.J.* **517** (1999) 565–586, arXiv:astro-ph/9812133 [astro-ph].

[3] A. Blanchard, "Evidence for the Fifth Element Astrophysical status of Dark Energy," *Astron.Astrophys.Rev.* **18** (2010) 595–645, arXiv:1005.3765 [astro-ph.CO].

[4] A. Albrecht, G. Bernstein, R. Cahn, W. L. Freedman, J. Hewitt, *et al.*, "Report of the Dark Energy Task Force," arXiv:astro-ph/0609591 [astro-ph].

[5] F. Zwicky, "Spectral displacement of extra galactic nebulae," *Helv.Phys.Acta* **6** (1933) 110–127.

[6] P. Serra, "No Evidence for Dark Energy Evolution from a global analysis of cosmological data," arXiv:1005.2415 [astro-ph.CO].

[7] C. Shapiro, S. Dodelson, B. Hoyle, L. Samushia, and B. Flaugher, "Will Multiple Probes of Dark Energy find Modified Gravity?," *Phys.Rev.* **D82** (2010) 043520, arXiv:1004.4810 [astro-ph.CO].

[8] S. Nesseris and A. Shafieloo, "A model independent null test on the cosmological constant," *Mon.Not.Roy.Astron.Soc.* **408** (2010) 1879–1885, arXiv:1004.0960 [astro-ph.CO].

[9] J. Kratochvil, A. D. Linde, E. V. Linder, and M. Shmakova, "Testing the cosmological constant as a candidate for dark energy," *JCAP* **0407** (2004) 001, arXiv:astro-ph/0312183 [astro-ph].

[10] M. J. Mortonson, W. Hu, and D. Huterer, "Testable dark energy predictions from current data," *Phys.Rev.* **D81** (2010) 063007, arXiv:0912.3816 [astro-ph.CO].

[11] S. M. Carroll, "The Cosmological constant," *Living Rev.Rel.* **4** (2001) 1, arXiv:astro-ph/0004075 [astro-ph].

[12] N. Straumann, "The History of the cosmological constant problem," arXiv:gr-qc/0208027 [gr-qc].

[13] T. Padmanabhan, "Cosmological constant: The Weight of the vacuum," *Phys.Rept.* **380** (2003) 235–320, arXiv:hep-th/0212290 [hep-th].

[14] P. Peebles and B. Ratra, "The Cosmological constant and dark energy," *Rev.Mod.Phys.* **75** (2003) 559–606, arXiv:astro-ph/0207347 [astro-ph].

[15] A. Einstein, "The Foundation of the General Theory of Relativity," *Annalen Phys.* **49** (1916) 769–822.

[16] A. Einstein, "Cosmological Considerations in the General Theory of Relativity," *Sitzungsber.Preuss.Akad.Wiss.Berlin (Math.Phys.)* **1917** (1917) 142–152.

[17] A. Eddington, "On the Instability of Einstein's Spherical World," *Mon.Not.Roy.Astron.Soc.* **90** (1930) 668–678.

[18] A. Einstein, *The meaning of relativity*. Princeton University Press, New York, 1921.

[19] H. Robertson, "Relativistic Cosmology," *Rev.Mod.Phys.* **5** (1933) 62–90.

[20] V. M. Slipher, "Spectrographic Observations of Nebulae," *Popular Astronomy* **23** (Jan., 1915) 21–24.

[21] E. Hubble, "A Relation between Distance and Radial Velocity among Extra-Galactic Nebulae," *Proceedings of the National Academy of Science* **15** (Mar., 1929) 168–173.

[22] E. Bianchi and C. Rovelli, "Why all these prejudices against a constant?," arXiv:1002.3966 [astro-ph.CO].

[23] N. Dadhich, "On the enigmatic Λ - a true constant of spacetime," *Pramana* **77** (2011) 433–437, arXiv:1006.1552 [gr-qc].

[24] A. S. Eddington, *The nature of the physical world*. Cambridge University Press, Cambridge, 1929.

[25] S. M. Carroll, "Dark energy and the preposterous universe," arXiv:astro-ph/0107571 [astro-ph].

[26] C. A. Egan, "Dark Energy, Anthropic Selection Effects, Entropy and Life," arXiv:1005.0745 [astro-ph.CO].

[27] J. Al-Khalili. Pers. comm.

[28] S. Weinberg, "The Cosmological Constant Problem," *Rev.Mod.Phys.* **61** (1989) 1–23.

[29] R. Jaffe, "The Casimir effect and the quantum vacuum," *Phys.Rev.* **D72** (2005) 021301, arXiv:hep-th/0503158 [hep-th].

[30] R. Triay, "Dark Energy: Fiction or reality?," *AIP Conf.Proc.* **1246** (2010) 105–113, arXiv:1004.0091 [gr-qc].

[31] G. Hinshaw, D. Larson, E. Komatsu, D. Spergel, C. Bennett, *et al.*, "Nine-Year Wilkinson Microwave Anisotropy Probe (WMAP) Observations: Cosmological Parameter Results," arXiv:1212.5226 [astro-ph.CO].

[32] **Planck Collaboration** Collaboration, P. Ade *et al.*, "Planck 2013 results. XVI. Cosmological parameters," arXiv:1303.5076 [astro-ph.CO].

[33] R. Keisler, C. Reichardt, K. Aird, B. Benson, L. Bleem, *et al.*, "A Measurement of the Damping Tail of the Cosmic Microwave Background Power Spectrum with the South Pole Telescope," *Astrophys.J.* **743** (2011) 28, arXiv:1105.3182 [astro-ph.CO].

[34] J. L. Sievers, R. A. Hlozek, M. R. Nolta, V. Acquaviva, G. E. Addison, *et al.*, "The Atacama Cosmology Telescope: Cosmological parameters from three seasons of data," arXiv:1301.0824 [astro-ph.CO].

[35] A. Slosar, V. Irsic, D. Kirkby, S. Bailey, N. G. Busca, *et al.*, "Measurement of Baryon Acoustic Oscillations in the Lyman-alpha Forest Fluctuations in BOSS Data Release 9," arXiv:1301.3459 [astro-ph.CO].

[36] F. Beutler, C. Blake, M. Colless, D. H. Jones, L. Staveley-Smith, *et al.*, "The 6dF Galaxy Survey: Baryon Acoustic Oscillations and the Local Hubble Constant," *Mon.Not.Roy.Astron.Soc.* **416** (2011) 3017–3032, arXiv:1106.3366 [astro-ph.CO].

[37] N. Padmanabhan, X. Xu, D. J. Eisenstein, R. Scalzo, A. J. Cuesta, *et al.*, "A 2: Methods and Application to the Sloan Digital Sky Survey," arXiv:1202.0090 [astro-ph.CO].

[38] L. Anderson, E. Aubourg, S. Bailey, D. Bizyaev, M. Blanton, *et al.*, "The clustering of galaxies in the SDSS-III Baryon Oscillation Spectroscopic Survey: Baryon Acoustic Oscillations in the Data Release 9 Spectroscopic Galaxy Sample," *Mon.Not.Roy.Astron.Soc.* **428** (2013) 1036–1054, arXiv:1203.6594 [astro-ph.CO].

[39] M. Phillips, "The absolute magnitudes of Type IA supernovae," *Astrophys.J.* **413** (1993) L105–L108.

[40] A. G. Riess, L. Macri, S. Casertano, H. Lampeitl, H. C. Ferguson, *et al.*, "A 3Telescope and Wide Field Camera 3," *Astrophys.J.* **730** (2011) 119, arXiv:1103.2976 [astro-ph.CO].

[41] W. L. Freedman, B. F. Madore, V. Scowcroft, C. Burns, A. Monson, *et al.*, "Carnegie Hubble Program: A Mid-Infrared Calibration of the Hubble Constant," *Astrophys.J.* **758** (2012) 24, arXiv:1208.3281 [astro-ph.CO].

[42] S. Suyu, T. Treu, R. Blandford, W. Freedman, S. Hilbert, *et al.*, "The Hubble constant and new discoveries in cosmology," arXiv:1202.4459 [astro-ph.CO].

[43] **Planck Collaboration** Collaboration, P. Ade *et al.*, "Planck 2013 results. XX. Cosmology from Sunyaev-Zeldovich cluster counts," arXiv:1303.5080 [astro-ph.CO].

[44] Z. Haiman, J. J. Mohr, and G. P. Holder, "Clusters in the precision cosmology era," arXiv:astro-ph/0103049 [astro-ph].

[45] S. Allen, D. Rapetti, R. Schmidt, H. Ebeling, G. Morris, *et al.*, "Improved constraints on dark energy from Chandra X-ray observations of the largest relaxed galaxy clusters," *Mon.Not.Roy.Astron.Soc.* **383** (2008) 879–896, arXiv:0706.0033 [astro-ph].

[46] T. Erben, H. Hildebrandt, L. Miller, L. van Waerbeke, C. Heymans, *et al.*, "CFHTLenS: The Canada-France-Hawaii Telescope Lensing Survey - Imaging Data and Catalogue Products," arXiv:1210.8156 [astro-ph.CO].

[47] C. Heymans, L. Van Waerbeke, L. Miller, T. Erben, H. Hildebrandt, *et al.*, "CFHTLenS: The Canada-France-Hawaii Telescope Lensing Survey," arXiv:1210.0032 [astro-ph.CO].

[48] C. Heymans, E. Grocutt, A. Heavens, M. Kilbinger, T. D. Kitching, *et al.*, "CFHTLenS tomographic weak lensing cosmological parameter constraints: Mitigating the impact of intrinsic galaxy alignments," arXiv:1303.1808 [astro-ph.CO].

[49] B. A. Reid, W. J. Percival, D. J. Eisenstein, L. Verde, D. N. Spergel, *et al.*, "Cosmological Constraints from the Clustering of the Sloan Digital Sky Survey DR7 Luminous Red Galaxies," *Mon.Not.Roy.Astron.Soc.* **404** (2010) 60–85, arXiv:0907.1659 [astro-ph.CO].

[50] C. Blake, S. Brough, M. Colless, C. Contreras, W. Couch, *et al.*, "The WiggleZ Dark Energy Survey: the growth rate of cosmic structure since redshift z=0.9," *Mon.Not.Roy.Astron.Soc.* **415** (2011) 2876, arXiv:1104.2948 [astro-ph.CO].

[51] R. G. Crittenden and N. Turok, "Looking for Lambda with the Rees-Sciama effect," *Phys.Rev.Lett.* **76** (1996) 575, arXiv:astro-ph/9510072 [astro-ph].

[52] C. Alcock and B. Paczynski, "An evolution free test for non-zero cosmological constant," *Nature* **281** (1979) 358–359.

[53] B. E. Schaefer, "Gamma-ray burst hubble diagram to z=4.5," *Astrophys.J.* **583** (2003) L67–L70, arXiv:astro-ph/0212445 [astro-ph].

[54] J. Simon, L. Verde, and R. Jimenez, "Constraints on the redshift dependence of the dark energy potential," *Phys.Rev.* **D71** (2005) 123001, arXiv:astro-ph/0412269 [astro-ph].

[55] J. Santos, J. Alcaniz, M. Reboucas, and N. Pires, "Lookback time bounds from energy conditions," *Phys.Rev.* **D76** (2007) 043519, arXiv:0706.1779 [astro-ph].

[56] E. J. Copeland, M. Sami, and S. Tsujikawa, "Dynamics of dark energy," *Int. J. Mod. Phys.* **D15** (2006) 1753–1936, arXiv:hep-th/0603057.

[57] J. Frieman, M. Turner, and D. Huterer, "Dark Energy and the Accelerating Universe," *Ann.Rev.Astron.Astrophys.* **46** (2008) 385–432, arXiv:0803.0982 [astro-ph].

[58] A. Silvestri and M. Trodden, "Approaches to Understanding Cosmic Acceleration," *Rept.Prog.Phys.* **72** (2009) 096901, arXiv:0904.0024 [astro-ph.CO].

[59] R. R. Caldwell and M. Kamionkowski, "The Physics of Cosmic Acceleration," *Ann.Rev.Nucl.Part.Sci.* **59** (2009) 397–429, arXiv:0903.0866 [astro-ph.CO].

[60] S. Tsujikawa, "Modified gravity models of dark energy," *Lect. Notes Phys.* **800** (2010) 99–145, arXiv:1101.0191 [gr-qc].

[61] M. Li, X.-D. Li, S. Wang, and Y. Wang, "Dark Energy," *Commun.Theor.Phys.* **56** (2011) 525–604, arXiv:1103.5870 [astro-ph.CO].

[62] P. Brax, "Gif Lectures on Cosmic Acceleration," arXiv:0912.3610 [astro-ph.CO].

[63] R. Bean, "TASI Lectures on Cosmic Acceleration," arXiv:1003.4468 [astro-ph.CO].

[64] R. Durrer and R. Maartens, "Dark Energy and Modified Gravity," arXiv:0811.4132 [astro-ph].

[65] L. Amendola and S. Tsujikawa, *Dark Energy: Theory and Observations*. Cambridge Uni. Press, Cambridge, 2010.

[66] V. Sahni and A. Starobinsky, "Reconstructing Dark Energy," *Int.J.Mod.Phys.* **D15** (2006) 2105–2132, arXiv:astro-ph/0610026 [astro-ph].

[67] R. Crittenden, E. Majerotto, and F. Piazza, "Measuring deviations from a cosmological constant: A field-space parameterization," *Phys.Rev.Lett.* **98** (2007) 251301, arXiv:astro-ph/0702003 [astro-ph].

[68] M. Cortes and E. V. Linder, "Old Dark Energy," *Phys.Rev.* **D81** (2010) 063004, arXiv:0909.2251 [astro-ph.CO].

[69] R. G. Crittenden, L. Pogosian, and G.-B. Zhao, "Investigating dark energy experiments with principal components," *JCAP* **0912** (2009) 025, arXiv:astro-ph/0510293 [astro-ph].

[70] C. Clarkson and C. Zunckel, "Direct reconstruction of dark energy," *Phys.Rev.Lett.* **104** (2010) 211301, arXiv:1002.5004 [astro-ph.CO].

[71] R.-G. Cai, Q. Su, and H.-B. Zhang, "Probing the dynamical behavior of dark energy," *JCAP* **1004** (2010) 012, arXiv:1001.2207 [astro-ph.CO].

[72] G.-B. Zhao and X.-m. Zhang, "Probing Dark Energy Dynamics from Current and Future Cosmological Observations," *Phys.Rev.* **D81** (2010) 043518, arXiv:0908.1568 [astro-ph.CO].

[73] E. J. Copeland, A. R. Liddle, and D. Wands, "Exponential potentials and cosmological scaling solutions," *Phys.Rev.* **D57** (1998) 4686–4690, arXiv:gr-qc/9711068 [gr-qc].

[74] M. Malquarti and A. R. Liddle, "Initial conditions for quintessence after inflation," *Phys.Rev.* **D66** (2002) 023524, arXiv:astro-ph/0203232 [astro-ph].

[75] S. Capozziello and M. De Laurentis, "Extended Theories of Gravity," *Phys.Rept.* **509** (2011) 167–321, arXiv:1108.6266 [gr-qc].

[76] S. Nojiri and S. D. Odintsov, "Unified cosmic history in modified gravity: from F(R) theory to Lorentz non-invariant models," *Phys.Rept.* **505** (2011) 59–144, arXiv:1011.0544 [gr-qc].

[77] T. Clifton, P. G. Ferreira, A. Padilla, and C. Skordis, "Modified Gravity and Cosmology," *Phys.Rept.* **513** (2012) 1–189, arXiv:1106.2476 [astro-ph.CO].

[78] T. Buchert, "Dark Energy from Structure: A Status Report," *Gen.Rel.Grav.* **40** (2008) 467–527, arXiv:0707.2153 [gr-qc].

[79] S. February, J. Larena, M. Smith, and C. Clarkson, "Rendering Dark Energy Void," *Mon.Not.Roy.Astron.Soc.* **405** (2010) 2231, arXiv:0909.1479 [astro-ph.CO].

[80] C. Clarkson and R. Maartens, "Inhomogeneity and the foundations of concordance cosmology," *Class.Quant.Grav.* **27** (2010) 124008, arXiv:1005.2165 [astro-ph.CO].

[81] K. A. Malik, "Cosmological perturbations in an inflationary universe," arXiv:astro-ph/0101563 [astro-ph].

[82] S. M. Carroll, *Spacetime and geometry: An introduction to general relativity*. Benjamin Cummings, London, 2004.

[83] R. M. Wald, *General Relativity*. University Of Chicago Press, Chicago, 1st ed., June, 1984.

[84] K. A. Malik and D. R. Matravers, "A Concise Introduction to Perturbation Theory in Cosmology," *Class.Quant.Grav.* **25** (2008) 193001, arXiv:0804.3276 [astro-ph].

[85] E. Lifshitz, "On the Gravitational stability of the expanding universe," *J.Phys.(USSR)* **10** (1946) 116.

[86] E. Lifshitz and I. Khalatnikov, "Investigations in relativistic cosmology," *Adv.Phys.* **12** (1963) 185–249.

[87] R. Sachs and A. Wolfe, "Perturbations of a cosmological model and angular variations of the microwave background," *Astrophys.J.* **147** (1967) 73–90.

[88] J. M. Bardeen, "Gauge Invariant Cosmological Perturbations," *Phys.Rev.* **D22** (1980) 1882–1905.

[89] H. Kodama and M. Sasaki, "Cosmological Perturbation Theory," *Prog.Theor.Phys.Suppl.* **78** (1984) 1–166.

[90] C.-P. Ma and E. Bertschinger, "Cosmological perturbation theory in the synchronous and conformal Newtonian gauges," *Astrophys.J.* **455** (1995) 7–25, arXiv:astro-ph/9506072 [astro-ph].

[91] E. Bertschinger, "Cosmological perturbation theory and structure formation," arXiv:astro-ph/0101009 [astro-ph].

[92] A. R. Liddle and D. Lyth, *Cosmological inflation and large scale structure*. Cambridge University Press, Cambridge, 2000.

[93] A. Lewis, A. Challinor, and A. Lasenby, "Efficient computation of CMB anisotropies in closed FRW models,"

Astrophys.J. **538** (2000) 473–476, arXiv:astro-ph/9911177 [astro-ph].

[94] P. J. E. Peebles, "Phenomenology of the Invisible Universe," *AIP Conf. Proc.* **1241** (2010) 175–182, arXiv:0910.5142 [astro-ph.CO].

[95] C. Wetterich, "Cosmology and the Fate of Dilatation Symmetry," *Nucl.Phys.* **B302** (1988) 668.

[96] W. Zimdahl and D. Pavon, "Interacting quintessence," *Phys. Lett.* **B521** (2001) 133–138, arXiv:astro-ph/0105479.

[97] E. R. Tarrant, C. van de Bruck, E. J. Copeland, and A. M. Green, "Coupled Quintessence and the Halo Mass Function," *Phys.Rev.* **D85** (2012) 023503, arXiv:1103.0694 [astro-ph.CO].

[98] J.-c. Hwang and H. Noh, "Cosmological perturbations with multiple fluids and fields," *Class.Quant.Grav.* **19** (2002) 527–550, arXiv:astro-ph/0103244 [astro-ph].

[99] K. A. Malik, D. Wands, and C. Ungarelli, "Large-scale curvature and entropy perturbations for multiple interacting fluids," *Phys. Rev.* **D67** (2003) 063516, arXiv:astro-ph/0211602.

[100] T. Koivisto, "Growth of perturbations in dark matter coupled with quintessence," *Phys. Rev.* **D72** (2005) 043516, arXiv:astro-ph/0504571.

[101] M. Kaplinghat and A. Rajaraman, "Stable models of super-acceleration," *Phys.Rev.* **D75** (2007) 103504, arXiv:astro-ph/0601517 [astro-ph].

[102] R. Bean, E. E. Flanagan, and M. Trodden, "The Adiabatic Instability on Cosmology's Dark Side," *New J. Phys.* **10** (2008) 033006, arXiv:0709.1124 [astro-ph].

[103] R. Bean, E. E. Flanagan, and M. Trodden, "Adiabatic instability in coupled dark energy-dark matter models," *Phys. Rev.* **D78** (2008) 023009, arXiv:0709.1128 [astro-ph].

[104] P. S. Corasaniti, "Slow-Roll Suppression of Adiabatic Instabilities in Coupled Scalar Field-Dark Matter Models," *Phys. Rev.* **D78** (2008) 083538, arXiv:0808.1646 [astro-ph].

[105] N. Afshordi, M. Zaldarriaga, and K. Kohri, "On the stability of dark energy with mass-varying neutrinos," *Phys.Rev.* **D72** (2005) 065024, arXiv:astro-ph/0506663 [astro-ph].

[106] O. E. Bjaelde, A. W. Brookfield, C. van de Bruck, S. Hannestad, D. F. Mota, *et al.*, "Neutrino Dark Energy – Revisiting the Stability Issue," *JCAP* **0801** (2008) 026, arXiv:0705.2018 [astro-ph].

[107] J. Valiviita, E. Majerotto, and R. Maartens, "Instability in interacting dark energy and dark matter fluids," *JCAP* **0807** (2008) 020, arXiv:0804.0232 [astro-ph].

[108] M. B. Gavela, D. Hernandez, L. Lopez Honorez, O. Mena, and S. Rigolin, "Dark coupling," *JCAP* **0907** (2009) 034, arXiv:0901.1611 [astro-ph].

[109] J.-H. He, B. Wang, and E. Abdalla, "Stability of the curvature perturbation in dark sectors' mutual interacting models," *Phys. Lett.* **B671** (2009) 139–145, arXiv:0807.3471 [gr-qc].

[110] B. M. Jackson, A. Taylor, and A. Berera, "On the large-scale instability in interacting dark energy and dark matter fluids," *Phys. Rev.* **D79** (2009) 043526, arXiv:0901.3272 [astro-ph.CO].

[111] L. L. Honorez and 0. Mena, "Instabilities in dark coupled models and constraints from cosmological data," *AIP Conf. Proc.* **1241** (2010) 1016–1024, arXiv:0911.3269 [astro-ph.CO].

[112] N. A. Koshelev, "On the growth of perturbations in interacting dark energy and dark matter fluids," *Gen. Rel. Grav.* **43** (2011) 1309–1321, arXiv:0912.0120 [gr-qc].

[113] C. Brans and R. Dicke, "Mach's principle and a relativistic theory of gravitation," *Phys.Rev.* **124** (1961) 925–935.

[114] R. Dicke, "Mach's principle and invariance under transformation of units," *Phys.Rev.* **125** (1962) 2163–2167.

[115] T. Kaluza, "On the Problem of Unity in Physics," *Sitzungsber.Preuss.Akad.Wiss.Berlin (Math.Phys.)* **1921** (1921) 966–972.

[116] O. Klein, "Quantum Theory and Five-Dimensional Theory of Relativity. (In German and English)," *Z.Phys.* **37** (1926) 895–906.

[117] P. Jordan, *Schwerkraft und Weltall*, vol. 107. Vieweg, Braunschweig, 1955.

[118] J. R. Ellis, S. Kalara, K. A. Olive, and C. Wetterich, "Density Dependent Couplings and Astrophysical Bounds on Light Scalar Particles," *Phys.Lett.* **B228** (1989) 264.

[119] C. Wetterich, "The Cosmon model for an asymptotically vanishing time dependent cosmological 'constant'," *Astron.Astrophys.* **301** (1995) 321–328, arXiv:hep-th/9408025 [hep-th].

[120] A. A. Starobinsky, "Relict Gravitation Radiation Spectrum and Initial State of the Universe. (In Russian)," *JETP Lett.* **30** (1979) 682–685.

[121] A. H. Guth, "The Inflationary Universe: A Possible Solution to the Horizon and Flatness Problems," *Phys.Rev.* **D23** (1981) 347–356.

[122] G. F. R. Ellis, "The expanding universe: a history of cosmology from 1917 to 1960.," in *Einstein and the History of General Relativity*, D. Howard and J. Stachel, eds., pp. 367–431. Birkhauser, Boston, 1989.

[123] E. W. Kolb, "Dynamics of the inflationary era," arXiv:hep-ph/9910311 [hep-ph].

[124] L. Amendola, D. Bellisai, and F. Occhionero, "Inflationary attractors and perturbation spectra in generally coupled gravity," *Phys.Rev.* **D47** (1993) 4267–4272, arXiv:gr-qc/9303023 [gr-qc].

[125] D. Wands, E. J. Copeland, and A. R. Liddle, "Exponential Potentials, Scaling Solutions, and Inflation," in *Texas/PASCOS '92: Relativistic Astrophysics and Particle Cosmology*, C. W. Akerlof and M. A. Srednicki, eds., vol. 688 of *Annals of the New York Academy of Sciences*, p. 647. 1993.

[126] A. P. Billyard and A. A. Coley, "Interactions in scalar field cosmology," *Phys. Rev.* **D61** (2000) 083503, arXiv:astro-ph/9908224.

[127] L. Amendola, "Scaling solutions in general non-minimal coupling theories," *Phys. Rev.* **D60** (1999) 043501, arXiv:astro-ph/9904120.

[128] D. J. Holden and D. Wands, "Self-similar cosmological solutions with a non-minimally coupled scalar field," *Phys. Rev.* **D61** (2000) 043506, arXiv:gr-qc/9908026.

[129] S. M. Carroll, "Quintessence and the rest of the world," *Phys.Rev.Lett.* **81** (1998) 3067–3070, arXiv:astro-ph/9806099 [astro-ph].

[130] C. G. Boehmer, G. Caldera-Cabral, R. Lazkoz, and R. Maartens, "Dynamics of dark energy with a coupling to dark matter," *Phys. Rev.* **D78** (2008) 023505, arXiv:0801.1565 [gr-qc].

[131] Y. Fujii and K. Maeda, *The scalar-tensor theory of gravitation*. Cambridge University Press, Cambridge, 2003.

[132] T. Damour, "Gravitation, experiment and cosmology," arXiv:gr-qc/9606079 [gr-qc].

[133] C. M. Will, "The Confrontation between general relativity and experiment," *Living Rev.Rel.* **9** (2006) 3, arXiv:gr-qc/0510072 [gr-qc].

[134] J. Bovy and G. R. Farrar, "Connection between a possible fifth force and the direct detection of Dark Matter," *Phys.Rev.Lett.* **102** (2009) 101301, arXiv:0807.3060 [hep-ph].

[135] S. M. Carroll, S. Mantry, M. J. Ramsey-Musolf, and C. W. Stubbs, "Dark-Matter-Induced Weak Equivalence Principle Violation," *Phys.Rev.Lett.* **103** (2009) 011301, arXiv:0807.4363 [hep-ph].

[136] T. Damour, G. Gibbons, and C. Gundlach, "Dark Matter, Time Varying G, and a Dilaton Field," *Phys.Rev.Lett.* **64** (1990) 123–126.

[137] J. Casas, J. Garcia-Bellido, and M. Quiros, "Scalar - tensor theories of gravity with phi dependent masses," *Class.Quant.Grav.* **9** (1992) 1371–1384, arXiv:hep-ph/9204213 [hep-ph].

[138] J. Khoury and A. Weltman, "Chameleon cosmology," *Phys.Rev.* **D69** (2004) 044026, arXiv:astro-ph/0309411 [astro-ph].

[139] I. Navarro and K. Van Acoleyen, "f(R) actions, cosmic acceleration and local tests of gravity," *JCAP* **0702** (2007) 022, arXiv:gr-qc/0611127 [gr-qc].

[140] T. Faulkner, M. Tegmark, E. F. Bunn, and Y. Mao, "Constraining f(R) Gravity as a Scalar Tensor Theory,"

Phys.Rev. **D76** (2007) 063505, arXiv:astro-ph/0612569 [astro-ph].

[141] G. W. Horndeski, "Second-order scalar-tensor field equations in a four-dimensional space," *Int.J.Theor.Phys.* **10** (1974) 363–384.

[142] L. Amendola, "Dark energy and the Boomerang data," *Phys.Rev.Lett.* **86** (2001) 196–199, arXiv:astro-ph/0006300 [astro-ph].

[143] L. Amendola and C. Quercellini, "Tracking and coupled dark energy as seen by WMAP," *Phys.Rev.* **D68** (2003) 023514, arXiv:astro-ph/0303228 [astro-ph].

[144] L. Amendola, "Perturbations in a coupled scalar field cosmology," *Mon. Not. Roy. Astron. Soc.* **312** (2000) 521, arXiv:astro-ph/9906073.

[145] L. Amendola, "Coupled quintessence," *Phys. Rev.* **D62** (2000) 043511, arXiv:astro-ph/9908023.

[146] D. Tocchini-Valentini and L. Amendola, "Stationary dark energy with a baryon dominated era: Solving the coincidence problem with a linear coupling," *Phys. Rev.* **D65** (2002) 063508, arXiv:astro-ph/0108143.

[147] L. Amendola and D. Tocchini-Valentini, "Stationary dark energy: The Present universe as a global attractor," *Phys.Rev.* **D64** (2001) 043509, arXiv:astro-ph/0011243 [astro-ph].

[148] L. Amendola and D. Tocchini-Valentini, "Baryon bias and structure formation in an accelerating universe," *Phys.Rev.* **D66** (2002) 043528, arXiv:astro-ph/0111535 [astro-ph].

[149] L. Amendola, M. Gasperini, and F. Piazza, "Fitting type Ia supernovae with coupled dark energy," *JCAP* **0409** (2004) 014, arXiv:astro-ph/0407573 [astro-ph].

[150] X. Zhang, "Statefinder diagnostic for coupled quintessence," *Phys.Lett.* **B611** (2005) 1–7, arXiv:astro-ph/0503075 [astro-ph].

[151] L. Amendola, "Linear and non-linear perturbations in dark energy models," *Phys. Rev.* **D69** (2004) 103524, arXiv:astro-ph/0311175.

[152] L. Amendola, M. Quartin, S. Tsujikawa, and I. Waga, "Challenges for scaling cosmologies," *Phys. Rev.* **D74** (2006) 023525, arXiv:astro-ph/0605488.

[153] L. Lopez Honorez, O. Mena, and G. Panotopoulos, "Higher-order coupled quintessence," *Phys.Rev.* **D82** (2010) 123525, arXiv:1009.5263 [astro-ph.CO].

[154] S. Lee, G.-C. Liu, and K.-W. Ng, "Constraints on the coupled quintessence from cosmic microwave background anisotropy and matter power spectrum," *Phys.Rev.* **D73** (2006) 083516, arXiv:astro-ph/0601333 [astro-ph].

[155] S. Lee, G.-C. Liu, and K.-W. Ng, "Effects on the two-point correlation function from the coupling of quintessence to dark matter," *Phys.Rev.* **D81** (2010) 061302, arXiv:0910.2175 [astro-ph.CO].

[156] H. Farajollahi and A. Salehi, "Observational constraint in FRW cosmology with a nonminimal scalar field-matter coupling," arXiv:1207.1642 [gr-qc].

[157] L. Vergani, L. P. Colombo, G. La Vacca, and S. A. Bonometto, "Dark Matter - Dark Energy coupling biasing parameter estimates from CMB data," *Astrophys.J.* **697** (2009) 1946–1955, arXiv:0804.0285 [astro-ph].

[158] A. Lewis and S. Bridle, "Cosmological parameters from CMB and other data: a Monte- Carlo approach," *Phys. Rev.* **D66** (2002) 103511, arXiv:astro-ph/0205436.

[159] J.-Q. Xia, "Constraint on coupled dark energy models from observations," *Phys. Rev.* **D80** (2009) 103514, arXiv:0911.4820 [astro-ph.CO].

[160] R. Giambo and J. Miritzis, "Energy exchange for homogeneous and isotropic universes with a scalar field coupled to matter," *Class.Quant.Grav.* **27** (2010) 095003, arXiv:0908.3452 [gr-qc].

[161] M. Manera and D. F. Mota, "Cluster number counts dependence on dark energy inhomogeneities and coupling to dark matter," *Mon. Not. Roy. Astron. Soc.* **371** (2006) 1373, arXiv:astro-ph/0504519.

[162] F. Saracco, M. Pietroni, N. Tetradis, V. Pettorino, and G. Robbers, "Non-linear Matter Spectra in Coupled Quintessence," *Phys.Rev.* **D82** (2010) 023528, arXiv:0911.5396 [astro-ph.CO].

[163] F. Shojai and A. Shojai, "Non-minimal quintessence: Dynamics and coincidence problem," *Pramana* **77** (Dec., 2011) 1179–1189, arXiv:1109.2189 [gr-qc].

[164] L. Amendola, V. Pettorino, C. Quercellini, and A. Vollmer, "Testing coupled dark energy with next-generation large-scale observations," *Phys.Rev.* **D85** (2012) 103008, arXiv:1111.1404 [astro-ph.CO].

[165] V. Pettorino, L. Amendola, C. Baccigalupi, and C. Quercellini, "Constraints on coupled dark energy using CMB data from WMAP and SPT," *Phys.Rev.* **D86** (2012) 103507, arXiv:1207.3293 [astro-ph.CO].

[166] S. Lee, K. A. Olive, and M. Pospelov, "Quintessence models and the cosmological evolution of alpha," *Phys.Rev.* **D70** (2004) 083503, arXiv:astro-ph/0406039 [astro-ph].

[167] D. Comelli, M. Pietroni, and A. Riotto, "Dark energy and dark matter," *Phys. Lett.* **B571** (2003) 115–120, arXiv:hep-ph/0302080.

[168] G. W. Anderson and S. M. Carroll, "Dark matter with time dependent mass," arXiv:astro-ph/9711288 [astro-ph].

[169] U. Franca and R. Rosenfeld, "Age constraints and fine tuning in VAMP models," *Phys.Rev.* **D69** (2004) 063517, arXiv:astro-ph/0308149 [astro-ph].

[170] R. Bean and J. Magueijo, "Dilaton derived quintessence scenario leading naturally to the late time acceleration of the universe," *Phys.Lett.* **B517** (2001) 177–183, arXiv:astro-ph/0007199 [astro-ph].

[171] M. Thorsrud, D. F. Mota, and S. Hervik, "Cosmology of a Scalar Field Coupled to Matter and an Isotropy-Violating Maxwell Field," *JHEP* **1210** (2012) 066, arXiv:1205.6261 [hep-th].

[172] M. Thorsrud, "Quintessence with Kaluza-Klein type couplings to matter and an isotropy-violating vector field," arXiv:1303.2469 [gr-qc].

[173] G. R. Farrar and P. J. E. Peebles, "Interacting dark matter and dark energy," *Astrophys.J.* **604** (2004) 1–11, arXiv:astro-ph/0307316 [astro-ph].

[174] G. Huey and B. D. Wandelt, "Interacting quintessence. The Coincidence problem and cosmic acceleration," *Phys.Rev.* **D74** (2006) 023519, arXiv:astro-ph/0407196 [astro-ph].

[175] S. Micheletti, E. Abdalla, and B. Wang, "A Field Theory Model for Dark Matter and Dark Energy in Interaction," *Phys.Rev.* **D79** (2009) 123506, arXiv:0902.0318 [gr-qc].

[176] O. Bertolami, P. Carrilho, and J. Paramos, "Two-scalar-field model for the interaction of dark energy and dark matter," *Phys.Rev.* **D86** (2012) 103522, arXiv:1206.2589 [gr-qc].

[177] A. Pavan, E. G. Ferreira, S. Micheletti, J. de Souza, and E. Abdalla, "Exact cosmological solutions of models with an interacting dark sector," *Phys.Rev.* **D86** (2012) 103521, arXiv:1111.6526 [gr-qc].

[178] D. Bazeia, C. Gomes, L. Losano, and R. Menezes, "First-order formalism and dark energy," *Phys.Lett.* **B633** (2006) 415–419, arXiv:astro-ph/0512197 [astro-ph].

[179] T. S. Koivisto and N. J. Nunes, "Coupled three-form dark energy," arXiv:1212.2541 [astro-ph.CO].

[180] S. Kumar, S. Panda, and A. A. Sen, "Cosmology With Axionic-quintessence Coupled with Dark Matter," *Class.Quant.Grav.* **30** (2013) 155011, arXiv:1302.1331 [astro-ph.CO].

[181] A. Brookfield, C. van de Bruck, and L. M. Hall, "New interactions in the dark sector mediated by dark energy," *Phys.Rev.* **D77** (2008) 043006, arXiv:0709.2297 [astro-ph].

[182] M. Baldi, "Multiple Dark Matter as a self-regulating mechanism for dark sector interactions," *Annalen Phys.* **524** (2012) 602–617, arXiv:1204.0514 [astro-ph.CO].

[183] M. Baldi, "Structure formation in Multiple Dark Matter cosmologies with long-range scalar interactions," arXiv:1206.2348 [astro-ph.CO].

[184] G. La Vacca, S. Bonometto, and L. Colombo, "Higher neutrino mass allowed if DM and DE are coupled," *New Astron.* **14** (2009) 435–442, arXiv:0810.0127 [astro-ph].

[185] G. La Vacca, J. R. Kristiansen, L. P. L. Colombo, R. Mainini, and S. A. Bonometto, "Do WMAP data favor neutrino mass and a coupling between Cold Dark Matter and Dark Energy?," *JCAP* **0904** (2009) 007, arXiv:0902.2711 [astro-ph.CO].

[186] J. Kristiansen, G. La Vacca, L. Colombo, R. Mainini, and S. Bonometto, "Coupling between cold dark matter and dark energy from neutrino mass experiments," *New Astron.* **15** (2010) 609–613, arXiv:0902.2737 [astro-ph.CO].

[187] H. V. Klapdor-Kleingrothaus, "First evidence for neutrinoless doubly beta decay: And world status of double beta experiments," arXiv:hep-ph/0512263 [hep-ph].

[188] G. Drexlin, V. Hannen, S. Mertens, and C. Weinheimer, "Current direct neutrino mass experiments," *Adv.High Energy Phys.* **2013** (2013) 293986.

[189] R. Mainini and D. F. Mota, "ISW-LSS cross-correlation in coupled Dark Energy models with massive neutrinos," *Astrophys.J.* **744** (2012) 3, arXiv:1011.0083 [astro-ph.CO].

[190] R. Mainini, "Voids and overdensities of coupled Dark Energy," *JCAP* **0904** (2009) 017, arXiv:0903.0574 [astro-ph.CO].

[191] W. Cui, M. Baldi, and S. Borgani, "The halo mass function in interacting Dark Energy models," arXiv:1201.3568 [astro-ph.CO].

[192] M. Le Delliou and T. Barreiro, "Interacting dark energy collapse with matter components separation," *JCAP* **1302** (2013) 037, arXiv:1208.6373 [astro-ph.CO].

[193] A. V. Maccio, C. Quercellini, R. Mainini, L. Amendola, and S. A. Bonometto, "N-body simulations for coupled dark energy: Halo mass function and density profiles," *Phys.Rev.* **D69** (2004) 123516, arXiv:astro-ph/0309671 [astro-ph].

[194] J. F. Navarro, C. S. Frenk, and S. D. White, "A Universal density profile from hierarchical clustering," *Astrophys.J.* **490** (1997) 493–508, arXiv:astro-ph/9611107 [astro-ph].

[195] V. Pettorino and C. Baccigalupi, "Coupled and Extended Quintessence: theoretical differences and structure formation," *Phys.Rev.* **D77** (2008) 103003, arXiv:0802.1086 [astro-ph].

[196] B. Li and H. Zhao, "Structure Formation by Fifth Force I: N-Body vs. Linear Simulations," *Phys. Rev.* **D80** (2009) 044027, arXiv:0906.3880 [astro-ph.CO].

[197] H. Zhao, A. Maccio', B. Li, H. Hoekstra, and M. Feix, "Structure Formation by Fifth Force: Power Spectrum from N-Body Simulations," *Astrophys.J.* **712** (2010) L179–L183, arXiv:0910.3207 [astro-ph.CO].

[198] B. Li and H. Zhao, "Structure Formation by the Fifth Force III: Segregation of Baryons and Dark Matter," *Phys. Rev.* **D81** (2010) 104047, arXiv:1001.3152 [astro-ph.CO].

[199] B. Li and J. D. Barrow, "N-Body Simulations for Coupled Scalar Field Cosmology," *Phys. Rev.* **D83** (2011) 024007, arXiv:1005.4231 [astro-ph.CO].

[200] B. Li, "Voids in Coupled Scalar Field Cosmology," *Mon.Not.Roy.Astron.Soc.* **411** (2011) 2615, arXiv:1009.1406 [astro-ph.CO].

[201] B. Li and J. D. Barrow, "On the Effects of Coupled Scalar Fields on Structure Formation," *Mon.Not.Roy.Astron.Soc.* **413** (2011) 262–270, arXiv:1010.3748 [astro-ph.CO].

[202] M. Baldi, "The CoDECS project: a publicly available suite of cosmological N-body simulations for interacting dark energy models," *Mon.Not.Roy.Astron.Soc.* **422** (2012) 1028–1044, arXiv:1109.5695 [astro-ph.CO].

[203] V. Springel, "The Cosmological simulation code GADGET-2," *Mon.Not.Roy.Astron.Soc.* **364** (2005) 1105–1134, arXiv:astro-ph/0505010 [astro-ph].

[204] M. Baldi, "Simulations of structure formation in interacting dark energy cosmologies," *Nucl.Phys.Proc.Suppl.* **194** (2009) 178–184, arXiv:0906.5353 [astro-ph.CO].

[205] G. Ballesteros and J. Lesgourgues, "Dark energy with non-adiabatic sound speed: initial conditions and detectability," *JCAP* **1010** (2010) 014, arXiv:1004.5509 [astro-ph.CO].

[206] M. Baldi and M. Viel, "The Impact of Coupled Dark Energy Cosmologies on the High- Redshift Intergalactic Medium," *Mon. Not. Roy. Astron. Soc.* **409** (2010) 89, arXiv:1007.3736 [astro-ph.CO].

[207] M. Baldi, J. Lee, and A. V. Maccio, "The Effect of Coupled Dark Energy on the Alignment between Dark Matter and Galaxy Distributions in Clusters," *Astrophys.J.* **732** (2011) 112, arXiv:1101.5761 [astro-ph.CO].

[208] M. Oguri, M. Takada, N. Okabe, and G. P. Smith, "Direct measurement of dark matter halo ellipticity from two-dimensional lensing shear maps of 25 massive clusters,"

Mon.Not.Roy.Astron.Soc. **405** (2010) 2215–2230, arXiv:1004.4214 [astro-ph.CO].

[209] J. Lee, "The Spin Alignments in Galaxy Pairs as a Test of Bouncing Coupled Dark Energy," arXiv:1111.5886 [astro-ph.CO].

[210] M. Baldi and V. Pettorino, "High-z massive clusters as a test for dynamical coupled dark energy," *Mon. Not. Roy. Astron. Soc.* **412** (2011) L1, arXiv:1006.3761 [astro-ph.CO].

[211] M. Baldi, "Early massive clusters and the bouncing coupled dark energy," *Mon.Not.Roy.Astron.Soc.* **420** (2012) 430–440, arXiv:1107.5049 [astro-ph.CO].

[212] J. Lee and M. Baldi, "Can Coupled Dark Energy Speed Up the Bullet Cluster?," *Astrophys.J.* **747** (2012) 45, arXiv:1110.0015 [astro-ph.CO].

[213] V. D. V. Cervantes, F. Marulli, L. Moscardini, M. Baldi, and A. Cimatti, "Exploiting the shift of baryonic acoustic oscillations as a dynamical probe for dark interactions," arXiv:1212.0853 [astro-ph.CO].

[214] C. Giocoli, F. Marulli, M. Baldi, L. Moscardini, and R. B. Metcalf, "Characterizing dark interactions with the halo mass accretion history and structural properties," arXiv:1301.3151 [astro-ph.CO].

[215] E. Beynon, M. Baldi, D. J. Bacon, K. Koyama, and C. Sabiu, "Weak lensing predictions for coupled dark energy cosmologies at non-linear scales," *Mon.Not.Roy.Astron.Soc.* **422** (2012) 3546–3553, arXiv:1111.6974 [astro-ph.CO].

[216] F. Marulli, M. Baldi, and L. Moscardini, "Clustering and redshift-space distortions in interacting dark energy cosmologies,"

Mon.Not.Roy.Astron.Soc. **420** (2012) 2377, arXiv:1110.3045 [astro-ph.CO].

[217] M. Baldi, "Time dependent couplings in the dark sector: from background evolution to nonlinear structure formation," *Mon. Not. Roy. Astron. Soc.* **411** (2011) 1077, arXiv:1005.2188 [astro-ph.CO].

[218] M. Baldi, "Clarifying the effects of interacting dark energy on linear and nonlinear structure formation processes," *Mon. Not. Roy. Astron. Soc.* **414** (2011) 116, arXiv:1012.0002 [astro-ph.CO].

[219] M. Baldi and P. Salucci, "Constraints on interacting dark energy models from galaxy Rotation Curves," *JCAP* **1202** (2012) 014, arXiv:1111.3953 [astro-ph.CO].

[220] C. Eckart, "The Thermodynamics of irreversible processes. 3.. Relativistic theory of the simple fluid," *Phys.Rev.* **58** (1940) 919–924.

[221] M. B. Gavela, L. Lopez Honorez, O. Mena, and S. Rigolin, "Dark Coupling and Gauge Invariance," *JCAP* **1011** (2010) 044, arXiv:1005.0295 [astro-ph.CO].

[222] L. P. Chimento, A. S. Jakubi, D. Pavon, and W. Zimdahl, "Interacting quintessence solution to the coincidence problem," *Phys. Rev.* **D67** (2003) 083513, arXiv:astro-ph/0303145.

[223] W. Zimdahl and D. Pavon, "Statefinder parameters for interacting dark energy," *Gen.Rel.Grav.* **36** (2004) 1483–1491, arXiv:gr-qc/0311067 [gr-qc].

[224] H. M. Sadjadi and M. Alimohammadi, "Cosmological coincidence problem in interacting dark energy models," *Phys. Rev.* **D74** (2006) 103007, arXiv:gr-qc/0610080.

[225] G. Olivares, F. Atrio-Barandela, and D. Pavon, "Dynamics of Interacting Quintessence Models: Observational Constraints," *Phys. Rev.* **D77** (2008) 063513, arXiv:0706.3860 [astro-ph].

[226] M. Quartin, M. O. Calvao, S. E. Joras, R. R. R. Reis, and I. Waga, "Dark Interactions and Cosmological Fine-Tuning," *JCAP* **0805** (2008) 007, arXiv:0802.0546 [astro-ph].

[227] M. Cataldo, F. Arevalo, and P. Minning, "On a class of scaling FRW cosmological models," *JCAP* **1002** (2010) 024, arXiv:1002.3415 [astro-ph.CO].

[228] J.-H. he he, B. Wang, and Y. P. Jing, "Effects of dark sectors' mutual interaction on the growth of structures," *JCAP* **0907** (2009) 030. http://arxiv.org/abs/0902.0660.

[229] C. Quercellini, M. Bruni, A. Balbi, and D. Pietrobon, "Late universe dynamics with scale-independent linear couplings in the dark sector," *Phys. Rev.* **D78** (2008) 063527, arXiv:0803.1976 [astro-ph].

[230] X. ming Chen, Y. gui Gong, and E. N. Saridakis, "Phase-space analysis of interacting phantom cosmology," *JCAP* **0904** (2009) 001, arXiv:0812.1117 [gr-qc].

[231] J. D. Barrow and T. Clifton, "Cosmologies with energy exchange," *Phys.Rev.* **D73** (2006) 103520, arXiv:gr-qc/0604063 [gr-qc].

[232] L. P. Chimento, M. I. Forte, and G. M. Kremer, "Cosmological model with interactions in the dark sector," *Gen.Rel.Grav.* **41** (2009) 1125–1137, arXiv:0711.2646 [astro-ph].

[233] J. Lu, Y. Wu, Y. Jin, and Y. Wang, "Investigate the interaction between dark matter and dark energy," *Results in Physics* **2** (Jan., 2012) 14–21, arXiv:1203.4905 [astro-ph.CO].

[234] Z.-K. Guo, N. Ohta, and S. Tsujikawa, "Probing the Coupling between Dark Components of the Universe," *Phys. Rev.* **D76** (2007) 023508, arXiv:astro-ph/0702015.

[235] G. M. Kremer and O. A. Sobreiro, "Bulk viscous cosmological model with interacting dark fluids," *Braz.J.Phys.* **42** (2012) 77–83, arXiv:1109.5068 [gr-qc].

[236] X.-m. Chen, Y. Gong, E. N. Saridakis, Y. Gong, and E. N. Saridakis, "Time-dependent interacting dark energy and transient acceleration," arXiv:1111.6743 [astro-ph.CO].

[237] Y.-H. Li and X. Zhang, "Running coupling: Does the coupling between dark energy and dark matter change sign during the cosmological evolution?," *Eur. Phys. J.* **C71** (2011) 1700, arXiv:1103.3185 [astro-ph.CO].

[238] M. Chevallier and D. Polarski, "Accelerating universes with scaling dark matter," *Int.J.Mod.Phys.* **D10** (2001) 213–224, arXiv:gr-qc/0009008 [gr-qc].

[239] E. V. Linder, "Strong gravitational lensing and dark energy complementarity," *Phys. Rev. D* **70** no. 4, (Aug, 2004) 043534.

[240] J. C. Fabris, B. Fraga, N. Pinto-Neto, and W. Zimdahl, "Transient cosmic acceleration from interacting fluids," *JCAP* **1004** (2010) 008, arXiv:0910.3246 [astro-ph.CO].

[241] A. Shafieloo, V. Sahni, and A. A. Starobinsky, "Is cosmic acceleration slowing down?," *Phys.Rev.* **D80** (2009) 101301, arXiv:0903.5141 [astro-ph.CO].

[242] C. Z. Vargas, W. S. Hipolito-Ricaldi, and W. Zimdahl, "Perturbations for transient acceleration," *JCAP* **1204** (2012) 032, arXiv:1112.5337 [astro-ph.CO].

[243] W. Zimdahl, C. Vargas, and W. Hipólito-Ricaldi, "Interacting dark energy and transient accelerated expansion," arXiv:1302.1347 [astro-ph.CO].

[244] L. Amendola, G. Camargo Campos, and R. Rosenfeld, "Consequences of dark matter-dark energy interaction on cosmological parameters derived from SNIa data," *Phys.Rev.* **D75** (2007) 083506, arXiv:astro-ph/0610806 [astro-ph].

[245] C. Feng, B. Wang, E. Abdalla, and R.-K. Su, "Observational constraints on the dark energy and dark matter mutual coupling," *Phys.Lett.* **B665** (2008) 111–119, arXiv:0804.0110 [astro-ph].

[246] J.-H. He, B. Wang, and E. Abdalla, "Testing the interaction between dark energy and dark matter via latest observations," *Phys. Rev.* **D83** (2011) 063515, arXiv:1012.3904 [astro-ph.CO].

[247] J.-H. He and B. Wang, "Effects of the interaction between dark energy and dark matter on cosmological parameters," *JCAP* **0806** (2008) 010, arXiv:0801.4233 [astro-ph].

[248] X. Chen, B. Wang, N. Pan, and Y. Gong, "Constraining the interacting dark energy models from weak gravity conjecture and recent observations," *Phys. Lett.* **B695** (2011) 30–36, arXiv:1008.3455 [astro-ph.CO].

[249] M. Martinelli, L. Lopez Honorez, A. Melchiorri, and O. Mena, "Future CMB cosmological constraints in a dark coupled universe," *Phys.Rev.* **D81** (2010) 103534, arXiv:1004.2410 [astro-ph.CO].

[250] X.-D. Xu, J.-H. He, and B. Wang, "Breaking parameter degeneracy in interacting dark energy models from observations," *Phys. Lett.* **B701** (2011) 513–519, arXiv:1103.2632 [astro-ph.CO].

[251] T. Barreiro, O. Bertolami, and P. Torres, "Gamma-Ray Bursts and Dark Energy - Dark Matter interaction," *Mon.Not.Roy.Astron.Soc.* **409** (2010) 750–754, arXiv:1004.4562 [astro-ph.CO].

[252] Y. Pan, S. Cao, Y. Gong, K. Liao, and Z.-H. Zhu, "Testing the interaction model with cosmological data and gamma-ray bursts," *Phys.Lett.* **B718** (2013) 699–703, arXiv:1211.0184 [astro-ph.CO].

[253] O. Bertolami, F. Gil Pedro, and M. Le Delliou, "Dark Energy-Dark Matter Interaction and the Violation of the Equivalence Principle from the Abell Cluster A586," *Phys.Lett.* **B654** (2007) 165–169, arXiv:astro-ph/0703462 [ASTRO-PH].

[254] O. Bertolami, F. Gil Pedro, and M. Le Delliou, "Testing the interaction of dark energy to dark matter through the analysis of virial relaxation of clusters Abell Clusters A586 and A1689 using realistic density profiles," *Gen.Rel.Grav.* **44** (2012) 1073–1088, arXiv:1105.3033 [astro-ph.CO].

[255] E. Abdalla, L. R. W. Abramo, J. L. Sodre, and B. Wang, "Signature of the interaction between dark energy and dark matter in galaxy clusters," *Phys. Lett.* **B673** (2009) 107–110, arXiv:0710.1198 [astro-ph].

[256] E. Abdalla, L. R. Abramo, and J. C. de Souza, "Signature of the interaction between dark energy and dark matter in observations," *Phys.Rev.* **D82** (2010) 023508, arXiv:0910.5236 [gr-qc].

[257] J.-H. He, B. Wang, E. Abdalla, and D. Pavon, "The Imprint of the interaction between dark sectors in galaxy clusters," *JCAP* **1012** (2010) 022, arXiv:1001.0079 [gr-qc].

[258] C. Pellicer, E. G. Ferreira, D. C. Guariento, A. A. Costa, L. L. Graef, *et al.*, "The role of Dark Matter interaction in galaxy clusters,"

Mod.Phys.Lett. **A27** (2012) 1250144, arXiv:1102.5113 [astro-ph.CO].

[259] J. Lee, "The Misalignments between Matter and Galaxy Distributions in Triaxial Clusters: A Signature of a Possible Fifth Force?," arXiv:1008.4620 [astro-ph.CO].

[260] G. 't Hooft, "Dimensional reduction in quantum gravity," arXiv:gr-qc/9310026 [gr-qc].

[261] B. Wang, C.-Y. Lin, D. Pavon, and E. Abdalla, "Thermodynamical description of the interaction between dark energy and dark matter," *Phys.Lett.* **B662** (2008) 1–6, arXiv:0711.2214 [hep-th].

[262] D. Pavon and W. Zimdahl, "Holographic dark energy and cosmic coincidence," *Phys.Lett.* **B628** (2005) 206–210, arXiv:gr-qc/0505020 [gr-qc].

[263] B. Wang, Y. gui Gong, and E. Abdalla, "Transition of the dark energy equation of state in an interacting holographic dark energy model," *Phys. Lett.* **B624** (2005) 141–146, arXiv:hep-th/0506069.

[264] Q. Wu, Y. Gong, A. Wang, and J. Alcaniz, "Current constraints on interacting holographic dark energy," *Phys.Lett.* **B659** (2008) 34–39, arXiv:0705.1006 [astro-ph].

[265] C. Feng, B. Wang, Y. Gong, and R.-K. Su, "Testing the viability of the interacting holographic dark energy model by using combined observational constraints," *JCAP* **0709** (2007) 005, arXiv:0706.4033 [astro-ph].

[266] A. Rozas-Fernandez, D. Brizuela, and N. Cruz, "Interacting holographic tachyon model of dark energy," *Int.J.Mod.Phys.* **D19** (2010) 573, arXiv:1002.2929 [gr-qc].

[267] K. Xiao and J.-Y. Zhu, "Dynamical behavior of interacting dark energy in loop quantum cosmology," *Int.J.Mod.Phys.* **A25** (2010) 4993–5007, arXiv:1006.5377 [gr-qc].

[268] S. Li and Y. Ma, "Dark Energy Interacting with Dark Matter in Classical Einstein and Loop Quantum Cosmology," *Eur.Phys.J.* **C68** (2010) 227–239, arXiv:1004.4350 [astro-ph.CO].

[269] O. Lemets and D. Yerokhin, "Interacting dark energy models in fractal cosmology," arXiv:1202.3457 [astro-ph.CO].

[270] A. Sheykhi and M. Sadegh Movahed, "Interacting Ghost Dark Energy in Non-Flat Universe," *Gen.Rel.Grav.* **44** (2012) 449–465, arXiv:1104.4713 [hep-th].

[271] M. Malekjani and A. Khodam-Mohammadi, "Statefinder diagnosis and the interacting ghost model of dark energy," *Astrophys.Space Sci.* **343** (2013) 451–461, arXiv:1202.4154 [gr-qc].

[272] M. Malekjani, "Statefinder description of interacting generalized QCD ghost dark energy," *In. J. Mod. Phys D* **22** (2013) 1350084, arXiv:1212.4673 [gr-qc].

[273] M. Jamil, "A Single model of interacting dark energy: Generalized phantom energy or generalized Chaplygin gas," *Int.J.Theor.Phys.* **49** (2010) 144–151, arXiv:0912.4468 [hep-th].

[274] H. Amirhashchi, A. Pradhan, and H. Zainuddin, "Interacting Two-Fluid Viscous Dark Energy Models In Non-Flat Universe," *Res.Astron.Astrophys.* **13** (2013) 129–138, arXiv:1210.4637 [astro-ph.CO].

[275] G. Olivares, F. Atrio-Barandela, and D. Pavon, "Observational constraints on interacting quintessence models,"

Phys.Rev. **D71** (2005) 063523, arXiv:astro-ph/0503242 [astro-ph].

[276] G. Olivares, F. Atrio-Barandela, and D. Pavon, "Matter density perturbations in interacting quintessence models," *Phys. Rev.* **D74** (2006) 043521, arXiv:astro-ph/0607604.

[277] L. L. Honorez, "Non-adiabatic instability in coupled dark sectors," arXiv:0905.2352 [astro-ph.CO].

[278] F. De Bernardis, M. Martinelli, A. Melchiorri, O. Mena, and A. Cooray, "Future weak lensing constraints in a dark coupled universe," *Phys. Rev.* **D84** (2011) 023504, arXiv:1104.0652 [astro-ph.CO].

[279] G. Izquierdo and D. Pavon, "Limits on the parameters of the equation of state for interacting dark energy," *Phys.Lett.* **B688** (2010) 115–124, arXiv:1004.2360 [astro-ph.CO].

[280] S. A. Bludman, "Tracking quintessence would require two cosmic coincidences," *Phys.Rev.* **D69** (2004) 122002, arXiv:astro-ph/0403526 [astro-ph].

[281] M. Capone, C. Rubano, and P. Scudellaro, "Slow rolling, inflation, and quintessence," *Europhys.Lett.* **73** (2006) 149–155, arXiv:astro-ph/0607556 [astro-ph].

[282] E. V. Linder, "The paths of quintessence," *Phys.Rev.* **D73** (2006) 063010, arXiv:astro-ph/0601052 [astro-ph].

[283] R. N. Cahn, R. de Putter, and E. V. Linder, "Field Flows of Dark Energy," *JCAP* **0811** (2008) 015, arXiv:0807.1346 [astro-ph].

[284] D. Pavon and B. Wang, "Le Chatelier-Braun principle in cosmological physics," *Gen.Rel.Grav.* **41** (2009) 1–5, arXiv:0712.0565 [gr-qc].

[285] J. S. Alcaniz and J. Lima, "Interpreting cosmological vacuum decay," *Phys.Rev.* **D72** (2005) 063516, arXiv:astro-ph/0507372 [astro-ph].

[286] S. Pereira and J. Jesus, "Can Dark Matter Decay in Dark Energy?," *Phys.Rev.* **D79** (2009) 043517, arXiv:0811.0099 [astro-ph].

[287] S. Cotsakis and G. Kittou, "Singularities in cosmologies with interacting fluids," *Phys.Lett.* **B712** (2012) 16–21, arXiv:1202.1407 [gr-qc].

[288] S. Cotsakis and G. Kittou, "Limits of isotropic universes with interacting fluids," arXiv:1302.4345 [gr-qc].

[289] H. Amirhashchi, A. Pradhan, and B. Saha, "An Interacting Two-Fluid Scenario for Dark Energy in FRW Universe," *Chin. Phys. Lett.* **28** (2011) 039801, arXiv:1011.3940 [gr-qc].

[290] B. Gumjudpai and K. Thepsuriya, "Scalar field power-law cosmology with spatial curvature and dark energy-dark matter interaction," *Astrophys.Space Sci.* **342** (2012) 537–547, arXiv:1207.2920 [astro-ph.CO].

[291] W. Cui, Y. Zhang, and Z. Fu, "Transient Accelerating Scalar Models with Exponential Potential," arXiv:1303.2315 [astro-ph.CO].

[292] R. Cen, "Decaying cold dark matter model and small-scale power," *Astrophys.J.* **546** (2001) L77–L80, arXiv:astro-ph/0005206 [astro-ph].

[293] M. Oguri, K. Takahashi, H. Ohno, and K. Kotake, "Decaying cold dark matter and the evolution of the cluster abundance," *Astrophys.J.* **597** (2003) 645–649, arXiv:astro-ph/0306020 [astro-ph].

[294] H. Ziaeepour, "Quintessence From The Decay of a Superheavy Dark Matter," *Phys. Rev.* **D69** (2004) 063512, arXiv:astro-ph/0308515.

[295] B. M. Schaefer, "The integrated Sachs-Wolfe effect in cosmologies with coupled dark matter and dark energy," *Mon.Not.Roy.Astron.Soc.* **388** (2008) 1403–1408, arXiv:0803.2239 [astro-ph].

[296] B. M. Schaefer, G. A. Caldera-Cabral, and R. Maartens, "Constraints on the decay of dark matter to dark energy from weak lensing bispectrum tomography," arXiv:0803.2154 [astro-ph].

[297] G. Caldera-Cabral, R. Maartens, and L. A. Urena-Lopez, "Dynamics of interacting dark energy," *Phys. Rev.* **D79** (2009) 063518, arXiv:0812.1827 [gr-qc].

[298] G. Caldera-Cabral, R. Maartens, and B. M. Schaefer, "The Growth of Structure in Interacting Dark Energy Models," *JCAP* **0907** (2009) 027, arXiv:0905.0492 [astro-ph.CO].

[299] K. Koyama, R. Maartens, and Y.-S. Song, "Velocities as a probe of dark sector interactions," *JCAP* **0910** (2009) 017, arXiv:0907.2126 [astro-ph.CO].

[300] L. L. Honorez, B. A. Reid, O. Mena, L. Verde, and R. Jimenez, "Coupled dark matter-dark energy in light of near Universe observations," *JCAP* **1009** (2010) 029, arXiv:1006.0877 [astro-ph.CO].

[301] G. Mangano, G. Miele, and V. Pettorino, "Coupled quintessence and the coincidence problem," *Mod.Phys.Lett.* **A18** (2003) 831–842, arXiv:astro-ph/0212518 [astro-ph].

[302] N. Cruz, G. Palma, D. Zambrano, and A. Avelino, "Interacting warm dark matter," arXiv:1211.6657 [astro-ph.CO].

[303] S. Z. W. Lip, "Interacting Cosmological Fluids and the Coincidence Problem," *Phys. Rev.* **D83** (2011) 023528, arXiv:1009.4942 [gr-qc].

[304] C. G. Boehmer, G. Caldera-Cabral, N. Chan, R. Lazkoz, and R. Maartens, "Quintessence with quadratic coupling to dark matter," *Phys. Rev.* **D81** (2010) 083003, arXiv:0911.3089 [gr-qc].

[305] E. Majerotto, J. Valiviita, and R. Maartens, "Adiabatic initial conditions for perturbations in interacting dark energy models," *Mon. Not. Roy. Astron. Soc.* **402** (2010) 2344–2354, arXiv:0907.4981 [astro-ph.CO].

[306] J. Valiviita, R. Maartens, and E. Majerotto, "Observational constraints on an interacting dark energy model," *Mon. Not. Roy. Astron. Soc.* **402** (2010) 2355–2368, arXiv:0907.4987 [astro-ph.CO].

[307] M. Doran, C. M. Muller, G. Schafer, and C. Wetterich, "Gauge-invariant initial conditions and early time perturbations in quintessence universes," *Phys.Rev.* **D68** (2003) 063505, arXiv:astro-ph/0304212 [astro-ph].

[308] W. J. Potter and S. Chongchitnan, "A gauge-invariant approach to interactions in the dark sector," *JCAP* **1109** (2011) 005, arXiv:1108.4414 [astro-ph.CO].

[309] H. Wei and R.-G. Cai, "A New Model of Agegraphic Dark Energy," *Phys.Lett.* **B660** (2008) 113–117, arXiv:0708.0884 [astro-ph].

[310] K. Karami and A. Abdolmaleki, "Reconstructing interacting new agegraphic polytropic gas model in non-flat FRW universe," *Astrophys.Space Sci.* **330** (2010) 133, arXiv:1010.4294 [hep-th].

[311] M. Malekjani, A. Khodam-Mohammadi, and M. Taji, "Statefinder diagnostic and $w - w'$ analysis for interacting polytropic gas dark

energy model," *Int.J.Theor.Phys.* **51** (2012) 3141–3151, arXiv:1201.0589 [gr-qc].

[312] R. C. de Souza and G. M. Kremer, "Dark Sector from Interacting Canonical and Non-Canonical Scalar Fields," *Class.Quant.Grav.* **27** (2010) 175006, arXiv:1006.3146 [gr-qc].

[313] E. Abdalla, L. Graef, and B. Wang, "A Model for Dark Energy decay," arXiv:1202.0499 [gr-qc].

[314] M. Khurshudyan, "A Dark Energy Model interacting with Dark Matter described by an effective EoS," arXiv:1302.1220 [gr-qc].

[315] S. del Campo, R. Herrera, and D. Pavon, "Soft coincidence in late acceleration," *Phys.Rev.* **D71** (2005) 123529, arXiv:astro-ph/0506482 [astro-ph].

[316] S. del Campo, R. Herrera, G. Olivares, and D. Pavon, "Interacting models of soft coincidence," *Phys.Rev.* **D74** (2006) 023501, arXiv:astro-ph/0606520 [astro-ph].

[317] R.-G. Cai and Q. Su, "On the Dark Sector Interactions," *Phys.Rev.* **D81** (2010) 103514, arXiv:0912.1943 [astro-ph.CO].

[318] H. Wei, "Cosmological Evolution of Quintessence and Phantom with a New Type of Interaction in Dark Sector," *Nucl.Phys.* **B845** (2011) 381–392, arXiv:1008.4968 [gr-qc].

[319] H. Wei, "Cosmological Constraints on the Sign-Changeable Interactions," *Commun.Theor.Phys.* **56** (2011) 972–980, arXiv:1010.1074 [gr-qc].

[320] C.-Y. Sun and R.-H. Yue, "New Interaction between Dark Energy and Dark Matter Changes Sign during Cosmological Evolution," *Phys.Rev.* **D85** (2012) 043010, arXiv:1009.1214 [gr-qc].

[321] L. P. Chimento, "Linear and nonlinear interactions in the dark sector," *Phys.Rev.* **D81** (2010) 043525, arXiv:0911.5687 [astro-ph.CO].

[322] L. P. Chimento, "Exactly solved models of interacting dark matter and dark energy," in *American Institute of Physics Conference Series*, J. Alcaniz, S. Carneiro, L. P. Chimento, S. Del Campo, J. C. Fabris, J. A. S. Lima, and W. Zimdahl, eds., vol. 1471 of *American Institute of Physics Conference Series*, pp. 30–38. Oct., 2012. arXiv:1204.5797 [gr-qc].

[323] T. Ngampitipan and P. Wongjun, "Dynamics of three-form dark energy with dark matter couplings," *JCAP* **1111** (2011) 036, arXiv:1108.0140 [hep-ph].

[324] N. Dalal, K. Abazajian, E. E. Jenkins, and A. V. Manohar, "Testing the cosmic coincidence problem and the nature of dark energy," *Phys.Rev.Lett.* **87** (2001) 141302, arXiv:astro-ph/0105317 [astro-ph].

[325] I. Ferreras, A. Melchiorri, and D. Tocchini-Valentini, "Using bright ellipticals as dark energy cosmic clocks," *Mon.Not.Roy.Astron.Soc.* **344** (2003) 257, arXiv:astro-ph/0302180 [astro-ph].

[326] L. M. Krauss and B. Chaboyer, "New globular cluster age estimates and constraints on the cosmic equation of state and the matter density of the universe," arXiv:astro-ph/0111597 [astro-ph].

[327] I. Ferreras, A. Melchiorri, and J. Silk, "How old is the universe? Setting new constraints on the age of the universe," *Mon.Not.Roy.Astron.Soc.* **327** (2001) L47, arXiv:astro-ph/0105384 [astro-ph].

[328] W. Zimdahl and D. Pavon, "Scaling cosmology," *Gen.Rel.Grav.* **35** (2003) 413–422, arXiv:astro-ph/0210484 [astro-ph].

[329] D. Pavon, S. Sen, and W. Zimdahl, "CMB constraints on interacting cosmological models," *JCAP* **0405** (2004) 009, arXiv:astro-ph/0402067 [astro-ph].

[330] Y. Chen, Z.-H. Zhu, J. Alcaniz, and Y. Gong, "Using A Phenomenological Model to Test the Coincidence Problem of Dark Energy," *Astrophys.J.* **711** (2010) 439–444, arXiv:1001.1489 [astro-ph.CO].

[331] P. Wang and X.-H. Meng, "Can vacuum decay in our universe?," *Class.Quant.Grav.* **22** (2005) 283–294, arXiv:astro-ph/0408495 [astro-ph].

[332] F. Costa, J. Barboza, E.M., and J. Alcaniz, "Cosmology with interaction in the dark sector," *Phys.Rev.* **D79** (2009) 127302, arXiv:0905.0672 [astro-ph.CO].

[333] J. Jesus, R. Santos, J. Alcaniz, and J. Lima, "New coupled quintessence cosmology," *Phys.Rev.* **D78** (2008) 063514, arXiv:0806.1366 [astro-ph].

[334] M. de Campos, "Observational consequences of a dark interaction model," *Braz.J.Phys.* **40** (2010) 398, arXiv:0912.1143 [gr-qc].

[335] F. Simpson, B. M. Jackson, and J. A. Peacock, "Unmodified Gravity," *Mon. Not. Roy. Astron. Soc.* **411** (Feb., 2011) 1053–1058, arXiv:1004.1920 [astro-ph.CO].

[336] P. Ferreira, J. Carvalho, and J. Alcaniz, "Probing interaction in the dark sector," *Phys.Rev.* **D87** (2013) 087301, arXiv:1212.2492 [astro-ph.CO].

[337] R. Herrera, D. Pavon, and W. Zimdahl, "Exact solutions for the interacting tachyonic - dark matter system," *Gen.Rel.Grav.* **36** (2004) 2161–2169, arXiv:astro-ph/0404086 [astro-ph].

[338] M. Bento, O. Bertolami, and A. A. Sen, "The Revival of the unified dark energy - dark matter model?," *Phys.Rev.* **D70** (2004) 083519, arXiv:astro-ph/0407239 [astro-ph].

[339] P. Avelino and H. da Silva, "Effective dark energy equation of state in interacting dark energy models," *Phys.Lett.* **B714** (2012) 6–10, arXiv:1201.0550 [astro-ph.CO].

[340] F. Costa and J. Alcaniz, "Cosmological consequences of a possible Λ-dark matter interaction," *Phys.Rev.* **D81** (2010) 043506, arXiv:0908.4251 [astro-ph.CO].

[341] H. Wei, "Revisiting the Cosmological Constraints on the Interacting Dark Energy Models," *Phys.Lett.* **B691** (2010) 173–182, arXiv:1004.0492 [gr-qc].

[342] F. C. Solano and U. Nucamendi, "Reconstruction of the interaction term between dark matter and dark energy using SNe Ia," *JCAP* **1204** (2012) 011, arXiv:1109.1303 [astro-ph.CO].

[343] F. C. Solano and U. Nucamendi, "Reconstruction of the interaction term between dark matter and dark energy using SNe Ia, BAO, CMB, H(z) and X-ray gas mass fraction," arXiv:1207.0250 [astro-ph.CO].

[344] H. Wei and S. N. Zhang, "How to distinguish dark energy and modified gravity?," *Phys.Rev.D* **78** (2008) 023011. http://arxiv.org/abs/0803.3292.

[345] L. Amendola, M. Baldi, and C. Wetterich, "Quintessence cosmologies with a growing matter component," *Phys.Rev.* **D78** (2008) 023015, arXiv:0706.3064 [astro-ph].

[346] A. Aviles and J. L. Cervantes-Cota, "The dark degeneracy and interacting cosmic components," *Phys. Rev.* **D84** (2011) 083515, arXiv:1108.2457 [astro-ph.CO].

[347] M. Jamil, E. N. Saridakis, and M. Setare, "Thermodynamics of dark energy interacting with dark matter and radiation," *Phys.Rev.* **D81** (2010) 023007, arXiv:0910.0822 [hep-th].

[348] T. Harko and F. S. Lobo, "Irreversible thermodynamic description of interacting dark energy - dark matter cosmological models," *Phys. Rev.* **D87** (2013) 044018, arXiv:1210.3617 [gr-qc].

[349] J. Beyer, S. Nurmi, and C. Wetterich, "Coupled dark energy and dark matter from dilatation anomaly," *Phys. Rev.* **D84** (2011) 023010, arXiv:1012.1175 [astro-ph.CO].

[350] M. Tong, Y. Zhang, and Z. Fu, "Crossing $w = -1$ by a single scalar field coupling with matter and the observational constraints," *Class.Quant.Grav.* **28** (2011) 055006, arXiv:1101.5199 [astro-ph.CO].

[351] F. Simpson, "Scattering of Dark Matter and Dark Energy," *Phys. Rev.* **D82** (2010) 083505, arXiv:1007.1034 [astro-ph.CO].

[352] X.-D. Xu, B. Wang, and E. Abdalla, "The signature of the scattering between dark sectors in large scale cosmic microwave background anisotropies," *Phys.Rev.* **D85** (2012) 083513, arXiv:1112.1128 [astro-ph.CO].

[353] F. Costa, J. Alcaniz, and D. Jain, "An interacting model for the cosmological dark sector," *Phys.Rev.* **D85** (2012) 107302, arXiv:1204.3066 [astro-ph.CO].

[354] F. Costa, J. Lima, and F. Oliveira, "Decaying Vacuum Cosmology and its Scalar Field Description," arXiv:1204.1864 [astro-ph.CO].

[355] J. De-Santiago, D. Wands, and Y. Wang, "Inhomogeneous and interacting vacuum energy," arXiv:1209.0563 [astro-ph.CO].

[356] V. Poitras, "Constraints on $\Lambda(t)$-cosmology with power law interacting dark sectors," *JCAP* **1206** (2012) 039, arXiv:1205.6766 [astro-ph.CO].

[357] A. G. Riess, L. Macri, S. Casertano, M. Sosey, H. Lampeitl, *et al.*, "A Redetermination of the Hubble Constant with the Hubble Space Telescope from a Differential Distance Ladder," *Astrophys.J.* **699** (2009) 539–563, arXiv:0905.0695 [astro-ph.CO].

[358] R. R. Caldwell, "A Phantom Menace?," *Phys. Lett.* **B545** (2002) 23–29, arXiv:astro-ph/9908168.

[359] C. Deffayet, O. Pujolas, I. Sawicki, and A. Vikman, "Imperfect Dark Energy from Kinetic Gravity Braiding," *JCAP* **1010** (2010) 026, arXiv:1008.0048 [hep-th].

[360] A. J. Christopherson and K. A. Malik, "The non-adiabatic pressure in general scalar field systems," *Phys.Lett.* **B675** (2009) 159–163, arXiv:0809.3518 [astro-ph].

[361] I. Huston and A. J. Christopherson, "Calculating Non-adiabatic Pressure Perturbations during Multi-field Inflation," *Phys.Rev.* **D85** (2012) 063507, arXiv:1111.6919 [astro-ph.CO].

[362] W. J. Percival, S. Cole, D. J. Eisenstein, R. C. Nichol, J. A. Peacock, *et al.*, "Measuring the Baryon Acoustic Oscillation scale using the SDSS and 2dFGRS," *Mon.Not.Roy.Astron.Soc.* **381** (2007) 1053–1066, arXiv:0705.3323 [astro-ph].

[363] **WMAP Collaboration** Collaboration, E. Komatsu *et al.*, "Seven-Year Wilkinson Microwave Anisotropy Probe (WMAP) Observations: Cosmological Interpretation," *Astrophys.J.Suppl.* **192** (2011) 18, arXiv:1001.4538 [astro-ph.CO].

[364] R. Kessler, A. Becker, D. Cinabro, J. Vanderplas, J. A. Frieman, *et al.*, "First-year Sloan Digital Sky Survey-II (SDSS-II) Supernova Results: Hubble Diagram and Cosmological Parameters," *Astrophys.J.Suppl.* **185** (2009) 32–84, arXiv:0908.4274 [astro-ph.CO].

[365] S. Burles, K. M. Nollett, and M. S. Turner, "Big bang nucleosynthesis predictions for precision cosmology," *Astrophys.J.* **552** (2001) L1–L6, arXiv:astro-ph/0010171 [astro-ph].

[366] B. Feng, X.-L. Wang, and X.-M. Zhang, "Dark Energy Constraints from the Cosmic Age and Supernova," *Phys. Lett.* **B607** (2005) 35–41, arXiv:astro-ph/0404224.

[367] H. Ziaeepour, "Discrimination between Lambda-CDM, quintessence, and modified gravity models using wide area surveys," *Phys.Rev.* **D86** (2012) 043503, arXiv:1112.6025 [astro-ph.CO].

[368] V. Faraoni, E. Gunzig, and P. Nardone, "Conformal transformations in classical gravitational theories and in cosmology," *Fund.Cosmic Phys.* **20** (1999) 121, arXiv:gr-qc/9811047 [gr-qc].

[369] N. Deruelle and M. Sasaki, "Conformal equivalence in classical gravity: the example of 'veiled' General Relativity," arXiv:1007.3563 [gr-qc].

[370] Y. Bisabr, "Cosmic Acceleration in Brans-Dicke Cosmology," *Gen.Rel.Grav.* **44** (2012) 427–435, arXiv:1110.3421 [gr-qc].

[371] B. Bertotti, L. Iess, and P. Tortora, "A test of general relativity using radio links with the Cassini spacecraft," *Nature* **425** (2003) 374.

[372] A. Avilez and C. Skordis, "Cosmological constraints on Brans-Dicke theory," arXiv:1303.4330 [astro-ph.CO].

[373] R. Nagata, T. Chiba, and N. Sugiyama, "Observational consequences of evolution of primordial fluctuations in scalar - tensor cosmology," *Phys.Rev.* **D66** (2002) 103510, arXiv:astro-ph/0209140 [astro-ph].

[374] S. Capozziello, V. F. Cardone, and A. Troisi, "Reconciling dark energy models with f(R) theories," *Phys.Rev.* **D71** (2005) 043503, arXiv:astro-ph/0501426 [astro-ph].

[375] S. Nojiri and S. D. Odintsov, "Modified f(R) gravity consistent with realistic cosmology: From matter dominated epoch to dark energy universe," *Phys.Rev.* **D74** (2006) 086005, arXiv:hep-th/0608008 [hep-th].

[376] Y.-S. Song, W. Hu, and I. Sawicki, "The Large Scale Structure of f(R) Gravity," *Phys.Rev.* **D75** (2007) 044004, arXiv:astro-ph/0610532 [astro-ph].

[377] E. V. Linder, "Cosmic growth history and expansion history," *Phys.Rev.* **D72** (2005) 043529, arXiv:astro-ph/0507263 [astro-ph].

[378] M. Ishak, A. Upadhye, and D. N. Spergel, "Probing cosmic acceleration beyond the equation of state: Distinguishing between dark energy and modified gravity models," *Phys.Rev.* **D74** (2006) 043513, arXiv:astro-ph/0507184 [astro-ph].

[379] L. Knox, Y.-S. Song, and J. A. Tyson, "Distance-redshift and growth-redshift relations as two windows on acceleration and

gravitation: Dark energy or new gravity?,"
Phys.Rev. **D74** (2006) 023512,
arXiv:astro-ph/0503644 [astro-ph].

[380] S. Nesseris and L. Perivolaropoulos, "Evolving newton's constant, extended gravity theories and snia data analysis,"
Phys.Rev. **D73** (2006) 103511,
arXiv:astro-ph/0602053 [astro-ph].

[381] D. Polarski, "Dark Energy: Beyond General Relativity?,"
AIP Conf.Proc. **861** (2006) 1013–1018,
arXiv:astro-ph/0605532 [astro-ph].

[382] T. Chiba and R. Takahashi, "A Consistency Relation in Cosmology,"
Phys.Rev. **D75** (2007) 101301,
arXiv:astro-ph/0703347 [astro-ph].

[383] A. F. Heavens, T. Kitching, and L. Verde, "On model selection forecasting, Dark Energy and modified gravity,"
Mon.Not.Roy.Astron.Soc. **380** (2007) 1029–1035,
arXiv:astro-ph/0703191 [astro-ph].

[384] D. Huterer and E. V. Linder, "Separating Dark Physics from Physical Darkness: Minimalist Modified Gravity vs. Dark Energy,"
Phys.Rev. **D75** (2007) 023519,
arXiv:astro-ph/0608681 [astro-ph].

[385] E. V. Linder, "Theory Challenges of the Accelerating Universe,"
J.Phys.A **A40** (2007) 6697, arXiv:astro-ph/0610173 [astro-ph].

[386] J.-P. Uzan, "The acceleration of the universe and the physics behind it," *Gen.Rel.Grav.* **39** (2007) 307–342,
arXiv:astro-ph/0605313 [astro-ph].

[387] S. Wang, L. Hui, M. May, and Z. Haiman, "Is modified gravity required by observations? an empirical consistency test of dark

energy models," *Phys.Rev.D* **76** (2007) 063503. http://arxiv.org/abs/0705.0165.

[388] K. Yamamoto, D. Parkinson, T. Hamana, R. C. Nichol, and Y. Suto, "Optimizing future imaging survey of galaxies to confront dark energy and modified gravity models," *Phys.Rev.* **D76** (2007) 023504, arXiv:0704.2949 [astro-ph].

[389] V. Acquaviva, A. Hajian, D. N. Spergel, and S. Das, "Next Generation Redshift Surveys and the Origin of Cosmic Acceleration," *Phys.Rev.* **D78** (2008) 043514, arXiv:0803.2236 [astro-ph].

[390] L. Amendola, M. Kunz, and D. Sapone, "Measuring the dark side (with weak lensing)," *JCAP* **0804** (2008) 013, arXiv:0704.2421 [astro-ph].

[391] I. Laszlo and R. Bean, "Nonlinear growth in modified gravity theories of dark energy," *Phys.Rev.* **D77** (2008) 024048, arXiv:0709.0307 [astro-ph].

[392] Y. Wang, "Differentiating dark energy and modified gravity with galaxy redshift surveys," *JCAP* **0805** (2008) 021. http://arxiv.org/abs/0710.3885.

[393] W. Hu, "Acceleration from Modified Gravity: Lessons from Worked Examples," *Nucl.Phys.Proc.Suppl.* **194** (2009) 230–238, arXiv:0906.2024 [astro-ph.CO].

[394] P. Wu, H. Yu, and X. Fu, "A parametrization for the growth index of linear matter perturbations," *JCAP* **0906** (2009) 019. http://arxiv.org/abs/0905.3444.

[395] S. Baghram and S. Rahvar, "Structure formation in $f(R)$ gravity: A distinguishing probe between the dark energy and modified gravity," *JCAP* **1012** (2010) 008, arXiv:1004.3360 [astro-ph.CO].

[396] S. Chen and J. Jing, "Improved parametrization of the growth index for dark energy and DGP models," *Phys.Lett.* **B685** (2010) 185–189, arXiv:0908.4379 [gr-qc].

[397] D. Huterer, "Weak lensing, dark matter and dark energy," *Gen.Rel.Grav.* **42** (2010) 2177–2195, arXiv:1001.1758 [astro-ph.CO].

[398] F. Simpson and J. A. Peacock, "Difficulties Distinguishing Dark Energy from Modified Gravity via Redshift Distortions," *Phys.Rev.* **D81** (2010) 043512, arXiv:0910.3834 [astro-ph.CO].

[399] S. Lee, "Constraints on scalar-tensor theories of gravity from observations," *JCAP* **1103** (2011) 021, arXiv:1012.2646 [astro-ph.CO].

[400] E. Jennings, C. M. Baugh, and S. Pascoli, "Testing gravity using the growth of large scale structure in the Universe," *Astrophys.J.* **727** (2011) L9, arXiv:1011.2842 [astro-ph.CO].

[401] Y. Wang, "Observational Probes of Dark Energy," *AIP Conf.Proc.* **1458** (2011) 285–300, arXiv:1201.2110 [astro-ph.CO].

[402] M. Kunz and D. Sapone, "Dark Energy versus Modified Gravity," *Phys.Rev.Lett.* **98** (2007) 121301, arXiv:astro-ph/0612452 [astro-ph].

[403] E. Bertschinger and P. Zukin, "Distinguishing modified gravity from dark energy," *Phys.Rev.D* **78** (2008) 024015. http://arxiv.org/abs/0801.2431.

[404] D. Sapone, "Dark Energy in Practice," *Int.J.Mod.Phys.* **A25** (2010) 5253–5331, arXiv:1006.5694 [astro-ph.CO].

[405] B. Jain and P. Zhang, "Observational Tests of Modified Gravity," *Phys.Rev.* **D78** (2008) 063503, arXiv:0709.2375 [astro-ph].

[406] Y.-S. Song and K. Koyama, "Consistency test of general relativity from large scale structure of the Universe," *JCAP* **0901** (2009) 048, arXiv:0802.3897 [astro-ph].

[407] T. Clemson, K. Koyama, G.-B. Zhao, R. Maartens, and J. Valiviita, "Interacting Dark Energy – constraints and degeneracies," *Phys.Rev.* **D85** (2012) 043007, arXiv:1109.6234 [astro-ph.CO].

[408] Y.-S. Song, L. Hollenstein, G. Caldera-Cabral, and K. Koyama, "Theoretical Priors On Modified Growth Parametrisations," *JCAP* **1004** (2010) 018, arXiv:1001.0969 [astro-ph.CO].

[409] G. Dvali, G. Gabadadze, and M. Porrati, "4-D gravity on a brane in 5-D Minkowski space," *Phys.Lett.* **B485** (2000) 208–214, arXiv:hep-th/0005016 [hep-th].

[410] B. Boisseau, G. Esposito-Farese, D. Polarski, and A. A. Starobinsky, "Reconstruction of a scalar tensor theory of gravity in an accelerating universe," *Phys.Rev.Lett.* **85** (2000) 2236, arXiv:gr-qc/0001066 [gr-qc].

[411] R. Reyes, R. Mandelbaum, U. Seljak, T. Baldauf, J. E. Gunn, *et al.*, "Confirmation of general relativity on large scales from weak lensing and galaxy velocities," *Nature* **464** (2010) 256–258, arXiv:1003.2185 [astro-ph.CO].

[412] L. Pogosian, A. Silvestri, K. Koyama, and G.-B. Zhao, "How to optimally parametrize deviations from general relativity in the evolution of cosmological perturbations," *Phys.Rev.D* **81** (2010) 104023. http://arxiv.org/abs/1002.2382.

[413] T. Baker, P. G. Ferreira, C. Skordis, and J. Zuntz, "Towards a fully consistent parameterization of modified gravity," *Phys. Rev. D* **84** (2011) 124018. http://arxiv.org/abs/1107.0491.

[414] J. Zuntz, T. Baker, P. Ferreira, and C. Skordis, "Ambiguous tests of general relativity on cosmological scales," Apr., 2012. http://arxiv.org/abs/1110.3830.

[415] G.-B. Zhao, T. Giannantonio, L. Pogosian, A. Silvestri, D. J. Bacon, K. Koyama, R. C. Nichol, and Y.-S. Song, "Probing modifications of general relativity using current cosmological observations," *Phys.Rev.D* **81** (2010) 103510. http://arxiv.org/abs/1003.0001.

[416] P. Zhang, M. Liguori, R. Bean, and S. Dodelson, "A discriminating probe of gravity at cosmological scales," *Phys.Rev.Lett.* **99** (2007) 141302. http://arxiv.org/abs/0704.1932.

[417] S. Tsujikawa, K. Uddin, S. Mizuno, R. Tavakol, and J. Yokoyama, "Constraints on scalar-tensor models of dark energy from observational and local gravity tests," *Phys.Rev.* **D77** (2008) 103009, arXiv:0803.1106 [astro-ph].

[418] V. Acquaviva, C. Baccigalupi, S. M. Leach, A. R. Liddle, and F. Perrotta, "Structure formation constraints on the Jordan-Brans-Dicke theory," *Phys.Rev.* **D71** (2005) 104025, arXiv:astro-ph/0412052 [astro-ph].

[419] F. Wu and X. Chen, "Cosmic microwave background with Brans-Dicke gravity II: constraints with the WMAP and SDSS data," *Phys.Rev.* **D82** (2010) 083003, arXiv:0903.0385 [astro-ph.CO].

[420] R. Nagata, T. Chiba, and N. Sugiyama, "WMAP constraints on scalar- tensor cosmology and the variation of the gravitational

constant," *Phys.Rev.* **D69** (2004) 083512, arXiv:astro-ph/0311274 [astro-ph].

[421] T. Clifton, D. F. Mota, and J. D. Barrow, "Inhomogeneous gravity," *Mon.Not.Roy.Astron.Soc.* **358** (2005) 601, arXiv:gr-qc/0406001 [gr-qc].

[422] E. Gaztanaga, E. Garcia-Berro, J. Isern, E. Bravo, and I. Dominguez, "Bounds on the possible evolution of the gravitational constant from cosmological type Ia supernovae," *Phys.Rev.* **D65** (2002) 023506, arXiv:astro-ph/0109299 [astro-ph].

[423] V. Acquaviva and L. Verde, "Observational signatures of Jordan-Brans-Dicke theories of gravity," *JCAP* **0712** (2007) 001, arXiv:0709.0082 [astro-ph].